IEEE Access
Multidisciplinary ⋮ Rapid Review ⋮ Open Access Journal

Received 23 December 2022, accepted 4 February 2023, date of publication 16 February 2023, date of current version 23 February 2023.

Digital Object Identifier 10.1109/ACCESS.2023.3246182

RESEARCH ARTICLE

Decentralized H_∞ Observer-Based Attack-Tolerant Formation Tracking Network Control of Large-Scale LEO Satellites via HJIE-Reinforced Deep Learning Approach

BOR-SEN CHEN[1,2], (Life Fellow, IEEE), AND HUNG-YU LIN[1]
[1]Department of Electrical Engineering, National Tsing Hua University, Hsinchu 30013, Taiwan
[2]Department of Electrical Engineering, Yuan Ze University, Taoyuan 32003, Taiwan

Corresponding author: Bor-Sen Chen (bschen@ee.nthu.edu.tw)

This work was supported by the Ministry of Science and Technology of Taiwan under Grant MOST 108-2221-E-007-099-MY3.

ABSTRACT In this study, an H_∞ attack-tolerant decentralized observer-based formation tracking control strategy is designed for the network control system (NCS) of large-scale LEO satellite team under external disturbance and attack signal. First, smoothing signal models of attack signals are embedded in each satellite to avoid their corruption on state estimation of Luenberger observer and to compensate their effect on the formation tracking of large-scale satellites. In addition, the observer-based formation tracking NCS of each satellite must efficiently attenuate the external disturbance, measurement noise and coupling effect from adjacent satellites. For the proposed decentralized H_∞ attack-tolerant observer-based team formation NCS of large-scale satellites, each satellite needs to solve a very complicated but decoupled Hamilton Jacobi Isaacs equation (HJIE). Therefore, a proposed HJIE-reinforcement learning-based deep neural network (DNN) is employed for each satellite to directly solve a corresponding nonlinear partial differential control-observer-coupled $HJIE_i$ of decentralized H_∞ attack-tolerant control problem. When trained by the proposed HJIE-reinforcement Adam deep learning algorithm, DNN can be reinforced to solve $HJIE_i$ for H_∞ control gain and observer gain as well as the worst-case external disturbance, measurement noise, and coupling of each satellite of the team formation in the off-line training phase. That is, the proposed HJIE-reinforcement learning algorithm-based DNN scheme in each satellite NCS can achieve robust decentralized H_∞ attack-tolerant observer-based team formation control strategy. When the HJIE-reinforcement-based Adam learning algorithm converges, we can show that the proposed reinforcement learning-based DNN formation tracking control scheme of each satellite can approach the theoretical robust decentralized H_∞ attack-tolerant observer-based formation tracking strategy of large-scale satellites NCS. In the simulation example, a satellite team with external disturbance, measurement noise and wireless communication malicious attack are given to validate the effectiveness of proposed method separately.

INDEX TERMS Attack-tolerant control, observer-based formation control, large-scale satellite NCS, Hamilton Jacobi Isaacs equation (HJIE)-reinforcement learning, network control system (NCS) DNN, H_∞ decentralized observer-based formation tracking control, team formation of LEO satellites.

I. INTRODUCTION

At present, the LOW EARTH ORBIT (LEO) satellite has been a popular research topic in various fields [1]. In addition to the wide range of applications, the LEO satellites also have advantages such as low consumption and low transmission delay. According to the above systematic characteristics, the LEO satellites have also been used to develop large-scale team satellites and satellite constellation, e.g., spaceX's starlink project [2]. Large-scale satellite formations can

The associate editor coordinating the review of this manuscript and approving it for publication was Vivek Kumar Sehgal.

enable satellites to achieve the global coverage and solve the problem of satellite service coverage. Besides, the satellites can establish Laser Intersatellite Links(LISLs) with other satellites [3], so that the communication is not limited to the ground communication station. In this way, a more efficient satellite communication transmission can be achieved. In order to achieve an ideal large-scale satellite formation, the formation shape and attitude of the satellites must be changed according to the desired mission during the flying process. In this case, the formation tracking control of the satellites will be an important task.

Among the formation control methods, the common methods include the leader-follower (L-F) method, the behavior-based control method, the graph theory-based method, the virtual leader-based method [4], etc. For the methods mentioned above, the L-F method is relatively simple to implement. The designer can achieve the desired team formation shape by keeping the leader and the follower at a specific distance and attitude. However, once the leader is crushed, the entire formation system based on L-F method becomes unsustainable [5]. In this case, the virtual-leader (V-L) method is the most suitable strategy for formation control. Similar to the L-F method, but the leader in the V-S method is virtual. The virtual leader will not crash in a disturbed environment [6]. Therefore, the V-L method can completely avoid the problem of leader collapse.

In addition to the above formation methods, the formation coordination strategy is also an important part of the formation control system. In the formation control strategy, it can be divided into centralized formation control [7], [8] and decentralized formation control [9], [10]. The centralized control strategy is that all satellites are coordinated by a single controller. However, in a large-scale satellite team, proceeding the information of all subsystems at one time will greatly increase the design and computational complexity of the controller. In contrast, the decentralized control strategy can be independently designed for each subsystem. Therefore, decentralized satellite control strategy can be developed into a larger scale satellite formation control system. Many decentralized control methods have been studied in [11] and [12]. Therefore, in the satellite team formation, it is generally more preferred to use the decentralized control strategy. However, more effort is needed to design the decentralized team formation control strategy of large-scale LEO satellites.

Recently, with the development of wireless communication network technology, the multi-agent network control method has been applied in various research fields [13], [14]. In a large-scale satellite team formation, the network control system (NCS) is applied to the formation tracking control. NCS is a control method for transmitting state and control information through wireless network. When the state information of satellite team is transmitted to the ground control system (GCS), GCS calculates control commands and then sends the control input back to the satellite [15]. This method can be simply employed for the decentralized formation control of Large-scale satellite team. However, in the wireless network environment of NCS, the transmission of information may suffer from malicious attack signals. Therefore, the output information of satellite received by the GCS and the control commands received by the satellite may be incorrect, resulting in the degradation of the control performance. To address this issue, we proposed an observer-based attack-tolerant control (ATC) scheme to eliminate the effect of unknown interference signals on the team formation NCS of large-scale LEO satellites. The ATC scheme is a popular research topic and it aims to estimate these interference signals for attack signal compensation [16], [17], [18]. In general, the observer-based ATC scheme includes a conventional Luenberger observer to simultaneously estimate the state information and attack signal on each satellite. In the part of estimating the attack signals, the unavailable actuator and sensor attack signals are described by two nonsingular smoothed signal models. To prevent the corruption problem of attack signals, two smoothed signal models are embedded in each satellite dynamic model as an augmented system. By this way, the conventional Luenberger observer can estimate satellite state and attack signals on sensor and actuator for the attack-tolerant observer-based control design. Then, the actual unavailable attack signals on the satellite formation NCS can be compensated by the estimated attack signals.

From the point of view of satellite implementation, with the expansion of the satellite team formation NCS, the number of LEO satellites will increase significantly. In this case, the wireless communication network between satellites may have coupling effects, e.g., co-channel interference [19], [20]. Therefore, the effect of wireless network interconnected couplings in the satellite team formation NCS should be taken into account. Furthermore, it is inevitable that the satellite formation control system is affected by external disturbances and measurement noise. Common disturbances in the outer space environment include earth flattening, pressure of solar radiation, aerodynamic drag, [21], [22], [23], etc. Based on the above discussion, it is seen that team formation robustness is important for decentralized formation tracking control of large-scale team satellites. Thus, the robust decentralized H_∞ attack-tolerant team formation tracking control strategy is adopted as a control method as NCS of large-scale satellites in this study. For years, the robust H_∞ control techniques have been used in practice to attenuate the worst-case impact of external disturbance on nonlinear dynamic systems. The attitude control of spacecraft implemented by the sliding mode control law and adaptive control law for a satellite have been discussed in [24] and [25], respectively. The fault estimation of observer design with sensor and actuator failure was discussed in [50] and the observer-based control with DoS attacks was introduced in [51].

In general, we need to solve a highly nonlinear partial differential Hamilton Jacobi Isaacs Equation (HJIE) in the robust H_∞ tracking control design of nonlinear dynamic systems in the environment of co-channel coupling, external

disturbances and malicious attack. Currently no mathematical tool can solve this HJIE analytically and numerically. To deal with this problem, several methods of interpolating local linearized systems to approximate a nonlinear system have been proposed, such as fuzzy interpolation method [26], [27], [28], [29], global linearization method [30], [31], [32], gain scheduling method [33], [34], etc. By these methods, it is possible to reduce the complicated HJIE problem to the problem of solving a set of linear matrix inequalities (LMIs). Nevertheless, since the process of converting HJIE into a set of LMIs requires performing several inequality operations and selecting a quadratic Lyapunov function as the solution of HJIE, this will lead to a conservative result. In addition, for observer-based attack-tolerant decentralized formation tracking control of large-scale team satellites, we need to interpolate two corresponding large coupled sets of local control laws and local observer laws in the observer-based team formation tracking control, which makes an increase in the design complexity and computational load.

To avoid the above problems in solving the complicated HJIE for decentralized H_∞ attack-tolerant team formation tracking control, a HJIE-reinforcement learning DNN-based control scheme is proposed to implement robust H_∞ decentralized attack-tolerant observer-based formation tracking controller for large-scale LEO satellites. Deep neural network (DNN) was a discriminative model, which can be trained by specific parameter updating law [35]. By learning from large amounts of data, DNN can approximate complicated nonlinear systems. Through the characteristics of appealing global approximation, DNN can be trained to implement a wide range of tasks such as translation of language [36], image classification [37], [38], image segmentation [39], etc. Recently, DNN has been trained to solve the robust stabilization of nonlinear time-varying system [40]. However, there is still no direct application of DNN to H_∞ filter and tracking control strategy of nonlinear stochastic system simultaneously. From the viewpoint of robust H_∞ observer-based tracking control, DNN can directly solve highly nonlinear partial differential HJIE problems by HJIE-reinforcement deep learning algorithm to achieve H_∞ tracking control performance without any local linear system interpolation method and quadratic Lyapunov solution of HJIE.

In order to reduce the worst-case effects of external disturbance, malicious attack signal, interconnected coupling effect, and measurement noise on the state estimation error and formation tracking error in the NCS of large-scale LEO satellites, the minmax stochastic H_∞ Nash game strategy is employed for each satellite in the team formation. In the proposed robust decentralized H_∞ attack-tolerant observer-based formation tracking control of large-scale team satellites, based on the augmented time-varying reference tracking error system and estimation error dynamic system, a corresponding control-observer-coupled HJIE of decentralized H_∞ attack-tolerant observer-based output feedback formation tracking control design of large-scale satellites NCS needs to be solved at first for each satellite. According to the control-observer-coupled HJIE and the characteristics of system models, the reinforcement learning scheme can be employed to train a corresponding DNN for each satellite in the team to approach the decentralized H_∞ attack-tolerant observer-based formation tracking control strategy of large-scale satellites NCS. For the robust decentralized H_∞ observer-based attack-tolerant formation tracking control design problem of large-scale satellites NCS, our objective is to solve $\frac{\partial V(\tilde{X}_i(t),e_i(t),t)}{\partial[\tilde{X}_i^T(t)\ e_i^T(t)\ t]^T}$ of control-observer-coupled $HJIE_i$ by training DNN via reinforcement learning algorithm for calculating control law $u_i^*(t)$ and observer gain $L_i^*(\hat{X}_i(t))$ of the robust decentralized H_∞ attack-tolerant observer-based formation tracking control design for each satellite in the team. In this work, since the external disturbance $v_i(t)$, interconnected coupling effect $X_j(t)$ from other satellites and measurement noise $n_i(t)$ are unavailable for training DNN in the off-line training phase, the worst-case external disturbance $v_i^*(t)$, interconnected coupling effect $X_j^*(t)$ and measurement noise $n_i^*(t)$ of robust decentralized H_∞ attack-tolerant observer-based formation tracking control strategy are employed to replace the actual external disturbance $v_i(t)$, interconnected coupling effect $X_j(t)$ and measurement noise $n_i(t)$, respectively, without influence on the robust decentralized H_∞ attack-tolerant observer-based formation tracking performance because it is designed based on the worst-case $v_i^*(t)$, $X_j^*(t)$ and $n_i^*(t)$. Accordingly, we can generate the measurement output $Y_i(t)$ by system model of the ith satellite with control input $u_i^*(t)$, $v_i^*(t)$ and $n_i^*(t)$ and $X_j^*(t)$ in the off-line training phase. In this study, HJIE-reinforcement-based Adam learning algorithm [35] is employed to train DNN. After training, we can prove the DNN can approach $\frac{\partial V(\tilde{X}_i(t),\bar{e}_i(t),t)}{\partial[\tilde{X}_i^T(t)\ \bar{e}_i^T(t)\ t]^T}$ for each satellite in the team. Furthermore, it can be proven that when the learning error of HJIE-reinforcement-based Adam learning algorithm approaches to zero, the DNN with input $\tilde{X}_i(t)$ and $\bar{e}_i(t)$ will output $\frac{\partial V(\tilde{X}_i(t),\bar{e}_i(t),t)}{\partial[\tilde{X}_i^T(t)\ \bar{e}_i^T(t)\ t]^T}$, i.e, the HJIE-reinforcement learning-based DNN observer-based attack-tolerant formation tracking control scheme can approach to the decentralized H_∞ attack-tolerant observer-based formation tracking control strategy of nonlinear NCS of large-scale satellites with external disturbance, malicious attack, interconnected coupling effect and measurement noise.

The followings are the main contributions of this work:

1) In the network control of large-scale satellite team formation, we construct a novel dynamic smoothing model to describe the possible occurrence of malicious attack on actuator and sensor in wireless network environment. Then, the conventional Luenberger observer could be employed to precisely estimate state variables, actuator and sensor attack signals simultaneously for the robust decentralized H_∞ observer-based attack-tolerant formation control design. The proposed robust decentralized H_∞ attack-tolerant observer-based control method can efficiently

attenuate the influence of the malicious attack signal, external disturbance, measurement noise and coupling effect on the satellite team formation system. As a result, if external disturbance, attack signal, measurement noise and the wireless co-channel coupling are of finite energy, then quadratic asymptotic team formation tracking of the network satellite control system can be guaranteed even under malicous attack signals through wireless communication network in future 5G and 6G era [14], [15].

2) In this study, the HJIE-reinforcement-based DNN learning algorithm is combined with the robust H_∞ control observer-based decentralized formation control design [10], [11]. For nonlinear team formation satellite network control systems with external disturbance, interconnected delayed coupling effect, attack signal, and output measurement noise, a novel HJIE-reinforcement DNN-based robust H_∞ attack-tolerant observer-based formation tracking control strategy is proposed for large-scale LEO satellites. We adopted the HJIE-reinforcement DNN-based learning algorithm to solve control-observer-coupled HJIE in the off-line training process of robust H_∞ attack-tolerant observer-based formation tracking control design of large-scale satellite network control system, and then we can obtain the control law, observer gain, the worst-case external disturbance, unknown couplings, malicious attack signal and measurement noise.

3) Compared with traditional T-S fuzzy control method [29] by interpolating L local linearized systems to approximate the nonlinear satellite system and assuming that the state variables of satellite are available, which needs to solve L linear matrix inequalities (LMIs) and compute the complicated fuzzy interpolation of L local controllers, the HJIE-reinforcement learning DNN-based robust H_∞ decentralized observer-based tracking control scheme is trained and then applied to large-scale satellite team formation system with malicious attack, external disturbances, measurement noise and interconnected coupling effect. Obviously, the proposed method has a different design aspect of integrating reinforcement learning algorithm with deep neural network, which will have wide applications due to the clue of satellite model and the use of theoretic results based on model. Therefore, it can not only achieve a more powerful control design performance but also save a large amount of training time and training data than the conventional big data deep learning methods [36], [37], [38], [39].

The structure of this study is described as follows. In Section II, the satellite team formation system, smoothed dynamic model of attack signals and problem formulation are introduced. In Section III, a HJIE-reinforcement DNN-based H_∞ attack-tolerant observer-based reference tracking control scheme is applied to large-scale LEO satellite team formation systems with external disturbance and measurement noise. In section IV, the effectiveness of the proposed HJIE-reinforcement learning DNN-based robust H_∞ observer-based attack-tolerant decentralized team formation tracking controller is verified through a simulation example. In the end, the conclusion is made in Section V.

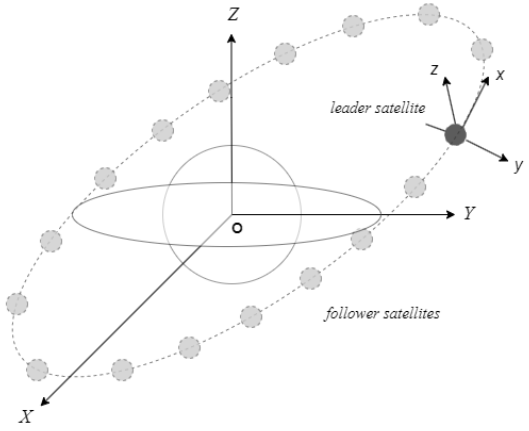

FIGURE 1. Large-scale satellite formation coordinate frames.

Notation:A^T denotes the transpose of vector or matrix A; $P = P^T \geq 0$ denotes semi-positive definite matrix P; $\frac{\partial V(\widetilde{X}_i(t),\bar{e}_i(t),t)}{\partial[\widetilde{X}_i^T(t)\ \bar{e}_i^T(t)\ t]^T} \triangleq \begin{bmatrix} \frac{\partial V(\widetilde{X}_i(t),\bar{e}_i(t),t)}{\partial \widetilde{X}_i(t)} \\ \frac{\partial V(\widetilde{X}_i(t),\bar{e}_i(t),t)}{\partial \bar{e}_i(t)} \\ \frac{\partial V(\widetilde{X}_i(t),\bar{e}_i(t),t)}{\partial t} \end{bmatrix}$; $\mathbb{R}^n$ denotes the set of n-tuple real vectors; $\mathcal{L}_2[0,\infty)$ denotes a set of real functions $X(t) \in \mathbb{R}^n$ with finite energy, i.e., $X(t) \in \mathcal{L}_2^F[0,\infty)$, if $\|X(t)\|_2 = (E\int_0^\infty X(t)^T X(t)dt)^{1/2} < \infty$; I_a denotes the identity matrix with dimension $a \times a$; $diag\{A, B\} \triangleq \begin{bmatrix} A & 0 \\ 0 & B \end{bmatrix}$

II. THE SYSTEM DYNAMIC MODEL OF SATELLITE AND PROBLEM FORMULATION

A. THE DYNAMIC MODEL OF SATELLITE

In this study, we employ the relative motion model of satellite position and attitude to describe the state of satellite team formation. The dynamic model of satellite team formation is divided into two parts, physical relative translation dynamic model and physical attitude dynamic model.

1) RELATIVE POSITION DYNAMIC MODEL OF LARGE-SCALE SATELLITE SYSTEM

In the multi-satellite formation, the team consists of a leader satellite and several follower satellites as shown in Fig. 1. The coordinate [X, Y, Z] is Earth-Centered-Inertial (ECI) frame with its origin at the Earth's center of mass. X-axis is pointing in the direction of the vernal equinox, the direction of the Z-axis represents the spin axis of the earth and the Y-axis is completely orthogonal to the other two axes. On the body of satellite, the distance between the virtual leader satellite and the follower satellites is expressed in the Local-Vertical-Local-Horizontal (LVLH) frame[x, y, z].

The x-axis is pointing in the direction of orbit operating, y-axis is pointing in the direction of radial, and z-axis is completely orthogonal to the other two axes. The following is the dynamic model of the i-th follower satellite's relative position to the leader satellite [23]:

$$\begin{aligned}
\ddot{x}_i &= \dot{\omega}_{ECI,z_i} y_i + 2\omega_{ECI,x_i}\dot{y}_i + \omega_{ECI,z_i} \\
&\quad \times(\omega_{ECI,z_i} x_i - \omega_{ECI,x_i} z_i) - \frac{u_e x_i}{R_i^3} + \frac{F_{x_i}}{m_i} + \frac{D_{d_{x_i}}}{m_i} \\
\ddot{y}_i &= \omega_{ECI,x_i}^2 y_i + 2\omega_{ECI,x_i}\dot{z} + \omega_{ECI,z_i}^2 y_i - 2\omega_{ECI,z_i}\dot{x}_i \\
&\quad -\dot{\omega}_{ECI,z_i} x_i + \dot{\omega}_{ECI,x_i} z_i - \frac{u_e(y_i + R_o)}{R_i^3} + \frac{u_e}{R_o^2} \\
&\quad + \frac{F_{y_i}}{m_i} + \frac{D_{d_{y_i}}}{m_i} \\
\ddot{z}_i &= -\dot{\omega}_{ECI,x_i} y_i - 2\omega_{ECI,x_i}\dot{y}_i - \omega_{ECI,x_i} \\
&\quad \times(\omega_{ECI,z_i} x_i - \omega_{ECI,x_i} z_i) - \frac{u_e z_i}{R_i^3} + \frac{F_{z_i}}{m_i} + \frac{D_{d_{z_i}}}{m_i}, \\
&\qquad i = 1, \ldots N
\end{aligned} \tag{1}$$

where ω_{ECI,x_i} and ω_{ECI,z_i} represent the ith satellite's orbital velocities in the X and Z directions, respectively. The gravitational constant of the Earth is u_e. R_o is the radial distance between the Earth and the virtual leader. $R_i = \sqrt{x_i^2 + (y_i + R_o)^2 + z_i^2}$ is the distance between the Earth and the ith follower mass center. $F_{x_i}, F_{y_i}, F_{z_i}$ denote the control torque of the ith follower satellites. $D_{d_{x_i}}, D_{d_{y_i}}, D_{d_{z_i}}$ represent the disturbance of the ith satellite. The formating team's satellite number is represented by N., and m_i is the the ith satellite mass. In this model, we set the leader satellite to be virtual-leader.

1: Each follower satellite's virtual leader information is constantly accessible.

2) RELATIVE ATTITUDE DYNAMIC MODEL OF LARGE-SCALE SATELLITE SYSTEM

In this subsection, the attitude model is taken into account to describe the orientation of the LEO satellite. As shown in Fig. 2, ECI frame $[X, Y, Z]$, orbital reference frame $[o_1^i, o_2^i, o_3^i]$, and body frame $[b_1^i, b_2^i, b_3^i]$ of the LEO satellite are considered. According to [29], we can get the nonlinear attitude dynamic model of each follower:

$$\begin{aligned}
\ddot{\theta}_1^i(t) &= F_{i_1}(t) + \frac{\tau_{\theta 1}^i}{J_1^i} + \frac{D_{\theta_1}^i}{J_1^i} + \sin\theta_2^i \ddot{\theta}_3^i \\
\ddot{\theta}_2^i(t) &= F_{i_2}(t) + \frac{\tau_{\theta 2}^i}{\cos\theta_1^i J_2^i} + \frac{D_{\theta_2}^i}{\cos\theta_1^i J_2^i} \\
&\quad - \frac{1}{\cos\theta_1^i}(\cos\theta_2^i \sin\theta_1^i \ddot{\theta}_3^i) \\
\ddot{\theta}_3^i(t) &= F_{i_3}(t) + \frac{\tau_{\theta 3}^i}{\cos\theta_1^i \cos\theta_2^i J_3^i} + \frac{D_{\theta_3}^i}{\cos\theta_1^i \cos\theta_2^i J_3^i} \\
&\quad + \frac{1}{\cos\theta_1^i \cos\theta_2^i}(\sin\theta_1^i \ddot{\theta}_2^i)
\end{aligned} \tag{2}$$

where J_k^i denotes the inertia principal moment of the ith satellite. τ_k^i is the control torque, and $D_{\theta_i}^i$ is the disturbance torque, for $k = 1, 2, 3$.

$$\begin{aligned}
F_{i_1}(t) = &-\omega_{ECI,z_i}\cos\theta_1^i \sin\theta_3^i \dot{\theta}_1^i - \cos\theta_3^i \sin\theta_1^i \dot{\theta}_3^i \\
&+ \cos\theta_1^i \cos\theta_2^i \cos\theta_3^i \dot{\theta}_2^i \\
&- \cos\theta_3^i \sin\theta_1^i \sin\theta_2^i \dot{\theta}_1^i - \cos\theta_1^i \sin\theta_2^i \\
&\times \sin\theta_3^i \dot{\theta}_3^i + \cos\theta_2^i \dot{\theta}_3^i \dot{\theta}_2^i \\
&+ \cos\theta_3^i \sin\theta_2^i \omega_{ECI,x_i} \dot{\theta}_2^i + \cos\theta_2^i \sin\theta_3^i \\
&\times \omega_{ECI,x_i} \dot{\theta}_3^i + \sin\theta_1^i \sin\theta_3^i \dot{v}_{ECI,z_i} - \cos\theta_2^i \cos\theta_3^i \\
&\times \dot{v}_{ECI,x_i} + \cos\theta_1^i \sin\theta_2^i \cos\theta_3^i \dot{\omega}_{ECI,x_i} \\
&+ \frac{(J_2^i - J_3^i)}{J_1^i}[-\cos\theta_1^i \times \sin\theta_1^i \dot{\theta}_2^i \dot{\theta}_2^i \\
&+ \cos\theta_1^i \cos\theta_2^i \cos\theta_1^i \dot{\theta}_2^i \dot{\theta}_3^i + \omega_{ECI,x_i} \cos\theta_1^i \\
&\times \sin\theta_2^i \dot{\theta}_2^i + \omega_{ECI,x_i} \cos\theta_2^i \sin\theta_1^i \dot{\theta}_2^i \\
&+ \omega_{ECI,x_i} \sin\theta_1^i \cos\theta_2^i \\
&\times \sin\theta_3^i \dot{\theta}_2^i - \omega_{ECI,x_i} \cos\theta_2^i \cos\theta_2^i \sin\theta_3^i \cos\theta_1^i \dot{\theta}_3^i \\
&- \omega_{ECI,x_i}\omega_{ECI,x_i} \cos\theta_2^i \times \sin\theta_3^i \sin\theta_2^i \\
&- \omega_{ECI,x_i}\omega_{ECI,z_i} \cos\theta_2^i \sin\theta_3^i \\
&\times \cos\theta_1^i \cos\theta_2^i + \cos\theta_1^i \cos\theta_1^i \cos\theta_2^i \omega_{ECI,z_i} \dot{\theta}_2^i \\
&- \cos\theta_2^i \sin\theta_1^i \sin\theta_1^i \dot{\theta}_2^i \dot{\theta}_3^i + \cos\theta_2^i \cos\theta_2^i \sin\theta_1^i \\
&\times \cos\theta_1^i \dot{\theta}_3^i \dot{\theta}_3^i + \omega_{ECI,z_i} \cos\theta_2^i \\
&\times \sin\theta_1^i \cos\theta_1^i \times \cos\theta_2^i \dot{\theta}_3^i - \omega_{ECI,z_i} \sin\theta_1^i \sin\theta_1^i \\
&\times \cos\theta_3^i \dot{\theta}_2^i - \omega_{ECI,z_i} \sin\theta_1^i \cos\theta_1^i \times \sin\theta_2^i \sin\theta_3^i \dot{\theta}_2^i \\
&+ \omega_{ECI,z_i} \sin\theta_1^i \cos\theta_3^i \cos\theta_2^i \cos\theta_1^i + \omega_{ECI,z_i} \cos\theta_1^i \\
&\times \cos\theta_2^i \cos\theta_1^i \sin\theta_2^i \sin\theta_3^i \\
&+ (\omega_{ECI,z_i})^2 \sin\theta_1^i \times \cos\theta_3^i \cos\theta_1^i \cos\theta_2^i \\
&+ (\omega_{ECI,z_i})^2 \cos\theta_1^i \\
&\times \cos\theta_1^i \cos\theta_2^i \sin\theta_2^i \times \sin\theta_3^i; \\
F_{i_2}(t) = &\frac{1}{\cos\theta_1^i}[-\omega_{ECI,z_i}\cos\theta_1^i \cos\theta_3^i \dot{\theta}_1^i + \sin\theta_1^i \sin\theta_3^i \dot{\theta}_3^i \\
&- \cos\theta_1^i \cos\theta_2^i \sin\theta_3^i \dot{\theta}_2^i - \cos\theta_1^i \cos\theta_3^i \sin\theta_2^i \dot{\theta}_3^i \\
&+ \sin\theta_1^i \sin\theta_2^i \sin\theta_3^i \dot{\theta}_1^i + \sin\theta_1^i \dot{\theta}_2^i \dot{\theta}_1^i \\
&- \cos\theta_1^i \cos\theta_2^i \dot{\theta}_3^i \dot{\theta}_1^i + \cos\theta_2^i \cos\theta_3^i \omega_{ECI,x_i} \dot{\theta}_3^i \\
&+ \sin\theta_1^i \sin\theta_2^i \dot{\theta}_3^i \dot{\theta}_2^i - \sin\theta_2^i \sin\theta_3^i \omega_{ECI,x_i} \dot{\theta}_2^i \\
&+ \cos\theta_2^i \sin\theta_3^i \dot{\omega}_{ECI,x_i} - \sin\theta_1^i \cos\theta_3^i \dot{v}_{ECI,z_i} \\
&- \cos\theta_1^i \sin\theta_2^i \sin\theta_3^i \dot{\omega}_{ECI,z_i} + \frac{(J_1^i - J_3^i)}{J_2^i} \\
&\times(-\sin\theta_1^i \dot{\theta}_1^i \dot{\theta}_2^i + \cos\theta_2^i \cos\theta_1^i \dot{\theta}_1^i \dot{\theta}_3^i \\
&+ \omega_{ECI,x_i} \sin\theta_2^i \dot{\theta}_1^i + \omega_{ECI,z_i} \cos\theta_1^i \cos\theta_2^i \dot{\theta}_1^i \\
&+ \sin\theta_1^i \sin\theta_2^i \dot{\theta}_2^i \dot{\theta}_3^i - \sin\theta_2^i \cos\theta_2^i \\
&\times \cos\theta_1^i \dot{\theta}_3^i \dot{\theta}_3^i - \omega_{ECI,x_i} \sin\theta_2^i \times \sin\theta_2^i \dot{\theta}_3^i
\end{aligned}$$

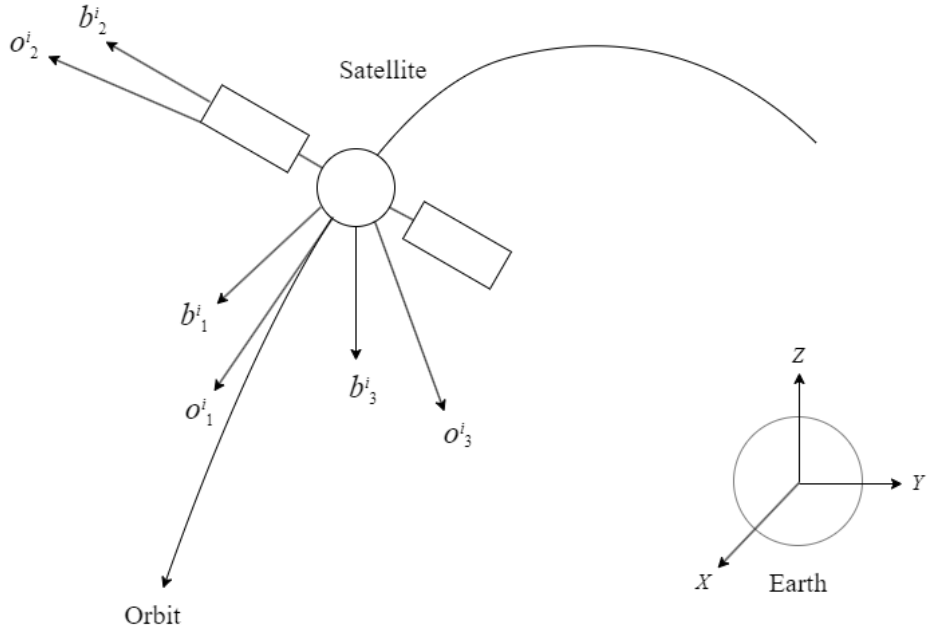

FIGURE 2. Body frame of LEO satellite, orbital reference frame and ECI frame in the space [50].

$$
\begin{aligned}
&-\omega_{ECI,z_i}\sin\theta_2^i\cos\theta_1^i\cos\theta_2^i\dot{\theta}_3^i-\omega_{ECI,x_i}\sin\theta_1^i\\
&\times\cos\theta_2^i\cos\theta_3^i\dot{\theta}_2^i+\omega_{ECI,x_i}\\
&\times\cos\theta_1^i\cos\theta_2^i\cos\theta_2^i\cos\theta_3^i\\
&+(\omega_{ECI,x_i})^2\cos\theta_2^i\cos\theta_3^i\sin\theta_2^i\\
&+\omega_{ECI,x_i}\omega_{ECI,z_i}\cos\theta_2^i\cos\theta_3^i\times\cos\theta_1^i\cos\theta_2^i\\
&-\omega_{ECI,z_i}\sin\theta_1^i\sin\theta_1^i\sin\theta_3^i\dot{\theta}_2^i+\omega_{ECI,z_i}\sin\theta_1^i\\
&\times\sin\theta_3^i\cos\theta_2^i\cos\theta_1^i\dot{\theta}_3^i+\omega_{ECI,x_i}\omega_{ECI,z_i}\sin\theta_1^i\\
&\times\sin\theta_2^i\sin\theta_3^i+(\omega_{ECI,z_i})^2\sin\theta_1^i\\
&\times\sin\theta_3^i\cos\theta_1^i\cos\theta_2^i+\omega_{ECI,z_i}\cos\theta_1^i\sin\theta_1^i\\
&\times\sin\theta_2^i\cos\theta_3^i\dot{\theta}_2^i\\
&-\omega_{ECI,z_i}\cos\theta_1^i\sin\theta_2^i\cos\theta_3^i\cos\theta_1^i\cos\theta_2^i\\
&-\omega_{ECI,x_i}\omega_{ECI,z_i}\cos\theta_1^i\sin\theta_2^i\cos\theta_3^i\sin\theta_2^i\\
&-(\omega_{ECI,z_i})^2\times\cos\theta_1^i\cos\theta_1^i\\
&\times\cos\theta_2^i\sin\theta_2^i\cos\theta_3^i)];
\end{aligned}
$$

$$
\begin{aligned}
F_{i_3}(t)=\frac{1}{\cos\theta_1^i\cos\theta_2^i}\times[&\cos\theta_1^i\dot{\theta}_1^i\dot{\theta}_2^i-\cos\theta_2^i\omega_{ECI,x_i}\dot{\theta}_2^i\\
&+\cos\theta_2^i\sin\theta_1^i\dot{\theta}_1^i\dot{\theta}_3^i+\cos\theta_1^i\sin\theta_2^i\dot{\theta}_2^i\dot{\theta}_3^i\\
&+\cos\theta_2^i\sin\theta_1^i\omega_{ECI,z_i}\dot{\theta}_1^i+\cos\theta_1^i\sin\theta_2^i\omega_{ECI,z_i}\dot{\theta}_2^i\\
&+\sin\theta_2^i\dot{\omega}_{ECI,x_i}+\cos\theta_1^i\cos\theta_2^i\\
&\times\dot{\omega}_{ECI,z_i}+\frac{(J_2^i-J_1^i)}{J_3^i}(\cos\theta_1^i\dot{\theta}_1^i\dot{\theta}_2^i+\cos\theta_2^i\sin\theta_1^i\\
&-\omega_{ECI,x_i}\cos\theta_2^i\sin\theta_3^i\dot{\theta}_1^i+\omega_{ECI,z_i}\sin\theta_1^i\cos\theta_3^i\dot{\theta}_1^i\\
&+\omega_{ECI,z_i}\cos\theta_1^i\sin\theta_2^i\sin\theta_3^i\dot{\theta}_1^i-\sin\theta_2^i\cos\theta_1^i\dot{\theta}_2^i\dot{\theta}_3^i\\
&-\sin\theta_2^i\sin\theta_1^i\cos\theta_2^i\dot{\theta}_3^i\dot{\theta}_3^i+\omega_{ECI,x_i}\sin\theta_2^i\\
&\times\cos\theta_2^i\sin\theta_3^i\dot{\theta}_3^i-\omega_{ECI,z_i}\sin\theta_1^i\cos\theta_3^i\sin\theta_2^i\dot{\theta}_3^i\\
&-\omega_{ECI,z_i}\cos\theta_1^i\sin\theta_2^i\sin\theta_3^i\sin\theta_2^i\dot{\theta}_3^i+\omega_{ECI,x_i}\cos\theta_2^i\\
&\times\cos\theta_3^i\cos\theta_1^i\dot{\theta}_2^i+\omega_{ECI,x_i}\cos\theta_2^i\cos\theta_3^i\cos\theta_2^i\\
&\times\sin\theta_1^i\dot{\theta}_3^i-(\omega_{ECI,x_i})^2\cos\theta_2^i\cos\theta_3^i\cos\theta_2^i\sin\theta_3^i\\
&+\omega_{ECI,x_i}\omega_{ECI,z_i}\cos\theta_2^i\sin\theta_1^i\times\cos\theta_3^i\cos\theta_3^i\\
&+\omega_{ECI,x_i}\omega_{ECI,z_i}\cos\theta_2^i\cos\theta_3^i\cos\theta_1^i\sin\theta_2^i\sin\theta_3^i\\
&-\omega_{ECI,z_i}\sin\theta_1^i\sin\theta_3^i\cos\theta_1^i\dot{\theta}_2^i-\omega_{ECI,z_i}\\
&\times\cos\theta_1^i\sin\theta_2^i\times\cos\theta_3^i\cos\theta_2^i\sin\theta_1^i\dot{\theta}_3^i\\
&+\omega_{ECI,x_i}\omega_{ECI,z_i}\cos\theta_1^i\sin\theta_2^i\cos\theta_3^i\times\cos\theta_2^i\sin\theta_3^i\\
&-(\omega_{ECI,z_i})^2\cos\theta_1^i\sin\theta_2^i\cos\theta_3^i\\
&\times\sin\theta_1^i\cos\theta_3^i-(\omega_{ECI,z_i})^2\cos\theta_1^i\sin\theta_2^i\cos\theta_3^i\\
&\times\cos\theta_1^i\sin\theta_2^i\sin\theta_3^i)]
\end{aligned}
$$

Obviously, the relative position and attitude dynamic model of each follower satellites in (1) and (2) are highly nonlinear and very complex. It is not easy to simultaneously to achieve the position and attitude control design of LEO satellite so that the conventional position and attitude control of LEO satellite are always designed separately. However, the desired position and attitude are all included in the team formation control design of each satellite in this study.

B. LARGE-SCALE SATELLITE FORMATION NCS WITH INTERCONNECTED COUPLING AND MALICIOUS ATTACK SIGNAL

In this study, a large-scale satellite formation NCS is represented by a set $S = \{S_1, S_2, \ldots, S_N\}$. The ith satellite

subsystem is represented by the S_i. N denotes the member number of the team formation. In practical applications, the satellite formation NCS will be disturbed by the external environment and malicious attacks in wireless network communications. Therefore, the problems of external interference attenuation and attack-tolerance must be taken into account. Besides, with the expansion of the satellite formation scale, the satellites also suffer from co-channel interference and non-ideal communications from adjacent satellites in the formation team. According to the above discussion, The following is a representation of the satellite team formation system:

$$\begin{aligned} S_i : \dot{X}_i(t) &= F_i(X_i(t)) + G_i(X_i(t))u_i(t) \\ &\quad + \sum_{j\in N_i} F_{ij}(X_i(t))X_j(t-\tau_{ij}(t)) + D_i v_i(t) \\ &\quad + D_a^i \gamma_a^i(t) \\ Y_i(t) &= C_i(X_i(t)) + n_i(t) + D_s^i \gamma_s^i(t) \end{aligned} \tag{3}$$

where $u_i(t) = [f_x^i(t), f_y^i(t), f_z^i(t), \tau_{\theta_1}^i(t), \tau_{\theta_2}^i(t), \tau_{\theta_3}^i(t)]^T$ represents control torque. $X_i(t) = [x_i, y_i, z_i, \dot{x}_i, \dot{y}_i, \dot{z}_i, \theta_1^i, \theta_2^i, \theta_3^i, \dot{\theta}_1^i, \dot{\theta}_2^i, \dot{\theta}_3^i]^T$ is the state vector of the position and attitude between the ith satellite and leader satellite in the formation team. $F_i(X_i(t)) = [\dot{x}_i, \dot{y}_i, \dot{z}_i, \dot{\omega}_{ECI,z_i} y_i + 2\omega_{ECI,x_i}\dot{y}_i + \omega_{ECI,z_i}(\omega_{ECI,z_i}x_i - \omega_{ECI,x_i}z_i), \omega_{ECI,x_i}^2 y_i + 2\omega_{ECI,x_i}\dot{z}_i + \dot{\omega}_{ECI,z_i}y_i - 2\omega_{ECI,z_i}\dot{x}_i - \dot{v}_{ECI,z_i}x_i + \dot{\omega}_{ECI,x_i}z_i - \dot{v}_{ECI,x_i}y_i - 2\omega_{ECI,x_i}\dot{y}_i - \omega_{ECI,x_i}(\omega_{ECI,z_i}x_i - \omega_{ECI,x_i}z_i), \dot{\theta}_1^i, \dot{\theta}_2^i, \dot{\theta}_3^i, F_{i,1}(t), F_{i,2}(t), F_{i,3}(t)]^T$ is the nonlinear dynamic matrix of the ith satellite. $G_i(X_i(t)) = [G_{i_1}^T, G_{i_2}^T, G_{i_3}^T, G_{i_4}^T]^T \in \mathbb{R}^{12\times 6}$ where $G_{i_1}^T = [0_{3\times 6}]$, $G_{i_2} = [\frac{1}{m_i}I_3, 0_{3\times 3}, diag(\frac{1}{J_1^i}, \frac{1}{\cos\theta_1^i J_2^i}, \frac{1}{\cos\theta_1^i \cos\theta_2^i J_3^i})]$, $G_{i_3}^T = [0_{3\times 6}]$, $G_{i_4} = [0_{3\times 3}, diag(\frac{1}{J_1^i}, \frac{1}{\cos\theta_1^i J_2^i}, \frac{1}{\cos\theta_1^i \cos\theta_2^i J_3^i})]$ are of the input matrix $G_i(X_i(t))$. $F_{ij}(X_i(t)) \in \mathbb{R}^{12\times 12}$ is the coupling matrix from the jth satellite to the i th satellite. $X_j(t-\tau_{ij}(t)) \in \mathbb{R}^{12}$ is the coupling caused by the influence of nearby wireless communication from the jth satellite to the ith satellite in the team. $\tau_{ij}(t)$ means time-varying delay. $D_i = [I_{12\times 12}]$ is the nonlinear system matrix of external disturbance torque. $v_i(t)$ represents the external disturbance with finite energy.$\gamma_a^i(t) \in \mathbb{R}$ and $\gamma_s^i(t) \in \mathbb{R}$ are the equivalent actuator malicious attack and sensor malicious attack on the ith satellite from wireless network communication, respectively. D_a^i is the actuator attack matrix; D_s^i is the sensor attack matrix. $Y_i(t)$ denotes the measurement output on the ith satellite. $n_i(t)$ is the noise of measurement output on the ith satellite.

In order to estimate attack signals $\gamma_a^i(t)$ and $\gamma_s^i(t)$ by the conventional Luenberger observer for the ATC design in the sequel, we proposed a novel dynamic smoothed model for malicious attack signal $\gamma_a^i(t)$ and $\gamma_s^i(t)$. To begin with, based on thederivative definition of $\dot{\gamma}_a^i(t) = \lim_{h\to 0}\frac{\gamma_a^i(t+h)-\gamma_a^i(t)}{h}$, the smoothed model of $\gamma_a^i(t)$ is given as follows [41]:

$$\begin{aligned} \dot{\gamma}_a^i(t) &= \frac{1}{h}(\gamma_a^i(t+h) - \gamma_a^i(t)) + \epsilon_{1,a}^i(t), \\ \dot{\gamma}_a^i(t-h) &= \frac{1}{h}(\gamma_a^i(t) - \gamma_a^i(t-h)) + \epsilon_{2,a}^i(t), \\ &\vdots \\ \dot{\gamma}_a^i(t-kh) &= \frac{1}{h}(\gamma_a^i(t-(k-1)h) - \gamma_a^i(t-kh)) + \epsilon_{k,a}^i(t) \end{aligned} \tag{4}$$

where $h > 0$ denotes small time interval, $k \in \mathbb{N}$ represents the attack signal estimation step, $\epsilon_{1,a}^i(t), \ldots, \epsilon_{k,a}^i(t)$ are approximation errors of the derivative at different smoothed time points for actuator attack signal $\gamma_a^i(t)$. By the extrapolation method, we could obtain the future attack signal $\gamma_a^i(t+h)$ as follows:

$$\gamma_a^i(t+h) = \sum_{j=0}^{k} a_j \gamma_a^i(t-jh) + \delta_a^i(t) \tag{5}$$

where $\{a_j\}_{j=0}^k$ are the extrapolation coefficients such as Lagrange extrapolation method [42] or other extrapolation methods of system attack signal $\gamma_a^i(t+h)$ and $\delta_a^i(t)$ is the extrapolation error of actuator attack signal $\gamma_a^i(t+h)$. Thereafter, we could obtain the following dynamic smoothed model of actuator attack signal $\gamma_a^i(t)$:

$$d\Gamma_a^i(t) = (A_a\Gamma_a^i(t) + \epsilon_a^i(t))dt \tag{6}$$

where $\Gamma_a^i(t) = [\gamma_a^{i^T}(t), \gamma_a^{i^T}(t-h), \ldots, \gamma_a^{i^T}(t-kh)]^T$, $\epsilon_a^i(t) = [(\epsilon_{1,a}^i(t) + \delta_a^i(t)/h)^T, \epsilon_{2,a}^{i^T}(t), \ldots, \epsilon_{k,a}^{i^T}(t)]^T$ represents the actuator attack signal approximation error vector, and

$$A_a = \begin{bmatrix} \frac{-1+a_0}{h}I & \frac{a_1}{h}I & \frac{a_2}{h}I & \ldots & \frac{a_k}{h}I \\ \frac{1}{h}I & -\frac{1}{h}I & 0 & \ldots & 0 \\ 0 & \frac{1}{h}I & -\frac{1}{h}I & \ldots & 0 \\ \vdots & & \vdots & \ddots & \vdots \\ 0 & \ldots & 0 & \frac{1}{h}I & -\frac{1}{h}I \end{bmatrix}$$

Again, by the extrapolation method, we could obtain the future sensor attack signal $\gamma_s^i(t+h)$ as follows:

$$\gamma_s^i(t+h) = \sum_{j=0}^{k} b_j \gamma_s^i(t-jh) + \delta_s^i(t) \tag{7}$$

$\{b_j\}_{j=0}^k$ are the extrapolation coefficients of sensor attack signal $\gamma_s^i(t+h)$ and $\delta_s^i(t)$ is the extrapolation error. The dynamic smoothed model of sensor attack signal $\gamma_s^i(t)$ can be constructed as [41]

$$d\Gamma_s^i(t) = (A_s\Gamma_s^i(t) + \epsilon_s^i(t))dt \tag{8}$$

where $\Gamma_s^i(t) = [\gamma_s^{i^T}(t), \gamma_s^{i^T}(t-h), \ldots, \gamma_s^{i^T}(t-kh)]^T$, $\epsilon_s^i(t) = [(\epsilon_{1,s}^i(t) + \delta_s^i(t)/h)^T, \epsilon_{2,s}^{i^T}(t), \ldots, \epsilon_{k,s}^{i^T}(t)]^T$ represents

the sensor attack signal approximation error vector, and

$$A_s = \begin{bmatrix} \frac{-1+b_0}{h}I & \frac{b_1}{h}I & \frac{b_2}{h}I & \dots & \frac{b_k}{h}I \\ \frac{1}{h}I & -\frac{1}{h}I & 0 & \dots & 0 \\ 0 & \frac{1}{h}I & -\frac{1}{h}I & \dots & 0 \\ \vdots & & \vdots & \ddots & \vdots \\ 0 & \dots & 0 & \frac{1}{h}I & -\frac{1}{h}I \end{bmatrix}$$

Remark 1: Since the prediction of future attack signal in (5) and (7) is based on the extrapolatory method, which is based on the smoothed method of past data, we therefore call the dynamic model in (6) and (8) the smoothed model. In smoothed dynamic models of actuator attack signal in (6) and sensor attack signal in (8), we can choose the desired number of extrapolation steps k. In general, when k is larger, the extrapolation performance is better, but it also leads to an increase in the matrix dimension of the dynamic model, i,e., the amount of calculation will become larger. Therefore, there is a trade-off between the computational complexity and the extrapolation performance of the attack signal modeling.

In order to estimate $X_i(t)$, $\gamma_a^i(t)$, and $\gamma_s^i(t)$ simultaneously for attack-tolerant observer-based team formation control in the sequel, we augment smoothed models of actuator attack signal in (6) and sensor attack signal in (8) with the ith satellite NCS as the following augmented stochastic system:

$$\begin{aligned} \dot{\bar{X}}_i(t) &= \bar{F}_i(\bar{X}_i(t)) + \bar{G}_i(\bar{X}_i(t))u_i(t) \\ &\quad + \sum_{j\in N_i} \bar{F}_{ij}(\bar{X}_i(t))\bar{X}_j(t-\tau_{ij}(t)) + \bar{D}_i(\bar{X}_i(t))\bar{v}_i(t) \\ Y_i(t) &= \bar{C}_i(\bar{X}_i(t)) + n_i(t) \end{aligned} \tag{9}$$

where

$$\bar{X}_i(t) = \left[\Gamma_a^{iT}(t)\ \ \Gamma_s^{iT}(t)\ X_i^T(t)\right]^T,$$

$$\bar{F}_i(\bar{X}_i(t)) = \begin{bmatrix} A_a\Gamma_a^i(t) \\ A_s\Gamma_s^i(t) \\ F_i(X_i(t)) + D_a^i S_a \Gamma_a^i(t) \end{bmatrix},$$

$$\bar{G}_i(\bar{X}_i(t)) = \begin{bmatrix} 0 \\ 0 \\ G_i(X_i(t)) \end{bmatrix},$$

$$\bar{D}_i(\overline{X}_i(t)) = \begin{bmatrix} I & 0 & 0 \\ 0 & I & 0 \\ 0 & 0 & D_i \end{bmatrix}, \quad \bar{v}_i(t) = \begin{bmatrix} \epsilon_a^i(t) \\ \epsilon_s^i(t) \\ v_i(t) \end{bmatrix},$$

$$S_a = [I, 0, \dots, 0], \quad S_s = [I, 0, \dots, 0],$$

$$\bar{C}_i(\bar{X}_i(t)) = C_i(X_i(t)) + D_s^i S_s \Gamma_s^i(t),$$

$$\bar{F}_{ij}(\bar{X}_i(t)) = \begin{bmatrix} I & 0 & 0 \\ 0 & I & 0 \\ 0 & 0 & F_{ij}(X_i(t)) \end{bmatrix},$$

$$\bar{X}_j(t-\tau_{ij}(t)) = \begin{bmatrix} 0 \\ 0 \\ X_j(t-\tau_{ij}(t)) \end{bmatrix}$$

The nonlinear observer-based controller is used to estimate the state of the ith satellite and the attack signals in the augmented stochastic system of the ith satellite NCS in (9). Before estimating the state $\bar{X}_i(t)$ of augmented system in (9), we need to guarantee the augmented state $\bar{X}_i(t)$ could be observable from $Y_i(t)$. In general, due to the nonlinearity of augmented system matrices $\bar{F}_i(\bar{X}_i(t)$ and $\bar{G}_i(\bar{X}_i(t))$, at present, the observability of augmented system in (9) can not be easily ensured by the conventional rank test condition. To address this issue, the following assumption is made.

2: The state $\bar{X}_i(t)$ of augmented system in (9) is observable from output measurement $Y_i(t)$ for each satellite in the formation team.

Then, the following nonlinear Luenberger observer-based control law for the augmented stochastic system of the ith satellite NCS in (9) is proposed as

$$\begin{aligned} \dot{\hat{\bar{X}}}_i(t) &= \bar{F}_i(\hat{\bar{X}}_i(t)) + \bar{G}_i(\hat{\bar{X}}_i(t))u_i(t) \\ &\quad + L_i(\hat{\bar{X}}_i(t))(Y_i(t) - \hat{Y}_i(t)) \\ \hat{Y}_i(t) &= \bar{C}_i(\hat{\bar{X}}_i(t)), u_i(t) = K_i(\hat{\bar{X}}_i(t)) \end{aligned} \tag{10}$$

where $\hat{\bar{X}}_i(t)$ is the estimated state of the ith satellite, $K_i(\hat{\bar{X}}_i(t))$ denotes the control gain and $L_i(\hat{\bar{X}}_i(t))$ is the observer gain of the ith satellite.

Remark 2: In (3), if we estimate the state $X_i(t)$ of the ith satellite from $Y_i(t)$, the state estimation will be corrupted by malicious attack signals $\gamma_a^i(t)$ and $\gamma_s^i(t)$ directly. After the actuator attack signals $\gamma_a^i(t)$ and sensor attack signals $\gamma_s^i(t)$ are embedded in the $\bar{X}_i(t)$ in the augmented stochastic system in (9), it not only enables the observer (10) to simultaneously estimate $X_i(t)$, $\gamma_a^i(t)$ and $\gamma_s^i(t)$ directly, but also avoid the corruption problem of attack signals on the augmented state estimation by the Luenberger observer in (10) can be avoided. Further, the estimation of the malicious attack signals in (10) will be employed to compensate their effect on the formation control of each satellite NCS by the H_∞ attack-tolerant observer-based formation tracking control strategy in the next section.

C. PROBLEM FORMULATION

In this article, the main task is to build a large-scale satellite formation NCS with robust H_∞ decentralized attack-tolerant observer-based network tracking control system under network malicious attack, delayed coupling and external disturbance in the outer space. The satellites formation NCS can change the shape attitude and attitude of the formation according to different applications. Fig. 3 presents the overall satellite team formation decentralized observer-based control framework via wireless communication network with malicious attack and delayed coupling effects from other satellites. First, we need to define the time-varying reference trajectory $r_i(t)$. $r_i(t)$ represents the reference state of the ith satellite in the team formation, i.e., $(r_1(t), \dots, r_i(t), \dots, r_N(t))^T$ denotes a desired time-varying team formation shape of N satellites, which is specified by the designer beforehand. Besides, in order to extend reference trajectory $r_i(t)$ to the augmented state $\bar{X}_i(t)$ containing the

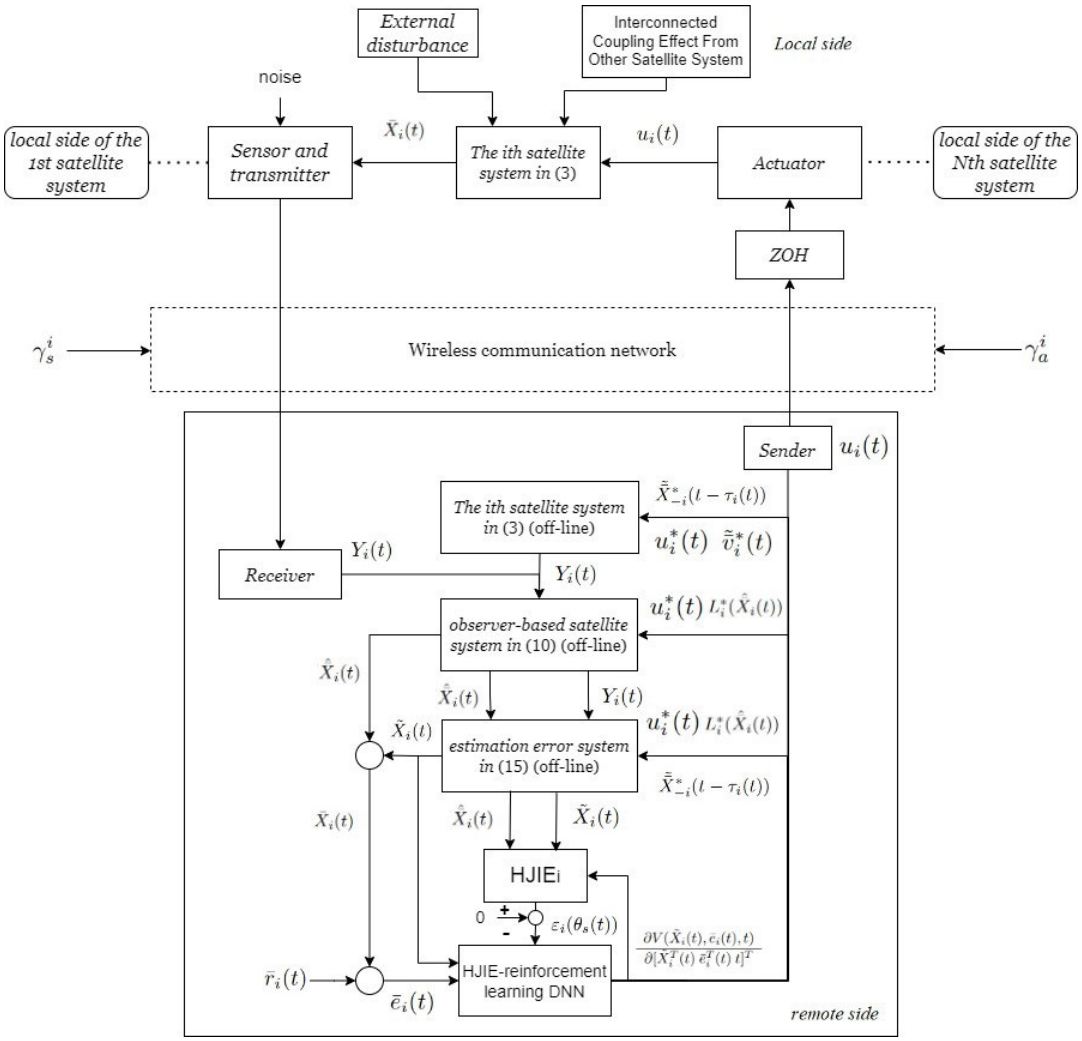

FIGURE 3. The team formation satellite control configuration in wireless communication network environment by HJIE-reinforced deep learning scheme at the remote side.

states of malicious attacks, we need to expand the reference trajectory $r_i(t)$ into $\bar{r}_i(t)$ for the ith satellite, where $\bar{r}_i(t) = [0, 0, r_i^T(t)]^T$. Therefore, the reference trajectory tracking error dynamic is indicated as follows:

$$\begin{aligned}\dot{\bar{e}}_i(t) &= \dot{\bar{X}}_i(t) - \dot{\bar{r}}_i(t)\\ &= \bar{F}_i(\bar{X}_i(t)) + \bar{G}_i(\bar{X}_i(t))u_i(t)\\ &\quad + \sum_{j\in N_i} \bar{F}_{ij}(\bar{X}_i(t))\bar{X}_j(t-\tau_{ij}(t))\\ &\quad + \bar{D}_i(\bar{X}_i(t))\bar{v}_i(t) - \dot{\bar{r}}_i(t)\\ &= \bar{F}_i(\bar{e}_i(t)+\bar{r}_i(t)) - \dot{\bar{r}}_i(t) + \bar{G}_i(\bar{e}_i(t)+\bar{r}_i(t))u_i(t)\\ &\quad + \sum_{j\in N_i} \bar{F}_{ij}(\bar{e}_i(t)+\bar{r}_i(t))\bar{X}_j(t-\tau_{ij}(t))\\ &\quad + \bar{D}_i(\bar{e}_i(t)+\bar{r}_i(t))\bar{v}_i(t) \qquad (11)\end{aligned}$$

Let us define

$$\begin{aligned}F_{e,i}(\bar{e}_i(t),t) &\triangleq \bar{F}_i(\bar{e}_i(t)+\bar{r}_i(t)) - \dot{\bar{r}}_i(t)\\ G_{e,i}(\bar{e}_i(t),t) &\triangleq \bar{G}_i(\bar{e}_i(t)+\bar{r}_i(t))\\ D_{e,i}(\bar{e}_i(t),t) &\triangleq \bar{D}_i(\bar{e}_i(t)+\bar{r}_i(t))\\ F_{e,ij}(\bar{e}_i(t),t) &\triangleq \bar{F}_{ij}(\bar{e}_i(t)+\bar{r}_i(t)) \qquad (12)\end{aligned}$$

After that, the formation tracking error time-varying dynamic equation of the ith satellite in the team formation can be further reformulated as

$$\begin{aligned}\dot{\bar{e}}_i(t) &= F_{e,i}(\bar{e}_i(t),t) + G_{e,i}(\bar{e}_i(t),t)u_i(t)\\ &\quad + D_{e,i}(\bar{e}_i(t),t)\bar{v}_i(t) + \sum_{j\in N_i} F_{e,ij}(\bar{e}_i(t),t)\bar{X}_j(t-\tau_{ij}(t))\end{aligned} \qquad (13)$$

In the previous subsection, we have also discussed malicious attack signals in the satellite team formation NCS and built an observer in (10) to estimate these false signals and system states of the ith satellite NCS. Our goal with this approach is to specify the observer gain $L_i(\hat{\bar{X}}_i(t))$ and corresponding controller $K_i(\hat{\bar{X}}_i(t))$ in (10) so that the formation tracking error $\bar{e}_i(t)$ and estimation error $\bar{X}_i(t) - \hat{\bar{X}}_i(t)$ for each satellite in the formation team will approach to zero.

At the same time, the effect of all possible disturbance $\bar{v}_i(t)$, measurement noise $n_i(t)$ and coupling effect $\bar{X}_j(t-\tau_{ij}(t))$ on the state estimation and formation tracking control as well as the control effort can be attenuated below a prescribed level ρ_i^2 by the following decentralized H_∞ attack-tolerant observer-based team formation tracking control strategy of large-scale satellites.

$$\min_{\substack{K_i(\hat{\bar{X}}_i(t),\ \bar{e}_i(t)) \\ L_i(\hat{\bar{X}}_i(t))}} \max_{\substack{\bar{v}_i(t) \\ n_i(t) \\ \sum_{j\in N_i}\bar{X}_j(t-\tau_{ij}(t))\in L_2[0,tf]}} \frac{\begin{array}{c} E\{\int_0^{t_f}(\bar{X}_i(t)-\hat{\bar{X}}_i(t))^T Q_{1,i}(\bar{X}_i(t)-\hat{\bar{X}}_i(t)) \\ +\bar{e}_i^T(t)Q_{2,i}\bar{e}_i(t)+u_i(t)^T R_i u_i(t)dt \\ -V(\bar{X}_i(0)-\hat{\bar{X}}_i(0),\bar{e}_i(0),0)\} \end{array}}{\begin{array}{c} E\{\int_0^{t_f}(\bar{v}_i^T(t)\bar{v}_i(t)+n_i^T(t)n_i(t) \\ +\sum_{j\in N_i}\bar{X}_j^T(t-\tau_{ij}(t))\bar{X}_j(t-\tau_{ij}(t)))dt\} \end{array}} \le \rho_i^2 \tag{14}$$

where t_f denotes the terminal time, $Q_{1,i}, Q_{2_i} \ge 0$ and $R_i = R_i^T > 0$ are the weighting matrices of state estimation, team formation tracking error and control input, respectively. In the decentralized H_∞ attack-tolerant observer-based formation control strategy of each satellite in (14), the worst-case effects of external disturbance, measurement noise and interconnected coupling effect on reference tracking error, state estimation error and control effort must be minimized and be attenuated below a prescribed level ρ_i^2 by specifying the minimum observer-based control $K_i(\bar{X}_i(t))$ and observer gain $L_i(\hat{\bar{X}}_i(t))$ in the Luenberger observer-based formation control law in (10). We also extract the effect of the initial conditions $\bar{X}_i(0)-\hat{\bar{X}}_i(0)$ and $e_i(0)$ in the H_∞ attack-tolerant observer-based formation tracking control strategy in (14). The term $V(\bar{X}_i(0)-\hat{\bar{X}}_i(0),\ e_i(0),0)$ presents the Lyapunov function(i.e., the energy) of the initial condition, which needs to be extracted in the H_∞ observer-based tracking control strategy. In addition, the designer can specify different weights $Q_{1,i}$, $Q_{2,i}$ and R_i and attenuation level ρ_i^2 according to the design purpose for different satellites in the formation. In this way, the corresponding team formation control requirements for each satellite NCS in the team formation can be achieved by the robust decentralized H_∞ attack-tolerant observer-based formation tracking strategy in (14).

Remark 3: The physical meaning of robust decentralized H_∞ attack-tolerant observer-based formation tracking strategy in (14) of each satellite in the team is that the worst-case effect of general external disturbance $\bar{v}_i(t)$, measurement noise $n_i(t)$ and interconnected coupling $\bar{X}_j(t-\tau_{ij}), j \in N_i$ of other satellites on the state estimation and formation tracking control must be minimized by the observer gain and control gain of each satellite in the team formation and below a prescribed attenuation level. Since the worst-case effects of $\bar{v}_i(t)$, $n_i(t)$ and coupling $\bar{X}_j(t-\tau_{ij})$, $j \in N_i$ are only dependent on the state $\bar{X}_i(t)$ of each satellite. Consequently, the decentralized robust attack-tolerant observer-based formation control design of satellite NCS can be achieved by the proposed H_∞ observer-based reference tracking control strategy in (14).

For design convenience, the state estimation error dynamic of $\tilde{X}_i(t) = \bar{X}_i(t) - \hat{\bar{X}}_i(t)$ from (9) and (10) can be formulated as follows:

$$\begin{aligned} \dot{\tilde{X}}_i(t) &= \tilde{F}_i(\tilde{X}_i(t)) + \tilde{G}_i(\tilde{X}_i(t))u_i(t) \\ &\quad -L_i(\bar{X}_i(t)-\hat{\bar{X}}_i(t))(\tilde{C}_i(\tilde{X}_i(t)) + n_i(t)) \\ &\quad +\sum_{j\in N_i}\bar{F}_{ij}(\hat{\bar{X}}_i(t)+\tilde{X}_i(t))\bar{X}_j(t-\tau_{ij}(t)) \\ &\quad +\bar{D}_i(\hat{\bar{X}}_i(t)+\tilde{X}_i(t))\bar{v}_i(t) \end{aligned} \tag{15}$$

where $\tilde{F}_i(\tilde{X}_i(t)) = \bar{F}_i(\bar{X}_i(t)) - \bar{F}_i(\hat{\bar{X}}_i(t))$, $\tilde{G}_i(\tilde{X}_i(t)) = \bar{G}_i(\bar{X}_i(t)) - \bar{G}_i(\hat{\bar{X}}_i(t))$ and $\tilde{C}_i(\tilde{X}_i(t)) = \bar{C}_i(\bar{X}(t)) - \bar{C}_i(\hat{\bar{X}}_i(t))$

Accordingly, we can reformulate the robust decentralized H_∞ attack-tolerant observer-based formation tracking control strategy in (15) as follows:

$$\min_{\substack{K_i(\hat{\bar{X}}_i(t),\ \bar{e}_i(t)) \\ L_i(\hat{\bar{X}}_i(t))}} \max_{\substack{\bar{v}_i(t) \\ n_i(t) \\ \sum_{j\in N_i}\bar{X}_j(t-\tau_{ij}(t))\in L_2[0,tf]}} \frac{\begin{array}{c} E\{\int_0^{t_f}\tilde{X}_i^T(t)Q_{1,i}\tilde{X}_i(t)+\bar{e}_i^T(t)Q_{2,i}\bar{e}_i(t) \\ +u_i(t)^T R_i u_i(t)dt - V(\tilde{X}_i(t),\ \bar{e}_i(0),0)\} \end{array}}{\begin{array}{c} E\{\int_0^{t_f}(\bar{v}_i^T(t)\bar{v}_i(t)+n_i^T(t)n_i(t) \\ +\sum_{j\in N_j}\bar{X}_j^T(t-\tau_{ij}(t))\bar{X}_j(t-\tau_{ij}(t)))dt\} \end{array}} \le \rho_i^2 \tag{16}$$

Moreover, we augment the reference tracking error $e_i(t)$ and state estimation error $\tilde{X}_i(t)$, then we can obtain the tracking augmented time-varying error system of satellite team formation NCS

$$\begin{aligned} \dot{\tilde{\bar{X}}}_i(t) &= \begin{bmatrix} \tilde{F}_i(\tilde{X}_i(t)) - L_i(\hat{\bar{X}}_i(t))\tilde{C}_i(\tilde{X}_i(t)) \\ F_{e,i}(\bar{e}_i(t),t) \end{bmatrix} \\ &\quad + \begin{bmatrix} \tilde{G}_i(\tilde{X}_i(t)) \\ G_{e,i}(\bar{e}_i(t),t) \end{bmatrix} u_i(t) \\ &\quad + \begin{bmatrix} \bar{D}_i(\bar{X}_i(t)) & -L_i(\hat{\bar{X}}_i(t)) \\ D_{e,i}(\bar{e}_i(t),t) & 0 \end{bmatrix} \tilde{\bar{v}}_i(t) \\ &\quad + \begin{bmatrix} \bar{F}_{-i}(\bar{X}_i(t)) \\ F_{e,-i}(\bar{e}_i(t),t) \end{bmatrix} \tilde{\bar{X}}_{-i}(t-\tau_{-i}(t)) \end{aligned} \tag{17}$$

where $\tilde{\bar{X}}(t) = \begin{bmatrix} \tilde{X}_i^T(t)\ \bar{e}_i^T(t) \end{bmatrix}^T$, $\bar{Q}_i = diag\{Q_{1,i}, Q_{2,i}\}$, $\tilde{\bar{v}}_i(t) = [\bar{v}_i^T(t)\ n_i^T(t)]^T$, $\bar{F}_{-i}(\bar{X}_i(t)) = \begin{bmatrix} \cdots \bar{F}_{ij}(\bar{X}_i(t)) \cdots \end{bmatrix}$, $F_{e,-i}(\bar{e}_i(t),t) = \begin{bmatrix} \cdots F_{e,ij}(\bar{e}_i(t),t) \cdots \end{bmatrix}$, $\tilde{\bar{X}}_{-i}(t-\tau_{-i}(t)) = \begin{bmatrix} \cdots \bar{X}_j^T(t-\tau_{ij}(t)) \cdots \end{bmatrix}^T$, $i \ne j$

Consequently, (16) can be further simplified as follows:

$$\frac{\min\limits_{\substack{K_i(\hat{\tilde{X}}_i(t),\ e_i(t))\\ L_i(\hat{\tilde{X}}_i(t))}}\ \max\limits_{\substack{\tilde{\bar{v}}_i(t\\ \tilde{\bar{X}}_{-i}(t-\tau_{-i}(t))\in L_2[0,tf]}} E\{\int_0^{tf}\tilde{\bar{X}}^T(t)\bar{Q}_i\tilde{\bar{X}}(t) +u_i(t)^T R_i u_i(t)dt - V(\tilde{\bar{X}}_i(0),0)\}}{E\{\int_0^{tf}(\tilde{\bar{v}}_i^T(t)\tilde{\bar{v}}_i(t)+\tilde{\bar{X}}_{-i}^T(t-\tau_{-i}(t))\tilde{\bar{X}}_{-i}(t-\tau_{-i}(t)))dt\}} \le \rho_i^2 \tag{18}$$

After the above rearrangement, the decentralized H_∞ attack-tolerant observer-based formation tracking control design problem of large-scale satellites in (14) can be converted into how to solve the minmax H_∞ stabilization design problem [43], [44] in (18) for the nonlinear augmented time-varying error system in (17), which greatly reduce the design complexity of the proposed control method of large-scale satellite team formation NCS.

In the nonlinear augmented error system of satellite team formation NCS in (17), it is challenging to directly solve the minmax H_∞ game problem of the fractional payoff function in (18) under the strategy that players $\tilde{\bar{v}}_i^T(t)$, $\tilde{\bar{X}}_{-i}(t-\tau_{ij})$, $j \neq i$ seek to maximize the payoff function while other players $K_i(\hat{\tilde{X}}_i(t),\ e_i(t))$ and $L_i(\hat{\tilde{X}}_i(t))$ seek to minimize the payoff function. In this case, we employ the indirect two-step method [43] in the following to solve minmax Nash game problem (18) [43], [44]. In the denominator of payoff function in (18), since the selections of players $\tilde{\bar{v}}_i(t)$ and $\tilde{\bar{X}}_{-i}(t-\tau_{ij})$ are independent on the selections of other players $K_i(\hat{\tilde{X}}_i(t),\ \bar{e}_i(t))$ and $L_i(\hat{\tilde{X}}_i(t))$, the minmax H_∞ game problem in (18) is equivalent to the following constrained Nash minmax quadratic game problem [43], [44]:

$$\begin{aligned}&\min_{\substack{K_i(\hat{\tilde{X}}_i(t),\ e_i(t))\\ L_i(\hat{\tilde{X}}_i(t))}}\ \max_{\substack{\tilde{\bar{v}}_i(t\\ \tilde{\bar{X}}_{-i}(t-\tau_{-i}(t))\in L_2[0,tf]}}\\ &E\{\int_0^{tf}(\tilde{\bar{X}}^T(t)\bar{Q}_i\tilde{\bar{X}}(t)+u_i(t)^T R_i u_i(t)\\ &-\rho_i^2(\tilde{\bar{v}}_i^T(t)\tilde{\bar{v}}_i(t)+\tilde{\bar{X}}_{-i}^T(t-\tau_{-i}(t))\tilde{\bar{X}}_{-i}(t-\tau_{-i}(t))))dt\}\\ &\le E\{V(\tilde{\bar{X}}_i(0),0)\},\\ &\quad for\ i=1,\ldots,N\end{aligned} \tag{19}$$

In (19), the above constrained minmax Nash quadratic game problem can be solved by two steps as follows: (i) At first step, the following minmax Nash quadratic game problem must be solved.

$$\begin{aligned}J_i = &\min_{\substack{K_i(\hat{\tilde{X}}_i(t),\ e_i(t))\\ L_i(\hat{\tilde{X}}_i(t))}}\ \max_{\substack{\tilde{\bar{v}}_i(t\\ \tilde{\bar{X}}_{-i}(t-\tau_{-i}(t))\in L_2[0,tf]}}\\ &\times E\{\int_0^{tf}(\tilde{\bar{X}}^T(t)\bar{Q}_i\tilde{\bar{X}}(t)+u_i(t)^T R_i u_i(t)-\rho_i^2(\tilde{\bar{v}}_i^T(t)\tilde{\bar{v}}_i(t)\\ &+\tilde{\bar{X}}_{-i}^T(t-\tau_{-i}(t))\tilde{\bar{X}}_{-i}(t-\tau_{-i}(t))))dt\},\\ &\quad for\ i=1,\ldots,N\end{aligned} \tag{20}$$

(ii) In the second step, $J_i \le E\{V(\tilde{\bar{X}}_i(0),0)\}$ must be guaranteed.

According to the above two-step method, the following theorem can solve the robust decentralized H_∞ attack-tolerant obsever-based formation tracking control strategy in (18).

Theorem 1: (a) The decentralized H_∞ attack-tolerant observer-based formation tracking control strategy for Luenberger observer-based control law in (10) of large-scale satellites NCS can be solved by the following H_∞ control gain $K_i^*(\hat{\tilde{X}}_i(t),\ e_i(t))$, observer gain $L_i^*(\hat{\tilde{X}}_i(t))$, as well as the worst-case external disturbance $\tilde{\bar{v}}_i^*(t)$ and interconnected coupling effect $\tilde{\bar{X}}_{-i}^*(t-\tau_{-i}(t))$:

$$\begin{aligned}u_i^*(t) &= K_i^*(\hat{\tilde{X}}_i(t),\bar{e}_i(t))\\ &= -\frac{1}{2}R_i^{-1}\begin{bmatrix}\tilde{G}_i(\tilde{X}_i(t))\\ G_{e,i}(\bar{e}_i(t),t)\end{bmatrix}^T\\ &\quad\times\left(\frac{\partial V(\tilde{X}_i(t),\bar{e}_i(t),t)}{\partial[\tilde{X}_i^T(t)\ \bar{e}_i^T(t)]^T}\right)\end{aligned} \tag{21}$$

$$L_i^*(\hat{\tilde{X}}_i(t)) = \frac{1}{2}\frac{\left(\frac{\partial V(\tilde{X}_i(t),\bar{e}_i(t),t)}{\partial\tilde{X}_i(t)}\right)}{\left\|\left(\frac{\partial V(\tilde{X}_i(t),\bar{e}_i(t),t)}{\partial\tilde{X}_i(t)}\right)\right\|^2}\tilde{C}_i^T(\tilde{X}_i(t)) \tag{22}$$

$$\begin{aligned}\tilde{\bar{v}}_i^*(t) &= \frac{1}{2\rho_i^2}\begin{bmatrix}\bar{D}_i(\bar{X}_i(t)) & -L_i(\hat{\tilde{X}}_i(t))\\ D_{e,i}(\bar{e}_i(t),t) & 0\end{bmatrix}^T\\ &\quad\times\left(\frac{\partial V(\tilde{X}_i(t),\bar{e}_i(t),t)}{\partial[\tilde{X}_i^T(t)\ \bar{e}_i^T(t)]^T}\right)\end{aligned} \tag{23}$$

$$\begin{aligned}\tilde{\bar{X}}_{-i}^*(t-\tau_i(t)) &= \frac{1}{2\rho_i^2}\begin{bmatrix}\bar{F}_{-i}(\bar{X}_i(t))\\ F_{e,-i}(\bar{e}_i(t),t)\end{bmatrix}^T\\ &\quad\times\left(\frac{\partial V(\tilde{X}_i(t),\bar{e}_i(t),t)}{\partial[\tilde{X}_i^T(t)\ \bar{e}_i^T(t)]^T}\right)\end{aligned} \tag{24}$$

where the Lyapunov function $V(\tilde{X}_i(t),\bar{e}_i(t),t) > 0$ with $V(0,0,t)=0$ is the solution of the following $HJIE_i$ for each satellite in the team.

$$\begin{aligned}HJIE_i = &\frac{\partial V(\tilde{X}_i(t),\bar{e}_i(t),t)}{\partial t}+\tilde{\bar{X}}_i^T(t)\bar{Q}_i\tilde{\bar{X}}_i(t)\\ &-\frac{1}{4}\left(\frac{\partial V(\tilde{X}_i(t),\bar{e}_i(t),t)}{\partial[\tilde{X}_i^T(t)\ \bar{e}_i^T(t)]^T}\right)^T\tilde{\bar{G}}_i(\tilde{X}_i(t),\bar{e}_i(t),t)\\ &\times R_i^{-1}\tilde{\bar{G}}_i^T(\tilde{X}_i(t),\bar{e}_i(t),t)\left(\frac{\partial V(\tilde{X}_i(t),\bar{e}_i(t),t)}{\partial[\tilde{X}_i^T(t)\ \bar{e}_i^T(t)]^T}\right)\\ &+\left(\frac{\partial V(\tilde{X}_i(t),\bar{e}_i(t),t)}{\partial[\tilde{X}_i^T(t)\ \bar{e}_i^T(t)]^T}\right)^T\tilde{\bar{F}}_i(\tilde{X}_i(t),\bar{e}_i(t),t)\\ &+\frac{1}{4\rho_i^2}\left(\frac{\partial V(\tilde{X}_i(t),\bar{e}_i(t),t)}{\partial[\tilde{X}_i^T(t)\bar{e}_i^T(t)]^T}\right)^T\tilde{\bar{D}}_i(\tilde{X}_i(t),\bar{e}_i(t),t)\end{aligned}$$

$$\times\left(\frac{\partial V(\tilde{X}_i(t),\bar{e}_i(t),t)}{\partial[\tilde{X}_i^T(t)\ \bar{e}_i^T(t)]^T}\right)$$
$$+\frac{1}{4\rho_i^2}\left(\frac{\partial V(\tilde{X}_i(t),\bar{e}_i(t),t)}{\partial[\tilde{X}_i^T(t)\bar{e}_i^T(t)]^T}\right)^T$$
$$\times\tilde{\bar{F}}_{-i}(\tilde{X}_i(t),\bar{e}_i(t),t)\left(\frac{\partial V(\tilde{X}_i(t),\bar{e}_i(t),t)}{\partial[\tilde{X}_i^T(t)\ \bar{e}_i^T(t)]^T}\right)$$
$$-\rho_i^2\tilde{C}_i^T(\tilde{X}_i(t))\tilde{C}_i(\tilde{X}_i(t))$$
$$=0 \tag{25}$$

where

$$\left(\frac{\partial V(\tilde{X}_i(t),\bar{e}_i(t),t)}{\partial[\tilde{X}_i^T(t)\ \bar{e}_i^T(t)]^T}\right)\triangleq\begin{bmatrix}\frac{\partial V(\tilde{X}_i(t),\bar{e}_i(t),t)}{\partial\tilde{X}_i(t)}\\ \frac{\partial V(\tilde{X}_i(t),\bar{e}_i(t),t)}{\partial\bar{e}_i(t)}\end{bmatrix}$$
$$\tilde{\bar{F}}_i(\tilde{X}_i(t),\bar{e}_i(t),t)=\begin{bmatrix}\tilde{F}_i(\tilde{X}_i(t))\\ F_{e,i}(\bar{e}_i(t),t)\end{bmatrix}$$
$$\tilde{\bar{G}}_i(\tilde{X}_i(t),\bar{e}_i(t),t)=\begin{bmatrix}\tilde{G}_i(\tilde{X}_i(t))\\ G_{e,i}(\bar{e}_i(t),t)\end{bmatrix}$$
$$\tilde{\bar{D}}_i(\tilde{X}_i(t),\bar{e}_i(t),t)=\begin{bmatrix}\bar{D}_i(\bar{X}_i(t))\bar{D}_i^T(\bar{X}_i(t)) & \bar{D}_i(\bar{X}_i(t))D_{e,i}^T(\bar{e}_i(t),t)\\ D_{e,i}(\bar{e}_i(t),t)\bar{D}_i^T(\bar{X}_i(t)) & D_{e,i}(\bar{e}_i(t),t)D_{e,i}^T(\bar{e}_i(t),t)\end{bmatrix}$$
$$\tilde{\bar{F}}_{-i}(\tilde{X}_i(t),\bar{e}_i(t),t)=\begin{bmatrix}\bar{F}_{-i}(\bar{X}_i(t))\bar{F}_{-i}^T(\bar{X}_i(t)) & \bar{F}_{-i}(\bar{X}_i(t))F_{e,-i}^T(\bar{e}_i(t),t)\\ F_{e,-i}(\bar{e}_i(t),t)\bar{F}_{-i}^T(\bar{X}_i(t)) & F_{e,-i}(\bar{e}_i(t),t)F_{e,-i}^T(\bar{e}_i(t),t)\end{bmatrix}$$

(b) If the nonlinear stochastic system of each satellite in (3) is with finite energy of external disturbance, attack signal estimation error $\bar{v}_i(t)$, measurement noise $n_i(t)$ and interconnected coupling effect $\tilde{\bar{X}}_{-i}(t-\tau_{-i}(t))$, i.e, $\bar{v}_i(t)$, $n_i(t)$, $\tilde{\bar{X}}_{-i}(t-\tau_{-i}(t))\in L_2[0,\infty]$, then the H_∞ observer-based control gain $K_i^*(\hat{\tilde{X}}_i(t),\ \bar{e}_i(t))$ and observer gain $L_i^*(\hat{\tilde{X}}_i(t))$ can achieve the asymptotical mean-square tracking and estimation ability,i.e., $E[\tilde{X}_i^T(t)\tilde{X}_i(0)]\to 0$ and $E[e_i^T(t)e_i(0)]\to 0$ as $t\to\infty$.

Proof: The proof is divided into part (a) and part (b) as follows:

(a) Based on the above indirect two-step method, we need to solve the minmax Nash quadratic game problem in (20) and then guarantee $J_i\le E\{V(\tilde{X}_i(0),\bar{e}_i(0),0)\}$.

From (20), we can get

$$J_i=\min_{\substack{K_i(\hat{\tilde{X}}_i(t),\ e_i(t))\\ L_i(\hat{\tilde{X}}_i(t))}}\ \max_{\substack{\tilde{\bar{v}}_i(t\\ \tilde{\bar{X}}_{-i}(t-\tau_{-i}(t))\in L_2[0,tf]}}$$
$$\times E\{\int_0^{tf}(\tilde{\bar{X}}^T(t)\bar{Q}_i\tilde{\bar{X}}(t)+u_i(t)^TR_iu_i(t)$$
$$-\rho_i^2(\tilde{\bar{v}}_i^T(t)\tilde{\bar{v}}_i(t)+\tilde{\bar{X}}_{-i}^T(t-\tau_{-i}(t))\tilde{\bar{X}}_{-i}(t-\tau_{-i}(t))))dt\}$$
$$=\min_{K_i(\hat{\tilde{X}}_i(t),\ \bar{e}_i(t)),L_i(\hat{\tilde{X}}_i(t))\tilde{\bar{v}}_i(t)\in L_2[0,tf],\tilde{\bar{X}}_{-i}(t-\tau_{-i}(t))\in L_2[0,tf]}\ \max$$
$$\times E\{-V(\tilde{X}_i(t_f),\bar{e}_i(t_f),t_f)+V(\tilde{X}_i(0),\bar{e}_i(0),0)$$
$$+\int_0^{tf}(\tilde{\bar{X}}^T(t)\bar{Q}_i\tilde{\bar{X}}(t)+u_i(t)^TR_iu_i(t)-\rho_i^2(\tilde{\bar{v}}_i^T(t)\tilde{\bar{v}}_i(t)$$
$$+\tilde{\bar{X}}_{-i}^T(t-\tau_{-i}(t))\tilde{\bar{X}}_{-i}(t-\tau_{-i}(t)))$$
$$+\frac{d}{dt}V(\tilde{X}_i(t),\bar{e}_i(t),t))dt\},$$
$$for\ i=1,\ldots,N \tag{26}$$

By chain rule from the augmented time-varying error system in (17), we have

$$\frac{dV(\tilde{X}_i(t),\bar{e}_i(t),t)}{dt}=\frac{\partial V(\tilde{X}_i(t),\bar{e}_i(t),t)}{\partial t}$$
$$+(\frac{\partial V(\tilde{X}_i(t),\bar{e}_i(t),t)}{\partial[\tilde{X}_i^T(t),\bar{e}_i^T(t)]^T})^T$$
$$\times(\begin{bmatrix}\tilde{F}_i(\tilde{X}_i(t))-L_i(\hat{\tilde{X}}_i(t))\tilde{C}_i(\tilde{X}_i(t))\\ F_{e,i}(\bar{e}_i(t),t)\end{bmatrix}$$
$$+\begin{bmatrix}\tilde{G}_i(\tilde{X}_i(t))\\ G_{e,i}(\bar{e}_i(t),t)\end{bmatrix}u_i(t)$$
$$+\begin{bmatrix}\bar{D}_i(\bar{X}_i(t)) & -L_i(\hat{\tilde{X}}_i(t))\\ D_{e,i}(\bar{e}_i(t),t) & 0\end{bmatrix}\tilde{\bar{v}}_i(t)$$
$$+\begin{bmatrix}\bar{F}_{-i}(\bar{X}_i(t))\\ F_{e,-i}(\bar{e}_i(t),t)\end{bmatrix}\tilde{\bar{X}}_{-i}(t-\tau_{-i}(t))),$$
$$for\ i=1,\ldots,N \tag{27}$$

Substituting (27) with $\tilde{\bar{G}}_i(\tilde{X}_i(t),\bar{e}_i(t),t)=\begin{bmatrix}\tilde{G}_i(\tilde{X}_i(t))\\ G_{e,i}(\bar{e}_i(t),t)\end{bmatrix}$ into (26), we have

$$J_i=\min_{\substack{K_i(\hat{\tilde{X}}_i(t),\ e_i(t))\\ L_i(\hat{\tilde{X}}_i(t))}}\ \max_{\substack{\tilde{\bar{v}}_i(t\\ \tilde{\bar{X}}_{-i}(t-\tau_{-i}(t))\in L_2[0,tf]}}$$
$$\times E\{-V(\tilde{X}_i(t_f),\bar{e}_i(t_f),t_f)+V(\tilde{X}_i(0),\bar{e}_i(0),0)$$
$$\times\int_0^{tf}(\frac{dV(\tilde{X}_i(t),\bar{e}_i(t),t)}{dt}+\tilde{\bar{X}}^T(t)\bar{Q}_i\tilde{\bar{X}}(t)$$
$$+u_i^T(t)R_iu_i(t)+(\frac{\partial V(\tilde{X}_i(t),\bar{e}_i(t),t)}{\partial[\tilde{X}_i^T(t),\bar{e}_i^T(t)]^T})^T$$
$$\times\begin{bmatrix}\tilde{F}_i(\tilde{X}_i(t))-L_i(\hat{\tilde{X}}_i(t))\tilde{C}_i(\tilde{X}_i(t))\\ F_{e,i}(\bar{e}_i(t),t)\end{bmatrix}$$
$$+(\frac{\partial V(\tilde{X}_i(t),\bar{e}_i(t),t)}{\partial[\tilde{X}_i^T(t),\bar{e}_i^T(t)]^T})^T\begin{bmatrix}\tilde{G}_i(\tilde{X}_i(t))\\ G_{e,i}(\bar{e}_i(t),t)\end{bmatrix}u_i(t)$$
$$+(\frac{\partial V(\tilde{X}_i(t),\bar{e}_i(t),t)}{\partial[\tilde{X}_i^T(t),\bar{e}_i^T(t)]^T})^T\begin{bmatrix}\bar{D}_i(\bar{X}_i(t)) & -L_i(\hat{\tilde{X}}_i(t))\\ D_{e,i}(\bar{e}_i(t),t) & 0\end{bmatrix}$$
$$\times\tilde{\bar{v}}_i(t)+(\frac{\partial V(\tilde{X}_i(t),\bar{e}_i(t),t)}{\partial[\tilde{X}_i^T(t),\bar{e}_i^T(t)]^T})^T\begin{bmatrix}\bar{F}_{-i}(\bar{X}_i(t))\\ F_{e,-i}(\bar{e}_i(t),t)\end{bmatrix}$$
$$\times\tilde{\bar{X}}_{-i}(t-\tau_{-i}(t)))-\rho_i^2(\tilde{\bar{v}}_i^T(t)\tilde{\bar{v}}_i(t)$$
$$+\tilde{\bar{X}}_{-i}^T(t-\tau_{-i}(t))\tilde{\bar{X}}_{-i}(t-\tau_{-i}(t))))dt\},$$
$$for\ i=1,\ldots,N \tag{28}$$

By the completing square method, we get

$$
\begin{aligned}
J_i = & \min_{\substack{K_i(\hat{\tilde{X}}_i(t),\ \bar{e}_i(t)) \\ L_i(\hat{\tilde{X}}_i(t))}} \max_{\substack{\tilde{\bar{v}}_i(t \\ \tilde{\bar{X}}_{-i}(t-\tau_{-i}(t)) \in L_2[0,tf]}} \\
& \times E\{-V(\tilde{X}_i(t_f), \bar{e}_i(t_f), t_f) + V(\tilde{X}_i(0), \bar{e}_i(0), 0) \\
& + \int_0^{t_f} \Big(\frac{dV(\tilde{X}_i(t), \bar{e}_i(t), t)}{dt} + \tilde{\bar{X}}^T(t) \bar{Q}_i \tilde{\bar{X}}(t) \\
& + u_i(t)^T R_i u_i(t) \\
& - \frac{1}{4} \Big(\frac{\partial V(\tilde{X}_i(t), \bar{e}_i(t), t)}{\partial [\tilde{X}_i^T(t), \bar{e}_i^T(t)]^T} \Big)^T \tilde{\bar{G}}_i(\tilde{X}_i(t), \bar{e}_i(t), t) R_i^{-1} \\
& \times \tilde{\bar{G}}_i^T(\tilde{X}_i(t), \bar{e}_i(t), t) \Big(\frac{\partial V(\tilde{X}_i(t), \bar{e}_i(t), t)}{\partial [\tilde{X}_i^T(t), \bar{e}_i^T(t)]^T} \Big) \\
& + \Big(\frac{1}{2} \tilde{\bar{G}}_i^T(\tilde{X}_i(t), \bar{e}_i(t), t) \Big(\frac{\partial V(\tilde{X}_i(t), \bar{e}_i(t), t)}{\partial [\tilde{X}_i^T(t), \bar{e}_i^T(t)]^T} \Big) \\
& + R_i u_i(t) \Big)^T R_i^{-1} \\
& \times \Big(\frac{1}{2} \tilde{\bar{G}}_i^T(\tilde{X}_i(t), \bar{e}_i(t), t) \Big(\frac{\partial V(\tilde{X}_i(t), \bar{e}_i(t), t)}{\partial [\tilde{X}_i^T(t), \bar{e}_i^T(t)]^T} \Big) + R_i u_i(t) \Big) \\
& + \Big(\frac{\partial V(\tilde{X}_i(t), \bar{e}_i(t), t)}{\partial [\tilde{X}_i^T(t), \bar{e}_i^T(t)]^T} \Big)^T \\
& \times \begin{bmatrix} \tilde{F}_i(\tilde{X}_i(t)) - L_i(\hat{\tilde{X}}_i(t)) \tilde{C}_i(\tilde{X}_i(t)) \\ F_{e,i}(\bar{e}_i(t), t) \end{bmatrix} \\
& + \frac{1}{4\rho_i^2} \Big(\frac{\partial V(\tilde{X}_i(t), \bar{e}_i(t), t)}{\partial [\tilde{X}_i^T(t), \bar{e}_i^T(t)]^T} \Big)^T \begin{bmatrix} \bar{D}_i(\bar{X}_i(t)) & -L_i(\hat{\tilde{X}}_i(t)) \\ D_{e,i}(\bar{e}_i(t), t) & 0 \end{bmatrix} \\
& \times \begin{bmatrix} \bar{D}_i(\bar{X}_i(t)) & -L_i(\hat{\tilde{X}}_i(t)) \\ D_{e,i}(\bar{e}_i(t), t) & 0 \end{bmatrix}^T \Big(\frac{\partial V(\tilde{X}_i(t), \bar{e}_i(t), t)}{\partial [\tilde{X}_i^T(t), \bar{e}_i^T(t)]^T} \Big) \\
& + \frac{1}{4\rho_i^2} \Big(\frac{\partial V(\tilde{X}_i(t), \bar{e}_i(t), t)}{\partial [\tilde{X}_i^T(t), \bar{e}_i^T(t)]^T} \Big)^T \begin{bmatrix} \bar{F}_{-i}(\bar{X}_i(t)) \\ F_{e,-i}(\bar{e}_i(t), t) \end{bmatrix} \\
& \times \begin{bmatrix} \bar{F}_{-i}(\bar{X}_i(t)) \\ F_{e,-i}(\bar{e}_i(t), t) \end{bmatrix}^T \Big(\frac{\partial V(\tilde{X}_i(t), \bar{e}_i(t), t)}{\partial [\tilde{X}_i^T(t), \bar{e}_i^T(t)]^T} \Big) \\
& - \Big(\frac{1}{2\rho_i^2} \begin{bmatrix} \bar{D}_i(\bar{X}_i(t)) & -L_i(\hat{\tilde{X}}_i(t)) \\ D_{e,i}(\bar{e}_i(t), t) & 0 \end{bmatrix}^T \\
& \times \Big(\frac{\partial V(\tilde{X}_i(t), \bar{e}_i(t), t)}{\partial [\tilde{X}_i^T(t), \bar{e}_i^T(t)]^T} \Big) - \rho_i \tilde{\bar{v}}_i(t) \Big)^T \\
& \times \Big(\frac{1}{2\rho_i^2} \begin{bmatrix} \bar{D}_i(\bar{X}_i(t)) & -L_i(\hat{\tilde{X}}_i(t)) \\ D_{e,i}(\bar{e}_i(t), t) & 0 \end{bmatrix}^T \Big(\frac{\partial V(\tilde{X}_i(t), \bar{e}_i(t), t)}{\partial [\tilde{X}_i^T(t), \bar{e}_i^T(t)]^T} \Big) \\
& - \rho_i \tilde{\bar{v}}_i(t) \Big) - \Big(\frac{1}{2\rho_i^2} \begin{bmatrix} \dots \bar{F}_{ij}(\bar{X}_i(t)) \dots \\ F_{e,-i}(\bar{e}_i(t), t) \end{bmatrix}^T \\
& \times \Big(\frac{\partial V(\tilde{X}_i(t), \bar{e}_i(t), t)}{\partial [\tilde{X}_i^T(t), \bar{e}_i^T(t)]^T} \Big) \\
& - \rho_i \tilde{\bar{X}}_{-i}(t - \tau_{-i}(t)))^T \Big(\frac{1}{2\rho_i^2} \begin{bmatrix} \dots \bar{F}_{ij}(\bar{X}_i(t)) \dots \\ F_{e,-i}(\bar{e}_i(t), t) \end{bmatrix}^T \\
& \times \Big(\frac{\partial V(\tilde{X}_i(t), \bar{e}_i(t), t)}{\partial [\tilde{X}_i^T(t), \bar{e}_i^T(t)]^T} \Big) - \rho_i \tilde{\bar{X}}_{-i}(t - \tau_{-i}(t))) dt\}, \\
& \quad for\ i = 1, \dots, N
\end{aligned} \tag{29}
$$

In (29), the optimal control input $u_i^*(t) = K_i(\hat{\tilde{X}}_i(t),\ \bar{e}_i(t))$ in (21) and the worst-case disturbance $\tilde{\bar{v}}_i^*(t)$ in (23) achieve Nash quadratic game $\min_{u_i(t)=K_i(\hat{\tilde{X}}_i(t),\ \bar{e}_i(t))} \max_{\tilde{\bar{v}}_i(t), \tilde{\bar{X}}_{-i}(t-\tau_{-i}(t))}$ by making the involved quadratic terms be zero. Then we can get

$$
\begin{aligned}
J_i = & \min_{L_i(\hat{\tilde{X}}_i(t))} E\{-V(\tilde{X}_i(t_f), \bar{e}_i(t_f), t_f) + V(\tilde{X}_i(0), \bar{e}_i(0), 0) \\
& + \int_0^{t_f} \Big(\frac{dV(\tilde{X}_i(t), \bar{e}_i(t), t)}{dt} + \tilde{\bar{X}}^T(t) \bar{Q}_i \tilde{\bar{X}}(t) \\
& - \frac{1}{4} \Big(\frac{\partial V(\tilde{X}_i(t), \bar{e}_i(t), t)}{\partial [\tilde{X}_i^T(t), \bar{e}_i^T(t)]^T} \Big)^T \tilde{\bar{G}}_i(\tilde{X}_i(t), \bar{e}_i(t), t) R_i^{-1} \\
& \times \tilde{\bar{G}}_i^T(\tilde{X}_i(t), \bar{e}_i(t), t) \Big(\frac{\partial V(\tilde{X}_i(t), \bar{e}_i(t), t)}{\partial [\tilde{X}_i^T(t), \bar{e}_i^T(t)]^T} \Big) \\
& + \Big(\frac{\partial V(\tilde{X}_i(t), \bar{e}_i(t), t)}{\partial [\tilde{X}_i^T(t), \bar{e}_i^T(t)]^T} \Big)^T \begin{bmatrix} \tilde{F}_i(\tilde{X}_i(t)) - L_i(\hat{\tilde{X}}_i(t)) \tilde{C}_i(\tilde{X}_i(t)) \\ F_{e,i}(\bar{e}_i(t), t) \end{bmatrix} \\
& + \frac{1}{4\rho_i^2} \Big(\frac{\partial V(\tilde{X}_i(t), \bar{e}_i(t), t)}{\partial [\tilde{X}_i^T(t), \bar{e}_i^T(t)]^T} \Big)^T \begin{bmatrix} \bar{D}_i(\bar{X}_i(t)) & -L_i(\hat{\tilde{X}}_i(t)) \\ & D_{e,i}(\bar{e}_i(t), t)\ 0 \end{bmatrix} \\
& \times \begin{bmatrix} \bar{D}_i(\bar{X}_i(t)) & -L_i(\hat{\tilde{X}}_i(t)) \\ D_{e,i}(\bar{e}_i(t), t) & 0 \end{bmatrix}^T \Big(\frac{\partial V(\tilde{X}_i(t), \bar{e}_i(t), t)}{\partial [\tilde{X}_i^T(t), \bar{e}_i^T(t)]^T} \Big) \\
& + \frac{1}{4\rho_i^2} \Big(\frac{\partial V(\tilde{X}_i(t), \bar{e}_i(t), t)}{\partial [\tilde{X}_i^T(t), \bar{e}_i^T(t)]^T} \Big)^T \begin{bmatrix} \bar{F}_{-i}(\bar{X}_i(t)) \\ F_{e,-i}(\bar{e}_i(t), t) \end{bmatrix} \\
& \times \begin{bmatrix} \bar{F}_{-i}(\bar{X}_i(t)) \\ F_{e,-i}(\bar{e}_i(t), t) \end{bmatrix}^T \Big(\frac{\partial V(\tilde{X}_i(t), \bar{e}_i(t), t)}{\partial [\tilde{X}_i^T(t), \bar{e}_i^T(t)]^T} \Big)) dt\}, \\
& \quad for\ i = 1, \dots, N
\end{aligned} \tag{30}
$$

By the fact

$$
\frac{\partial V(\tilde{X}_i(t), \bar{e}_i(t), t)}{\partial [\tilde{X}_i^T(t), \bar{e}_i^T(t)]^T} = \begin{bmatrix} \frac{\partial V(\tilde{X}_i(t), \bar{e}_i(t), t)}{\partial \tilde{X}_i(t)} \\ \frac{\partial V(\tilde{X}_i(t), \bar{e}_i(t), t)}{\partial \bar{e}_i(t)} \end{bmatrix} \quad for\ i = 1, \dots, N \tag{31}
$$

we have

$$
\begin{aligned}
& \Big(\frac{\partial V(\tilde{X}_i(t), \bar{e}_i(t), t)}{\partial [\tilde{X}_i^T(t), \bar{e}_i^T(t)]^T} \Big)^T \begin{bmatrix} \tilde{F}_i(\tilde{X}_i(t)) - L_i(\hat{\tilde{X}}_i(t)) \tilde{C}_i(\tilde{X}_i(t)) \\ F_{e,i}(\bar{e}_i(t), t) \end{bmatrix} \\
& = \Big(\frac{\partial V(\tilde{X}_i(t), \bar{e}_i(t), t)}{\partial \tilde{X}_i(t)} \Big)^T (\tilde{F}_i(\tilde{X}_i(t)) - L_i(\hat{\tilde{X}}_i(t)) \tilde{C}_i(\tilde{X}_i(t))) \\
& \quad + \Big(\frac{\partial V(\tilde{X}_i(t), \bar{e}_i(t), t)}{\partial \bar{e}_i(t)} \Big)^T F_{e,i}(\bar{e}_i(t), t), \\
& \quad for\ i = 1, \dots, N
\end{aligned} \tag{32}
$$

and

$$
\begin{aligned}
& \Big(\frac{\partial V(\tilde{X}_i(t), \bar{e}_i(t), t)}{\partial [\tilde{X}_i^T(t), \bar{e}_i^T(t)]^T} \Big)^T \begin{bmatrix} \bar{D}_i(\bar{X}_i(t)) & -L_i(\hat{\tilde{X}}_i(t)) \\ D_{e,i}(\bar{e}_i(t), t) & 0 \end{bmatrix} \\
& \quad \times \begin{bmatrix} \bar{D}_i(\bar{X}_i(t)) & -L_i(\hat{\tilde{X}}_i(t)) \\ D_{e,i}(\bar{e}_i(t), t) & 0 \end{bmatrix}^T \Big(\frac{\partial V(\tilde{X}_i(t), \bar{e}_i(t), t)}{\partial [\tilde{X}_i^T(t), \bar{e}_i^T(t)]^T} \Big)
\end{aligned}
$$

$$
\begin{aligned}
&= \left[\left(\tfrac{\partial V(\tilde{X}_i(t),\bar{e}_i(t),t)}{\partial \tilde{X}_i(t)}\right)^T \ \left(\tfrac{\partial V(\tilde{X}_i(t),\bar{e}_i(t),t)}{\partial \bar{e}_i(t)}\right)^T \right] \\
&\quad \times \begin{bmatrix} \bar{D}_i(\bar{X}_i(t))\bar{D}_i^T(\bar{X}_i(t)) + & \\ L_i(\hat{\tilde{X}}_i(t))L_i^T(\hat{\tilde{X}}_i(t)) & \bar{D}_i(\bar{X}_i(t))D_{e,i}^T(\bar{e}_i(t),t) \\ D_{e,i}(\bar{e}_i(t),t)\bar{D}_i^T(\bar{X}_i(t)) & D_{e,i}(\bar{e}_i(t),t)D_{e,i}^T(\bar{e}_i(t),t) \end{bmatrix} \\
&\quad \times \begin{bmatrix} \frac{\partial V(\tilde{X}_i(t),\bar{e}_i(t),t)}{\partial \tilde{X}_i(t)} \\ \frac{\partial V(\tilde{X}_i(t),\bar{e}_i(t),t)}{\partial \bar{e}_i(t)} \end{bmatrix} \\
&= \left(\frac{\partial V(\tilde{X}_i(t),\bar{e}_i(t),t)}{\partial \tilde{X}_i(t)}\right)^T (\bar{D}_i(\bar{X}_i(t))\bar{D}_i^T(\bar{X}_i(t)) \\
&\quad + L_i(\hat{\tilde{X}}_i(t))L_i^T(\hat{\tilde{X}}_i(t)))\left(\frac{\partial V(\tilde{X}_i(t),\bar{e}_i(t),t)}{\partial \bar{e}_i(t)}\right) \\
&\quad + \left(\frac{\partial V(\tilde{X}_i(t),\bar{e}_i(t),t)}{\partial \tilde{X}_i(t)}\right)^T \bar{D}_i(\bar{X}_i(t)) \\
&\quad \times D_{e,i}^T(\bar{e}_i(t),t)\left(\frac{\partial V(\tilde{X}_i(t),\bar{e}_i(t),t)}{\partial \bar{e}_i(t)}\right) \\
&\quad + \left(\frac{\partial V(\tilde{X}_i(t),\bar{e}_i(t),t)}{\partial \tilde{X}_i(t)}\right)^T D_{e,i}(\bar{e}_i(t),t) \\
&\quad \times \bar{D}_i^T(\bar{X}_i(t))\left(\frac{\partial V(\tilde{X}_i(t),\bar{e}_i(t),t)}{\partial \bar{e}_i(t)}\right) \\
&\quad + \left(\frac{\partial V(\tilde{X}_i(t),\bar{e}_i(t),t)}{\partial \tilde{X}_i(t)}\right)^T D_{e,i}(\bar{e}_i(t),t) \\
&\quad \times D_{e,i}^T(\bar{e}_i(t),t)\left(\frac{\partial V(\tilde{X}_i(t),\bar{e}_i(t),t)}{\partial \bar{e}_i(t)}\right) \\
&\qquad \textit{for } i = 1,\ldots,N
\end{aligned} \tag{33}
$$

$$
\begin{aligned}
&\left(\frac{\partial V(\tilde{X}_i(t),\bar{e}_i(t),t)}{\partial [\tilde{X}_i^T(t),\bar{e}_i^T(t)]^T}\right)^T \begin{bmatrix} \bar{F}_{-i}(\bar{X}_i(t)) \\ F_{e,-i}(\bar{e}_i(t),t) \end{bmatrix} \\
&\quad \times \begin{bmatrix} \bar{F}_{-i}(\bar{X}_i(t)) \\ F_{e,-i}(\bar{e}_i(t),t) \end{bmatrix}^T \left(\frac{\partial V(\tilde{X}_i(t),\bar{e}_i(t),t)}{\partial [\tilde{X}_i^T(t),\bar{e}_i^T(t)]^T}\right) \\
&= \left[\left(\tfrac{\partial V(\tilde{X}_i(t),\bar{e}_i(t),t)}{\partial \tilde{X}_i(t)}\right)^T \ \left(\tfrac{\partial V(\tilde{X}_i(t),\bar{e}_i(t),t)}{\partial \bar{e}_i(t)}\right)^T \right] \\
&\quad \times \begin{bmatrix} \bar{F}_{-i}(\bar{X}_i(t))\bar{F}_{-i}^T(\bar{X}_i(t)) & \bar{F}_{-i}(\bar{X}_i(t))F_{e,-i}^T(\bar{e}_i(t),t) \\ F_{e,-i}(\bar{e}_i(t),t)\bar{F}_{-i}^T(\bar{X}_i(t)) & F_{e,-i}(\bar{e}_i(t),t)F_{e,-i}^T(\bar{e}_i(t),t) \end{bmatrix} \\
&\quad \times \begin{bmatrix} \frac{\partial V(\tilde{X}_i(t),\bar{e}_i(t),t)}{\partial \tilde{X}_i(t)} \\ \frac{\partial V(\tilde{X}_i(t),\bar{e}_i(t),t)}{\partial \bar{e}_i(t)} \end{bmatrix} \\
&= \left(\frac{\partial V(\tilde{X}_i(t),\bar{e}_i(t),t)}{\partial \tilde{X}_i(t)}\right)^T \bar{F}_{-i}(\bar{X}_i(t)) \\
&\quad \times \bar{F}_{-i}^T(\bar{X}_i(t))\left(\frac{\partial V(\tilde{X}_i(t),\bar{e}_i(t),t)}{\partial \bar{e}_i(t)}\right) \\
&\quad + \left(\frac{\partial V(\tilde{X}_i(t),\bar{e}_i(t),t)}{\partial \tilde{X}_i(t)}\right)^T \bar{F}_{-i}(\bar{X}_i(t)) \\
&\quad \times F_{e,-i}^T(\bar{e}_i(t),t)\left(\frac{\partial V(\tilde{X}_i(t),\bar{e}_i(t),t)}{\partial \bar{e}_i(t)}\right) \\
&\quad + \left(\frac{\partial V(\tilde{X}_i(t),\bar{e}_i(t),t)}{\partial \tilde{X}_i(t)}\right)^T F_{e,-i}(\bar{e}_i(t),t) \\
&\quad \times \bar{F}_{-i}^T(\bar{X}_i(t))\left(\frac{\partial V(\tilde{X}_i(t),\bar{e}_i(t),t)}{\partial \bar{e}_i(t)}\right) \\
&\quad + \left(\frac{\partial V(\tilde{X}_i(t),\bar{e}_i(t),t)}{\partial \tilde{X}_i(t)}\right)^T F_{e,-i}(\bar{e}_i(t),t) \\
&\quad \times F_{e,-i}^T(\bar{e}_i(t),t)\left(\frac{\partial V(\tilde{X}_i(t),\bar{e}_i(t),t)}{\partial \bar{e}_i(t)}\right) \\
&\qquad \textit{for } i = 1,\ldots,N
\end{aligned} \tag{34}
$$

Substituting (31), (32),(33) and (34) into (30), we get

$$
\begin{aligned}
J_i = \min_{L_i(\hat{\tilde{X}}_i(t))} & E\{-V(\tilde{X}_i(t_f),\bar{e}_i(t_f),t_f) + V(\tilde{X}_i(0),\bar{e}_i(0),0) \\
&+ \int_0^{t_f} \Big(\frac{dV(\tilde{X}_i(t),\bar{e}_i(t),t)}{dt} + \tilde{\tilde{X}}^T(t)\bar{Q}_i\tilde{\tilde{X}}(t) \\
&- \frac{1}{4}\left(\frac{\partial V(\tilde{X}_i(t),\bar{e}_i(t),t)}{\partial [\tilde{X}_i^T(t),\bar{e}_i^T(t)]^T}\right)^T \tilde{\bar{G}}_i(\tilde{X}_i(t),\bar{e}_i(t),t)R_i^{-1} \\
&\times \tilde{\bar{G}}_i^T(\tilde{X}_i(t),\bar{e}_i(t),t)\left(\frac{\partial V(\tilde{X}_i(t),\bar{e}_i(t),t)}{\partial [\tilde{X}_i^T(t),\bar{e}_i^T(t)]^T}\right) \\
&+ \left(\frac{\partial V(\tilde{X}_i(t),\bar{e}_i(t),t)}{\partial \tilde{X}_i(t)}\right)^T (\tilde{F}_i(\tilde{X}_i(t)) - L_i(\hat{\tilde{X}}_i(t))\tilde{C}_i(\tilde{X}_i(t))) \\
&+ \left(\frac{\partial V(\tilde{X}_i(t),\bar{e}_i(t),t)}{\partial \bar{e}_i(t)}\right)^T F_{e,i}(\bar{e}_i(t),t) \\
&+ \frac{1}{4\rho_i^2}\left(\frac{\partial V(\tilde{X}_i(t),\bar{e}_i(t),t)}{\partial \tilde{X}_i(t)}\right)^T (\bar{D}_i(\bar{X}_i(t))\bar{D}_i^T(\bar{X}_i(t)) \\
&+ L_i(\hat{\tilde{X}}_i(t))L_i^T(\hat{\tilde{X}}_i(t)))\left(\frac{\partial V(\tilde{X}_i(t),\bar{e}_i(t),t)}{\partial \tilde{X}_i(t)}\right) \\
&+ \frac{1}{4\rho_i^2}\left(\frac{\partial V(\tilde{X}_i(t),\bar{e}_i(t),t)}{\partial \tilde{X}_i(t)}\right)^T \bar{D}_i(\bar{X}_i(t)) \\
&\times D_{e,i}^T(\bar{e}_i(t),t)\left(\frac{\partial V(\tilde{X}_i(t),\bar{e}_i(t),t)}{\partial \bar{e}_i(t)}\right) \\
&+ \frac{1}{4\rho_i^2}\left(\frac{\partial V(\tilde{X}_i(t),\bar{e}_i(t),t)}{\partial \bar{e}_i(t)}\right)^T D_{e,i}(\bar{e}_i(t),t) \\
&\times \bar{D}_i^T(\bar{X}_i(t))\left(\frac{\partial V(\tilde{X}_i(t),\bar{e}_i(t),t)}{\partial \tilde{X}_i(t)}\right) \\
&+ \frac{1}{4\rho_i^2}\left(\frac{\partial V(\tilde{X}_i(t),\bar{e}_i(t),t)}{\partial \bar{e}_i(t)}\right)^T D_{e,i}(\bar{e}_i(t),t) \\
&\times D_{e,i}^T(\bar{e}_i(t),t)\left(\frac{\partial V(\tilde{X}_i(t),\bar{e}_i(t),t)}{\partial \bar{e}_i(t)}\right) \\
&+ \frac{1}{4\rho_i^2}\left(\frac{\partial V(\tilde{X}_i(t),\bar{e}_i(t),t)}{\partial \tilde{X}_i(t)}\right)^T \bar{F}_{-i}(\bar{X}_i(t)) \\
&\times \bar{F}_{-i}^T(\bar{X}_i(t))\left(\frac{\partial V(\tilde{X}_i(t),\bar{e}_i(t),t)}{\partial \tilde{X}_i(t)}\right) \\
&+ \frac{1}{4\rho_i^2}\left(\frac{\partial V(\tilde{X}_i(t),\bar{e}_i(t),t)}{\partial \tilde{X}_i(t)}\right)^T \bar{F}_{-i}(\bar{X}_i(t)) \\
&\times F_{e,-i}^T(\bar{e}_i(t),t)\left(\frac{\partial V(\tilde{X}_i(t),\bar{e}_i(t),t)}{\partial \bar{e}_i(t)}\right) \\
&+ \frac{1}{4\rho_i^2}\left(\frac{\partial V(\tilde{X}_i(t),\bar{e}_i(t),t)}{\partial \bar{e}_i(t)}\right)^T F_{e,-i}(\bar{e}_i(t),t)
\end{aligned}
$$

$$\times \bar{F}_{-i}^T(\bar{X}_i(t))(\frac{\partial V(\tilde{X}_i(t),\bar{e}_i(t),t)}{\partial \tilde{X}_i(t)})$$
$$+\frac{1}{4\rho_i^2}(\frac{\partial V(\tilde{X}_i(t),\bar{e}_i(t),t)}{\partial \bar{e}_i(t)})^T F_{e,-i}(\bar{e}_i(t),t)$$
$$\times F_{e,-i}^T(\bar{e}_i(t),t)(\frac{\partial V(\tilde{X}_i(t),\bar{e}_i(t),t)}{\partial \bar{e}_i(t)}))dt\},$$
$$for\ i=1,\ldots,N$$
$$= \min_{L_i(\hat{\tilde{X}}_i(t))} E\{-V(\tilde{X}_i(t_f),\bar{e}_i(t_f),t_f)+V(\tilde{X}_i(0),\bar{e}_i(0),0)$$
$$+\int_0^{t_f}(\frac{dV(\tilde{X}_i(t),\bar{e}_i(t),t)}{dt}+\tilde{\bar{X}}^T(t)\bar{Q}_i\tilde{\bar{X}}(t)$$
$$-\frac{1}{4}(\frac{\partial V(\tilde{X}_i(t),\bar{e}_i(t),t)}{\partial[\tilde{X}_i^T(t),\bar{e}_i^T(t)]^T})^T\tilde{\bar{G}}_i(\tilde{X}_i(t),\bar{e}_i(t),t)R_i^{-1}$$
$$\times\tilde{\bar{G}}_i^T(\tilde{X}_i(t),\bar{e}_i(t),t)(\frac{\partial V(\tilde{X}_i(t),\bar{e}_i(t),t)}{\partial[\tilde{X}_i^T(t),\bar{e}_i^T(t)]^T})$$
$$+(\frac{\partial V(\tilde{X}_i(t),\bar{e}_i(t),t)}{\partial \tilde{X}_i(t)})^T\tilde{F}_i(\tilde{X}_i(t))$$
$$+(\frac{\partial V(\tilde{X}_i(t),\bar{e}_i(t),t)}{\partial \bar{e}_i(t)})^T F_{e,i}(\bar{e}_i(t),t)$$
$$+\frac{1}{4\rho_i^2}(\frac{\partial V(\tilde{X}_i(t),\bar{e}_i(t),t)}{\partial \tilde{X}_i(t)})^T\bar{D}_i(\bar{X}_i(t))$$
$$\times\bar{D}_i^T(\bar{X}_i(t))(\frac{\partial V(\tilde{X}_i(t),\bar{e}_i(t),t)}{\partial \tilde{X}_i(t)})$$
$$+\frac{1}{4\rho_i^2}(\frac{\partial V(\tilde{X}_i(t),\bar{e}_i(t),t)}{\partial \tilde{X}_i(t)})^T\bar{D}_i(\bar{X}_i(t))$$
$$\times D_{e,i}^T(\bar{e}_i(t),t)(\frac{\partial V(\tilde{X}_i(t),\bar{e}_i(t),t)}{\partial \bar{e}_i(t)})$$
$$+\frac{1}{4\rho_i^2}(\frac{\partial V(\tilde{X}_i(t),\bar{e}_i(t),t)}{\partial \bar{e}_i(t)})^T D_{e,i}(\bar{e}_i(t),t)$$
$$\times\bar{D}_i^T(\bar{X}_i(t))(\frac{\partial V(\tilde{X}_i(t),\bar{e}_i(t),t)}{\partial \tilde{X}_i(t)})$$
$$+\frac{1}{4\rho_i^2}(\frac{\partial V(\tilde{X}_i(t),\bar{e}_i(t),t)}{\partial \bar{e}_i(t)})^T D_{e,i}(\bar{e}_i(t),t)$$
$$\times D_{e,i}^T(\bar{e}_i(t),t)(\frac{\partial V(\tilde{X}_i(t),\bar{e}_i(t),t)}{\partial \bar{e}_i(t)})$$
$$+\frac{1}{4\rho_i^2}(\frac{\partial V(\tilde{X}_i(t),\bar{e}_i(t),t)}{\partial \tilde{X}_i(t)})^T\bar{F}_{-i}(\bar{X}_i(t))$$
$$\times\bar{F}_{-i}^T(\bar{X}_i(t))\frac{\partial V(\tilde{X}_i(t),\bar{e}_i(t),t)}{\partial \tilde{X}_i(t)})$$
$$+\frac{1}{4\rho_i^2}(\frac{\partial V(\tilde{X}_i(t),\bar{e}_i(t),t)}{\partial \tilde{X}_i(t)})^T\bar{F}_{-i}(\bar{X}_i(t))$$
$$\times F_{e,-i}^T(\bar{e}_i(t),t)(\frac{\partial V(\tilde{X}_i(t),\bar{e}_i(t),t)}{\partial \bar{e}_i(t)})$$
$$+\frac{1}{4\rho_i^2}(\frac{\partial V(\tilde{X}_i(t),\bar{e}_i(t),t)}{\partial \bar{e}_i(t)})^T F_{e,-i}(\bar{e}_i(t),t)$$
$$\times\bar{F}_{-i}^T(\bar{X}_i(t))(\frac{\partial V(\tilde{X}_i(t),\bar{e}_i(t),t)}{\partial \tilde{X}_i(t)})$$
$$+\frac{1}{4\rho_i^2}(\frac{\partial V(\tilde{X}_i(t),\bar{e}_i(t),t)}{\partial \bar{e}_i(t)})^T F_{e,-i}(\bar{e}_i(t),t)$$
$$\times F_{e,-i}^T(\bar{e}_i(t),t)(\frac{\partial V(\tilde{X}_i(t),\bar{e}_i(t),t)}{\partial \bar{e}_i(t)})$$
$$+\frac{1}{4\rho_i^2}(L_i^T(\hat{\tilde{X}}_i(t))(\frac{\partial V(\tilde{X}_i(t),\bar{e}_i(t),t)}{\partial \tilde{X}_i(t)})-2\rho_i^2\tilde{C}_i(\tilde{X}_i(t)))^T$$
$$\times(L_i^T(\hat{\tilde{X}}_i(t))(\frac{\partial V(\tilde{X}_i(t),\bar{e}_i(t),t)}{\partial \tilde{X}_i(t)})-2\rho_i^2\tilde{C}_i(\tilde{X}_i(t)))$$
$$-\rho_i^2\tilde{C}_i^T(\tilde{X}_i(t))\tilde{C}_i(\tilde{X}_i(t))dt\} \quad (35)$$

From $HJIE_i$ in (25), we get

$$J_i = \min_{L_i(\hat{\tilde{X}}_i(t))} E\{-V(\tilde{X}_i(t_f),\bar{e}_i(t_f),t_f)+V(\tilde{X}_i(0),\bar{e}_i(0),0)$$
$$+\frac{1}{4\rho_i^2}(L_i^T(\hat{\tilde{X}}_i(t))(\frac{\partial V(\tilde{X}_i(t),\bar{e}_i(t),t)}{\partial \tilde{X}_i(t)})-\frac{1}{2}\tilde{C}_i(\tilde{X}_i(t)))^T$$
$$\times(L_i^T(\hat{\tilde{X}}_i(t))(\frac{\partial V(\tilde{X}_i(t),\bar{e}_i(t),t)}{\partial \tilde{X}_i(t)})-\frac{1}{2}\tilde{C}_i(\tilde{X}_i(t)))dt\} \quad (36)$$

Then we get the optimal observer gain $L_i^*(t)$ in (22). Finally (36) becomes

$$J_i = E\{-V(\tilde{X}_i(t_f),\bar{e}_i(t_f),t_f)+V(\tilde{X}_i(0),\bar{e}_i(0),0)\}$$
$$\le E\{V(\tilde{X}_i(0),\bar{e}_i(0),0)\} \quad (37)$$

Therefore the proof in the second step is finished.

(b) If $\tilde{\bar{v}}_i(t)\in\mathcal{L}_2^F[0,\infty]$ and $\tilde{\bar{X}}_{-i}(t-\tau_i(t))\in\mathcal{L}_2^F[0,\infty]$, from the definition of J_i in (20), then (37) becomes

$$\min_{\substack{K_i(\hat{\tilde{X}}_i(t),\ \bar{e}_i(t))\\ L_i(\hat{\tilde{X}}_i(t))}} E\{\int_0^{t_f}\tilde{\bar{X}}^T(t)\bar{Q}_i\tilde{\bar{X}}(t)$$
$$+u_i(t)^T R_i u_i(t)dt\} \le E\{V(\tilde{X}_i(0),\bar{e}_i(0),0)$$
$$+\rho_i^2\int_0^{t_f}\tilde{\bar{v}}_i^T(t)\tilde{\bar{v}}_i(t)+\tilde{\bar{X}}_{-i}^T(t-\tau_{-i}(t))\tilde{\bar{X}}_{-i}(t-\tau_{-i}(t))dt\},$$
$$for\ i=1,\ldots,N \quad (38)$$

i.e., in the case external disturbance $\bar{v}_i(t)\in\mathcal{L}_2^F[0,\infty]$, measurement noise $n_i(t)\in\mathcal{L}_2^F[0,\infty]$ and coupling effect $\tilde{\bar{X}}_{-i}(t-\tau_{-i}(t))\in\mathcal{L}_2^F[0,\infty]$, the proposed robust decentralized H_∞ attack-tolerant observer-based output feedback formation tracking control is reduced to the optimal H_2 quadratic observer-based output feedback formation tracking problem. Since $\rho_i^2E\{\int_0^{t_f}\tilde{\bar{v}}_i^T(t)\tilde{\bar{v}}_i(t)+\tilde{\bar{X}}_{-i}^T(t-\tau_{-i}(t))\tilde{\bar{X}}_{-i}(t-\tau_{-i}(t))dt\}$ are finite, from (38), it is seen that $E[\tilde{X}_i^T(t)\tilde{X}_i(t)]\to 0$ and $E[\bar{e}_i^T\bar{e}_i(t)]\to 0$ as $t_f\to\infty$, i.e., the proposed robust decentralized H_∞ attack-tolerant observer-based output feedback formation tracking control will achieve the mean-square asymptotical estimation and team formation tracking ability for each satellite NCS in the large-scale satellite if external

disturbance $\bar{v}_i(t)$, measurement noise $n_i(t)$ and coupling effect $\tilde{\bar{X}}_{-i}(t-\tau_{-i}(t))$ in each satellite NCS in (17) are all of finite energy. The proof is completed. ■

Remark 4: For the conventional decentralized H_∞ attack-tolerant observer-based formation tracking control design problem of large scale satellites conventionally, we need to solve one HJIE for the H_∞ controller and another HJIE for the H_∞ observer. That is, it is necessary to solve two-coupled HJIEs. If state estimation error dynamic in (15) and reference tracking error dynamic in (13) are combined as the augmented nonlinear error stochastic system in (17), then the decentralized H_∞ attack-tolerant observer-based formation tracking control strategy in (14) can be employed for NCS of large-scale satellites, and we only need to solve a decoupled $HJIE_i$ in (25) for each satellite. Consequently, the decentralized H_∞ attack-tolerant observer-based formation reference tracking scheme design procedure of large-scale satellites NCS can be simplified by considering both reference tracking error and state estimation error simultaneously.

III. HJIE-REINFORCEMENT DNN-BASED H_∞ ATTACK-TOLERANT OBSERVER-BASED DECENTRALIZED FORMATION TRACKING CONTROL DESIGN OF TEAM FORMATION NCS OF LARGE-SCALE LEO SATELLITES

From Theorem 1, in order to complete the decentralized H_∞ attack-tolerant observer-based formation tracking control design for each satellite of large-scale satellites NCS, we need to solve the $\frac{\partial V(\tilde{X}_i(t),\bar{e}_i(t),t)}{\partial[\tilde{X}_i^T(t)\ \bar{e}_i^T(t)]^T}$ and $\frac{\partial V(\tilde{X}_i(t),\bar{e}_i(t),t)}{\partial t}$ for each satellite from the time-varying partial differential $HJIE_i$ to obtain the optimal control gain $K_i^*(\hat{\tilde{X}}_i(t),\bar{e}_i(t))$ in (21), the optimal observer gain $L_i^*(\hat{\tilde{X}}_i(t))$ in (22), and the worst-case external disturbance $\bar{v}_i^*(t)$ in (44), measurement noise $n_i^*(t)$, interconnected coupling effect $\tilde{\bar{X}}_{-i}^*(t-\tau_{-i}(t))$ in (24).

Remark 5: In the decentralized H_∞ fuzzy team formation state feedback control of large-scale satellites in [29], T-S fuzzy control method is used to interpolate L local linearized stochastic systems to approach the each nonlinear satellite system. Therefore the $HJIE_i$ can be interpolated by L Riccati-like equations, which can be transformed to L linear matrix inequalities(LMIs). However, in the decentralized H_∞ fuzzy observer-based team formation tracking control strategy in (14), fuzzy observer-based team formation controller needs to solve L^2 control-observer-coupled LMIs, then a very complicated two-step method is needed to solve fuzzy control gains and observer gains. Further, at every time instant, we need to compute a very complicated fuzzy observer-based controller $\hat{\tilde{X}}_i(t) = \sum_{i=1}^L \sum_{j=1}^L \phi_i(X_i(t))\phi_j(X_i(t))(F_i\hat{\tilde{X}}_i(t) + G_iu_i(t)+L_i(Y_i(t)-\hat{Y}_i(t)))$, $u_i(t)=\sum_{i=1}^L \phi_i(X_i(t))\hat{\tilde{X}}_i(t)$ where $\phi_i(X_i(t)), i = 1,\ldots L$ are the fuzzy interpolation function, for each satellite at every time instant, which is a very time-consuming loading.

In this study, in order to solve a decoupled HJIE in (25) for the decentralized H_∞ attack-tolerant observer-based formation control strategy of each satellite in Theorem 1 more efficiently, an HJIE-reinforcement learning-based DNN method is employed to approach the theoretical solution $\frac{\partial V(\tilde{X}_i(t),\bar{e}_i(t),t)}{\partial[\tilde{X}_i^T(t)\ \bar{e}_i^T(t)]^T}$ and $\frac{\partial V(\tilde{X}_i(t),\bar{e}_i(t),t)}{\partial t}$ of $HJIE_i$ in (25) directly. The reason is that if we solve Lyapunov function $V(\tilde{X}_i(t),\bar{e}_i(t),t)$ in (25) directly by the conventional method [29], it is very difficult to calculate $\frac{\partial V(\tilde{X}_i(t),\bar{e}_i(t),t)}{\partial[\tilde{X}_i^T(t)\ \bar{e}_i^T(t)]^T}$ and $\frac{\partial V(\tilde{X}_i(t),\bar{e}_i(t),t)}{\partial t}$ for $K_i^*(\hat{\tilde{X}}_i(t),\bar{e}_i(t))$, $L_i^*(\hat{\tilde{X}}_i(t))$, $\tilde{\bar{v}}_i^*(t)$ and $\tilde{\bar{X}}_{-i}^*(t-\tau_{-i}(t))$ in (21)-(24) in the real-time decentralized H_∞ attack-tolerant observer-based formation tracking control process.

To make design easier, we denote

$$\left(\frac{\partial V(\tilde{X}_i(t),\bar{e}_i(t),t)}{\partial[\tilde{X}_i^T(t)\ \bar{e}_i^T(t)\ t]^T}\right) \triangleq \begin{bmatrix} \frac{\partial V(\tilde{X}_i(t),\bar{e}_i(t),t)}{\partial \tilde{X}_i(t)} \\ \frac{\partial V(\tilde{X}_i(t),\bar{e}_i(t),t)}{\partial \bar{e}_i(t)} \\ \frac{\partial V(\tilde{X}_i(t),\bar{e}_i(t),t)}{\partial t} \end{bmatrix} \tag{39}$$

According to the (39), (25) can be reformulated as

$$\begin{aligned} HJIE_i = {} & \tilde{\bar{X}}_i^T(t)\bar{Q}_i\tilde{\bar{X}}_i(t) - \frac{1}{4}\left(\frac{\partial V(\tilde{X}_i(t),\bar{e}_i(t),t)}{\partial[\tilde{X}_i^T(t)\ \bar{e}_i^T(t)\ t]^T}\right)^T \\ & \times\begin{bmatrix}\tilde{\bar{G}}_i(\tilde{X}_i(t),\bar{e}_i(t),t)\\ 0\end{bmatrix} R_i^{-1}\begin{bmatrix}\tilde{\bar{G}}_i(\tilde{X}_i(t),\bar{e}_i(t),t)\\ 0\end{bmatrix}^T \\ & \times\left(\frac{\partial V(\tilde{X}_i(t),\bar{e}_i(t),t)}{\partial[\tilde{X}_i^T(t)\ \bar{e}_i^T(t)\ t]^T}\right) + \left(\frac{\partial V(\tilde{X}_i(t),\bar{e}_i(t),t)}{\partial[\tilde{X}_i^T(t)\ \bar{e}_i^T(t)\ t]^T}\right)^T \\ & \times\begin{bmatrix}\tilde{\bar{F}}_i(\tilde{X}_i(t),\bar{e}_i(t),t)\\ 1\end{bmatrix} + \frac{1}{4\rho_i^2}\left(\frac{\partial V(\tilde{X}_i(t),\bar{e}_i(t),t)}{\partial[\tilde{X}_i^T(t)\ \bar{e}_i^T(t)\ t]^T}\right)^T \\ & \times\begin{bmatrix}\tilde{\bar{D}}_i(\tilde{X}_i(t),\bar{e}_i(t),t) & 0\\ 0 & 0\end{bmatrix}\left(\frac{\partial V(\tilde{X}_i(t),\bar{e}_i(t),t)}{\partial[\tilde{X}_i^T(t)\ \bar{e}_i^T(t)\ t]^T}\right) \\ & + \frac{1}{4\rho_i^2}\left(\frac{\partial V(\tilde{X}_i(t),\bar{e}_i(t),t)}{\partial[\tilde{X}_i^T(t)\bar{e}_i^T(t)\ t]^T}\right)^T\begin{bmatrix}\tilde{\bar{F}}_{-i}(\tilde{X}_i(t),\bar{e}_i(t),t) & 0\\ 0 & 0\end{bmatrix} \\ & \times\left(\frac{\partial V(\tilde{X}_i(t),\bar{e}_i(t),t)}{\partial[\tilde{X}_i^T(t)\ \bar{e}_i^T(t)\ t]^T}\right) - \rho_i^2\tilde{C}_i^T(\tilde{X}_i(t))\tilde{C}_i(\tilde{X}_i(t)) \\ = {} & 0, \quad i=1,\ldots,N \end{aligned} \tag{40}$$

In (40), the design problem becomes how to solve partial differential $\left(\frac{\partial V(\tilde{X}_i(t),\bar{e}_i(t),t)}{\partial[\tilde{X}_i^T(t)\ \bar{e}_i^T(t)\ t]^T}\right)$ from $HJIE_i$ in (40) to obtain the control input $K_i^*(\hat{\tilde{X}}_i(t),\bar{e}_i(t))$, observer gain $L_i^*(\hat{\tilde{X}}_i(t))$, worst-case external disturbance $\bar{v}_i^*(t)$, measurement noise $n_i^*(t)$ and interconnected coupling effect $\tilde{\bar{X}}_{-i}^*(t-\tau_{-i}(t))$ in (21)-(24) by HJIE-reinforcement learning-based DNN scheme as shown in Fig. 4. The training of HJIE by reinforcement-based deep learning algorithm can be divided into the phase of off-line training and on-line operation. In the off-line training process, since the actual state, external disturbance, measurement noise, internal coupling, and malicious attack signals of each satellite are not available. We use the worst-case $\bar{v}_i^*(t)$,$n_i^*(t)$,$\tilde{\bar{X}}_{-i}^*(t-\tau_{-i}(t))$ to replace the real $\bar{v}_i(t)$,$n_i(t)$,$\tilde{\bar{X}}_{-i}(t-$

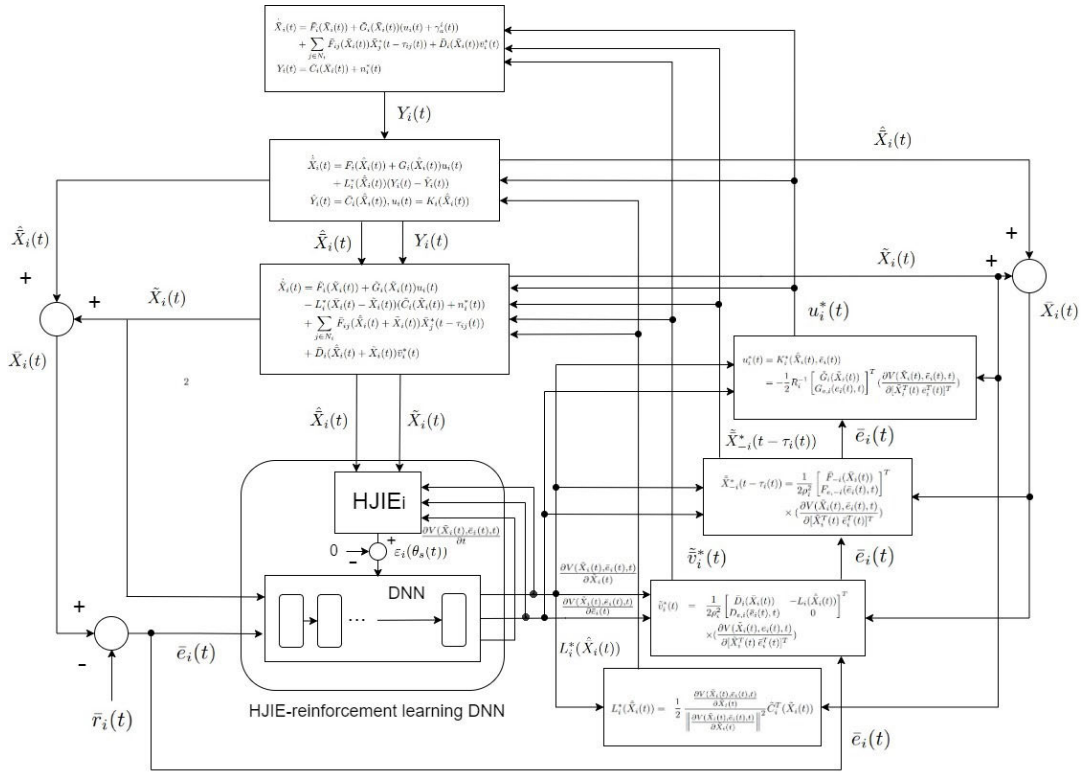

FIGURE 4. The flow chart of the HJIE-reinforcement DNN-based H_∞ observer-based attack-tolerant decentralized team formation tracking control scheme of the ith satellite at the remote side. In the off-line training phase, the worst-case generalized external disturbance $\tilde{\bar{v}}_i^*(t)$ and coupling effect $\tilde{\bar{X}}_{-i}^*(t)$ will be fed back to the satellite dynamic system to obtain the state $\bar{X}_i(t)$ and generate the tracking error $\bar{e}_i$ by reference $\bar{r}_i(t)$. Then, the control input $u_i^*(t)$ and observer gain $L_i^*(\hat{\bar{X}}_i(t))$ will be obtained through the output of HJIE-reinforcement learning DNN. In the on-line operation phase, the actual external disturbance $v_i(t)$, measurement noise $n_i(t)$ and coupling effect $\bar{X}_{-i}(t)$ will replace these worst-case external disturbance, measurement noise and coupling effect.

$\tau_{-i}(t)$) to generate output $Y_i(t)$ for state estimation. These replacements do not influence the H_∞ observer-based team formation tracking control performance because the H_∞ observer-based team formation tracking control is based on the worst-case $\bar{v}_i^*(t)$,$n_i^*(t)$ and $\tilde{\bar{X}}_{-i}^*(t-\tau_{-i}(t))$. To estimate the state $\hat{\bar{X}}_i(t)$, the Luenberger observer is proposed, and then the estimation error model is used to generate the estimation error $\tilde{X}_i(t)$ to calculate $\bar{X}_i(t) = \tilde{X}_i(t) + \hat{\bar{X}}_i(t)$. We can also get the tracking error $\bar{e}_i(t) = \bar{X}_i(t) - \hat{\bar{X}}_i(t)$. In this way, we can get the augmented state $\tilde{\bar{X}}_i(t) = [\tilde{X}_i^T(t)\ \bar{e}_i^T(t)]^T$. Taking the state $\tilde{\bar{X}}_i(t)$ as the input of the DNN, our objective is to solve the partial differential $HJIE_i$ by DNN after the HJIE-reinforcement training. Before the $HJIE_i$ approaches to zero in the reinforcement-based training process, $HJIE_i$ can be rewritten as the following formula.

$$
\begin{aligned}
HJIE_{\varepsilon,i} = {} & \tilde{\bar{X}}_i^T(t)\bar{Q}_i\tilde{\bar{X}}_i(t) - \frac{1}{4}\left(\frac{\partial V(\tilde{X}_i(t),\bar{e}_i(t),t)}{\partial[\tilde{X}_i^T(t)\ \bar{e}_i^T(t)\ t]^T}\right)_\varepsilon^T \\
& \times \begin{bmatrix} \tilde{\bar{G}}_i(\tilde{X}_i(t),\bar{e}_i(t),t) \\ 0 \end{bmatrix} R_i^{-1} \\
& \times \begin{bmatrix} \tilde{\bar{G}}_i(\tilde{X}_i(t),\bar{e}_i(t),t) \\ 0 \end{bmatrix}^T \\
& \times \left(\frac{\partial V(\tilde{X}_i(t),\bar{e}_i(t),t)}{\partial[\tilde{X}_i^T(t)\ \bar{e}_i^T(t)\ t]^T}\right)_\varepsilon \\
& + \left(\frac{\partial V(\tilde{X}_i(t),\bar{e}_i(t),t)}{\partial[\tilde{X}_i^T(t)\ \bar{e}_i^T(t)\ t]^T}\right)_\varepsilon^T \begin{bmatrix} \tilde{\bar{F}}_i(\tilde{X}_i(t),\bar{e}_i(t),t) \\ 1 \end{bmatrix} \\
& + \frac{1}{4\rho_i^2}\left(\frac{\partial V(\tilde{X}_i(t),\bar{e}_i(t),t)}{\partial[\tilde{X}_i^T(t)\bar{e}_i^T(t)\ t]^T}\right)_\varepsilon^T \\
& \times \begin{bmatrix} \tilde{\bar{D}}_i(\tilde{X}_i(t),\bar{e}_i(t),t) & 0 \\ 0 & 0 \end{bmatrix} \left(\frac{\partial V(\tilde{X}_i(t),\bar{e}_i(t),t)}{\partial[\tilde{X}_i^T(t)\ \bar{e}_i^T(t)\ t]^T}\right)_\varepsilon \\
& + \frac{1}{4\rho_i^2}\left(\frac{\partial V(\tilde{X}_i(t),\bar{e}_i(t),t)}{\partial[\tilde{X}_i^T(t)\bar{e}_i^T(t)\ t]^T}\right)_\varepsilon^T \\
& \times \begin{bmatrix} \tilde{\bar{F}}_{-i}(\tilde{X}_i(t),\bar{e}_i(t),t) & 0 \\ 0 & 0 \end{bmatrix} \left(\frac{\partial V(\tilde{X}_i(t),\bar{e}_i(t),t)}{\partial[\tilde{X}_i^T(t)\ \bar{e}_i^T(t)\ t]^T}\right)_\varepsilon \\
& - \rho_i^2 \tilde{C}_i^T(\tilde{X}_i(t))\tilde{C}_i(\tilde{X}_i(t)) \\
= {} & \varepsilon_i(\theta(t)), \quad i = 1,\ldots,N
\end{aligned} \tag{41}
$$

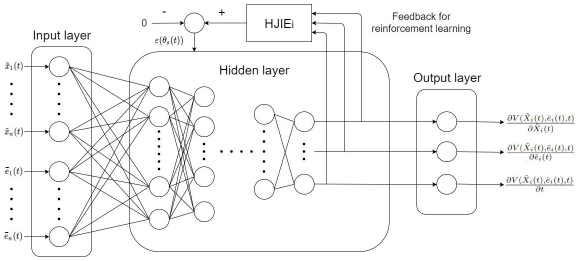

FIGURE 5. A HJIE-reinforcement DNN architecture trained using the Adam learning algorithm. It is able to find an appropriate solution to make HJIE approach zero [35].

The output $\left(\frac{\partial V(\tilde{X}_i(t),\bar{e}_i(t),t)}{\partial[\tilde{X}_i^T(t)\ \bar{e}_i^T(t)\ t]^T}\right)_\varepsilon$ of DNN is taken to calculate the $K_i^*(\hat{\tilde{X}}_i(t), \bar{e}_i(t))$, $L_i^*(\hat{\tilde{X}}_i(t))$, $\bar{\tilde{v}}_i^*(t)$, $\bar{\tilde{X}}_{-i}^*(t-\tau_{-i}(t))$ in the reinforcement training process during off-line training phase as shown in Fig. 4. According to the above steps, we can obtain $\tilde{X}_i(t)$ and $\bar{e}_i(t)$. Then take $\tilde{X}_i(t)$, $\bar{e}_i(t)$ as input to train DNN by HJIE-reinforcement learning algorithm and calculate the $\varepsilon_i(\theta(t))$ of $HJIE_i$ in (41) at the same time. Repeat this step and fedback $\varepsilon_i(\theta(t))$ to train the neuron weightings in DNN until the trained output $\left(\frac{\partial V(\tilde{X}_i(t),\bar{e}_i(t),t)}{\partial[\tilde{X}_i^T(t)\bar{e}_i^T(t)\ t]^T}\right)_\varepsilon$ of DNN approaches to the theoretical solution $\left(\frac{\partial V(\tilde{X}_i(t),\bar{e}_i(t),t)}{\partial[\tilde{X}_i^T(t)\ \bar{e}_i^T(t)\ t]^T}\right)$. When $\varepsilon_i(\theta(t))$ approaches to zero, the off-line training phase is over, and we switch the off-line training phase to the on-line operation phase. The well-trained DNN-based H_∞ attack-tolerant observer-based formation tracking scheme in Fig. 3 starts to operate. The on-line operation phase is different from the off-line training phase. External disturbance, measurement noise, and interconnected coupling effect on each satellite NCS are all real. So in the on-line operation phase we don't need to compute the worst-case $\bar{v}_i^*(t)$, $n_i^*(t)$ and $\bar{\tilde{X}}_{-i}^*(t-\tau_{-i}(t))$ again.

The HJIE-reinforcement learning-based DNN architecture of the robust decentralized H_∞ attack-tolerant observer-based formation tracking control scheme includes input layer, multiple hidden layers and output layer with a HJIE-reinforcement feedback as shown in Fig. 5. Inputs of deep neural network are tracking error $\bar{e}_i(t)$ and estimation error $\tilde{X}_i(t)$. The neurons in hidden layers use LeakyReLU as an ideal activation function in our case instead of the conventional ReLU in a dead neuron problem. When the input value of ReLU is negative, the output is always zero. Then the first derivative is always zero, which will cause the neuron to fail to update the parameters, that is, the neuron does not learn. This phenomenon is called dead neuron. Therefore we choose LeakyReLU as our activation function. When the input is negative, LeakyReLU is a constant gradient instead of zero [35]. This feature can well avoid the dead neuron problem of ReLU, i.e.,

$$I(X(t)) = \begin{cases} a_1 X(t)\ , \text{if } X(t) > 0 \\ a_2 X(t)\ , \text{if } X(t) \le 0 \end{cases}$$

where a_1 and a_2 are some constant with $a_1, a_2 \in [0, 1]$.

The $HJIE_{\varepsilon,i}$ in (41) with error $\varepsilon_i(\theta(t))$ is employed to train the weighting and bias parameters of DNN by Adam learning algorithm to minimize the objective function as the following HJIE-reinforcement learning-based Adam algorithm [35], [45]:

$$\theta_s(t) = \theta_{s-1}(t) - \frac{\psi}{\sqrt{\hat{v}_s(t)+\lambda}}\hat{m}_s(t), \quad s = 1, \ldots, S \tag{42}$$

$$\hat{m}_s(t) = \frac{m_s(t)}{1-\alpha_1^s},\ \hat{v}_s(t) = \frac{v_s(t)}{1-\alpha_2^s} \tag{43}$$

$$m_s(t) = \alpha_1 m_{s-1}(t) + (1-\alpha_1) g_s(t)$$

$$v_s(t) = \alpha_2 v_{s-1}(t) + (1-\alpha_2) g_s^2(t)$$

$$g_s(t) = \frac{\partial}{\partial \theta_s(t)} \sqrt{\frac{1}{P}\sum_{s=1}^{P} \varepsilon_i^2(\theta_s(t))} \tag{44}$$

where $\theta_s(t)$ denotes the weighting parameter vector to be trained for DNN to output $\left(\frac{\partial V(\tilde{X}_i(t),\bar{e}_i(t),t)}{\partial[\tilde{X}_i^T(t)\ \bar{e}_i^T(t)\ t]^T}\right)_\varepsilon$, ψ denotes the learning rate or stepsize at each time t and S denotes the number of training time steps. $\hat{m}_s(t)$ and $\hat{v}_s(t)$ are bias-corrected estimators [35]. P is batch size. The partial derivative of objective function with respect to $\theta_s(t)$ at time step s and time t. $\alpha_1, \alpha_2 \in [0, 1]$ in (44) represent the strength of the prior influence on the current direction. These two parameters can accelerate the learning process and prevent the HJIE-reinforcement deep learning from becoming caught by a local minimum [35], [45], which can be specified by the designer. According to the bias-corrected estimators in (43) and (44), the gradient will be reinforced if the current direction of gradient $g_s(t)$ of the square error $\varepsilon_i^2(\theta_s(t))$ of $HJIE_{\varepsilon,i}$ in (41) matches that of the accumulated gradient, otherwise, it will be weakened. The sth powers of α_1 and α_2 are α_1^s, α_2^s, respectively. λ is the gradient moving average, and $\hat{v}_s(t)$ is squared gradient of $g_s(t)$ at time t. Due to the benefit of $\hat{v}_s(t)$, the adaptive learning rate in (42) has a large starting value and small value close to the minimum. Since HJIE-reinforcement Adam learning algorithm has great performance and easy-to-use features, recently it has been one of the most common optimizer for deep learning algorithm.

Remark 6: In the HJIE-reinforced DNN control scheme trained by Adam learning algorithm, the updating weighting parameter vector $\theta_s(t)$ could converge to a globally optimal $\theta_s^*(t)$ with a linear convergence rate as $s \to \infty$ in (42)-(44) if the time steps and number of hidden neurons are large enough, which has been shown in [35].

According to the above architecture of HJIE-reinforcement learning-based DNN via Adam algorithm in (42)-(44), the output $\left(\frac{\partial V(\tilde{X}_i(t),\bar{e}_i(t),t)}{\partial[\tilde{X}_i^T(t)\ \bar{e}_i^T(t)\ t]^T}\right)_\varepsilon$ of DNN is transmitted to $\text{HJIE}_{\varepsilon,i}$ in (41) to obtain error $\varepsilon_i(\theta_s(t))$ at the sth training step in Fig. 4 as follows:

$$HJIE_{\varepsilon,i} = \bar{\tilde{X}}_i^T(t)\bar{Q}_i\bar{\tilde{X}}_i(t) - \frac{1}{4}\left(\frac{\partial V(\tilde{X}_i(t),\bar{e}_i(t),t)}{\partial[\tilde{X}_i^T(t)\ \bar{e}_i^T(t)\ t]^T}\right)_\varepsilon^T \times \begin{bmatrix} \bar{\tilde{G}}_i(\tilde{X}_i(t),\bar{e}_i(t),t) \\ 0 \end{bmatrix} R_i^{-1}$$

$$\times \begin{bmatrix} \tilde{\bar{G}}_i(\tilde{X}_i(t), \bar{e}_i(t), t) \\ 0 \end{bmatrix}^T \left(\frac{\partial V(\tilde{X}_i(t), \bar{e}_i(t), t)}{\partial [\tilde{X}_i^T(t)\ \bar{e}_i^T(t)\ t]^T} \right)_\varepsilon$$
$$+ \left(\frac{\partial V(\tilde{X}_i(t), \bar{e}_i(t), t)}{\partial [\tilde{X}_i^T(t)\ \bar{e}_i^T(t)\ t]^T} \right)_\varepsilon^T \begin{bmatrix} \tilde{\bar{F}}_i(\tilde{X}_i(t), \bar{e}_i(t), t) \\ 1 \end{bmatrix}$$
$$+ \frac{1}{4\rho_i^2} \left(\frac{\partial V(\tilde{X}_i(t), \bar{e}_i(t), t)}{\partial [\tilde{X}_i^T(t)\ \bar{e}_i^T(t)\ t]^T} \right)_\varepsilon^T$$
$$\times \begin{bmatrix} \tilde{\bar{D}}_i(\tilde{X}_i(t), \bar{e}_i(t), t) & 0 \\ 0 & 0 \end{bmatrix}$$
$$\times \left(\frac{\partial V(\tilde{X}_i(t), \bar{e}_i(t), t)}{\partial [\tilde{X}_i^T(t)\ \bar{e}_i^T(t)\ t]^T} \right)_\varepsilon$$
$$+ \frac{1}{4\rho_i^2} \left(\frac{\partial V(\tilde{X}_i(t), \bar{e}_i(t), t)}{\partial [\tilde{X}_i^T(t) \bar{e}_i^T(t)\ t]^T} \right)_\varepsilon^T$$
$$\times \begin{bmatrix} \tilde{\bar{F}}_{-i}(\tilde{X}_i(t), \bar{e}_i(t), t) & 0 \\ 0 & 0 \end{bmatrix} \left(\frac{\partial V(\tilde{X}_i(t), \bar{e}_i(t), t)}{\partial [\tilde{X}_i^T(t)\ \bar{e}_i^T(t)\ t]^T} \right)_\varepsilon$$
$$-\rho_i^2 \tilde{C}_i^T(\tilde{X}_i(t)) \tilde{C}_i(\tilde{X}_i(t)) = \varepsilon_i(\theta_s(t)),$$
$$i = 1, \ldots, N \tag{45}$$

The error $\varepsilon_i(\theta_s(t))$ of HJIE will be sent back to train DNN by HJIE-reinforcement-based Adam learning algorithm iteratively to generate the precise $\left(\frac{\partial V(\tilde{X}_i(t), \bar{e}_i(t), t)}{\partial [\tilde{X}_i^T(t)\ \bar{e}_i^T(t)\ t]^T} \right)$ finally, then we can obtain the decentralized H_∞ attack-tolerant observer-based formation tracking control law $u_i^*(t) = K_i^*(\hat{\tilde{X}}_i(t), \bar{e}_i(t)) = -\frac{1}{2} R_i^{-1} \begin{bmatrix} \tilde{G}_i(\tilde{X}_i(t)) \\ G_{e,i}(\bar{e}_i(t), t) \end{bmatrix}^T \left(\frac{\partial V(\tilde{X}_i(t), \bar{e}_i(t), t)}{\partial [\tilde{X}_i^T(t)\ \bar{e}_i^T(t)]^T} \right)$, the observer gain $L_i^*(\hat{\tilde{X}}_i(t)) = \frac{1}{2} \frac{\frac{\partial V(\tilde{X}_i(t), \bar{e}_i(t), t)}{\partial \tilde{X}_i(t)}}{\left\| \frac{\partial V(\tilde{X}_i(t), \bar{e}_i(t), t)}{\partial \tilde{X}_i(t)} \right\|^2} \tilde{C}_i^T(\tilde{X}_i(t))$, the worst-case external disturbance and measurement noise $\tilde{\bar{v}}_i^*(t) = \frac{1}{2\rho_i^2} \begin{bmatrix} \bar{D}_i(\bar{X}_i(t)) & -L_i(\hat{\bar{X}}_i(t)) \\ D_{e,i}(\bar{e}_i(t), t) & 0 \end{bmatrix}^T \left(\frac{\partial V(\tilde{X}_i(t), \bar{e}_i(t), t)}{\partial [\tilde{X}_i^T(t)\ \bar{e}_i^T(t)]^T} \right)$, the worst-case interconnected coupling effect $\tilde{\bar{X}}_{-i}^*(t - \tau_i(t)) = \frac{1}{2\rho_i^2} \begin{bmatrix} \bar{F}_{-i}(\bar{X}_i(t)) \\ F_{e,-i}(\bar{e}_i(t), t) \end{bmatrix}^T \left(\frac{\partial V(\tilde{X}_i(t), \bar{e}_i(t), t)}{\partial [\tilde{X}_i^T(t)\ \bar{e}_i^T(t)]^T} \right)$ after the training process by HJIE-reinforcement DNN-based Adam learning algorithm. The following theorem is to prove that when the error $\varepsilon_i(\theta_s(t))$ of HJIE-reinforcement learning-based DNN approaches to zero by Adam learning process, the output $\left(\frac{\partial V(\tilde{X}_i(t), \bar{e}_i(t), t)}{\partial [\tilde{X}_i^T(t)\ \bar{e}_i^T(t)\ t]^T} \right)_\varepsilon$ of DNN can approach to $\left(\frac{\partial V(\tilde{X}_i(t), \bar{e}_i(t), t)}{\partial [\tilde{X}_i^T(t) \bar{e}_i^T(t)\ t]^T} \right)$.

Theorem 2: If $\varepsilon_i(\theta_s(t)) \to 0$ in (45) by HJIE-reinforcement learning-based Adam algorithm in (42)-(44), then $\left(\frac{\partial V(\tilde{X}_i(t), \bar{e}_i(t), t)}{\partial [\tilde{X}_i^T(t) \bar{e}_i^T(t)\ t]^T} \right)_\varepsilon$ in (45) can approach to $\left(\frac{\partial V(\tilde{X}_i(t), \bar{e}_i(t), t)}{\partial [\tilde{X}_i^T(t)\ \bar{e}_i^T(t)\ t]^T} \right)$ in (40). In this case, the proposed HJIE-reinforced DNN-based robust observer-based output feedback formation tracking scheme of each satellite in the team will approach to the theoretical H_∞ observer-based output feedback decentralized formation tracking control design (21)-(24) of large-scale satellites NCS in Theorem 1.

Proof: At first, we suppose

$$\left(\frac{\partial V(\tilde{X}_i(t), \bar{e}_i(t), t)}{\partial [\tilde{X}_i^T(t)\ \bar{e}_i^T(t)\ t]^T} \right)_\varepsilon = \left(\frac{\partial V(\tilde{X}_i(t), \bar{e}_i(t), t)}{\partial [\tilde{X}_i^T(t)\ \bar{e}_i^T(t)\ t]^T} \right) + \Xi_i(\tilde{X}_i(t), \bar{e}_i(t), t),$$
$$for\ i = 1, \ldots, N \tag{46}$$

where $\Xi_i(\tilde{X}_i(t), \bar{e}_i(t), t)$ denotes the error function between $\left(\frac{\partial V(\tilde{X}_i(t), \bar{e}_i(t), t)}{\partial [\tilde{X}_i^T(t)\ \bar{e}_i^T(t)\ t]^T} \right)_\varepsilon$ and $\left(\frac{\partial V(\tilde{X}_i(t), \bar{e}_i(t), t)}{\partial [\tilde{X}_i^T(t)\ \bar{e}_i^T(t)\ t]^T} \right)$.

Subtracting (45) with (40), $\varepsilon_i(\theta_s(t))$ can be rewritten as follows:

$$\begin{aligned}
&\varepsilon_i(\theta_s(t)) \\
&= HJIE_{\varepsilon,i} - HJIE_i \\
&= \left(\left(\frac{\partial V(\tilde{X}_i(t), \bar{e}_i(t), t)}{\partial [\tilde{X}_i^T(t)\ \bar{e}_i^T(t)\ t]^T} \right)_\varepsilon^T - \left(\frac{\partial V(\tilde{X}_i(t), \bar{e}_i(t), t)}{\partial [\tilde{X}_i^T(t)\ \bar{e}_i^T(t)\ t]^T} \right)^T \right) \\
&\quad \times \begin{bmatrix} \tilde{\bar{F}}_i(\tilde{X}_i(t), \bar{e}_i(t), t) \\ 1 \end{bmatrix} - \frac{1}{4} \left(\frac{\partial V(\tilde{X}_i(t), \bar{e}_i(t), t)}{\partial [\tilde{X}_i^T(t)\ \bar{e}_i^T(t)\ t]^T} \right)_\varepsilon^T \\
&\quad \times \begin{bmatrix} \tilde{\bar{G}}_i(\tilde{X}_i(t), \bar{e}_i(t), t) \\ 0 \end{bmatrix} R_i^{-1} \\
&\quad \times \begin{bmatrix} \tilde{\bar{G}}_i(\tilde{X}_i(t), \bar{e}_i(t), t) \\ 0 \end{bmatrix}^T \left(\frac{\partial V(\tilde{X}_i(t), \bar{e}_i(t), t)}{\partial [\tilde{X}_i^T(t)\ \bar{e}_i^T(t)\ t]^T} \right)_\varepsilon \\
&\quad + \frac{1}{4} \left(\frac{\partial V(\tilde{X}_i(t), \bar{e}_i(t), t)}{\partial [\tilde{X}_i^T(t)\ \bar{e}_i^T(t)\ t]^T} \right)^T \begin{bmatrix} \tilde{\bar{G}}_i(\tilde{X}_i(t), \bar{e}_i(t), t) \\ 0 \end{bmatrix} \\
&\quad \times R_i^{-1} \begin{bmatrix} \tilde{\bar{G}}_i(\tilde{X}_i(t), \bar{e}_i(t), t) \\ 0 \end{bmatrix}^T \left(\frac{\partial V(\tilde{X}_i(t), \bar{e}_i(t), t)}{\partial [\tilde{X}_i^T(t)\ \bar{e}_i^T(t)\ t]^T} \right) \\
&\quad + \frac{1}{4\rho_i^2} \left(\frac{\partial V(\tilde{X}_i(t), \bar{e}_i(t), t)}{\partial [\tilde{X}_i^T(t)\ \bar{e}_i^T(t)\ t]^T} \right)_\varepsilon^T \begin{bmatrix} \tilde{\bar{D}}_i(\tilde{X}_i(t), \bar{e}_i(t), t) & 0 \\ 0 & 0 \end{bmatrix} \\
&\quad \times \left(\frac{\partial V(\tilde{X}_i(t), \bar{e}_i(t), t)}{\partial [\tilde{X}_i^T(t)\ \bar{e}_i^T(t)\ t]^T} \right)_\varepsilon - \frac{1}{4\rho_i^2} \left(\frac{\partial V(\tilde{X}_i(t), \bar{e}_i(t), t)}{\partial [\tilde{X}_i^T(t) \bar{e}_i^T(t)\ t]^T} \right)^T \\
&\quad \times \begin{bmatrix} \tilde{\bar{D}}_i(\tilde{X}_i(t), \bar{e}_i(t), t) & 0 \\ 0 & 0 \end{bmatrix} \left(\frac{\partial V(\tilde{X}_i(t), \bar{e}_i(t), t)}{\partial [\tilde{X}_i^T(t)\ \bar{e}_i^T(t)\ t]^T} \right) \\
&\quad + \frac{1}{4\rho_i^2} \left(\frac{\partial V(\tilde{X}_i(t), \bar{e}_i(t), t)}{\partial [\tilde{X}_i^T(t)\ \bar{e}_i^T(t)\ t]^T} \right)_\varepsilon^T \begin{bmatrix} \tilde{\bar{F}}_{-i}(\tilde{X}_i(t), \bar{e}_i(t), t) & 0 \\ 0 & 0 \end{bmatrix} \\
&\quad \times \left(\frac{\partial V(\tilde{X}_i(t), \bar{e}_i(t), t)}{\partial [\tilde{X}_i^T(t)\ \bar{e}_i^T(t)\ t]^T} \right)_\varepsilon - \frac{1}{4\rho_i^2} \left(\frac{\partial V(\tilde{X}_i(t), \bar{e}_i(t), t)}{\partial [\tilde{X}_i^T(t) \bar{e}_i^T(t)\ t]^T} \right)^T \\
&\quad \times \begin{bmatrix} \tilde{\bar{F}}_{-i}(\tilde{X}_i(t), \bar{e}_i(t), t) & 0 \\ 0 & 0 \end{bmatrix} \left(\frac{\partial V(\tilde{X}_i(t), \bar{e}_i(t), t)}{\partial [\tilde{X}_i^T(t)\ \bar{e}_i^T(t)\ t]^T} \right), \\
&\quad for\ i = 1, \ldots, N
\end{aligned} \tag{47}$$

By (46), we get

$$
\begin{aligned}
&\varepsilon_i(\theta_s(t)) \\
&= \Xi_i^T(\tilde{X}_i(t),\bar{e}_i(t),t)\begin{bmatrix}\tilde{\bar{F}}_i(\tilde{X}_i(t),\bar{e}_i(t),t)\\ 1\end{bmatrix} \\
&\quad -\frac{1}{4}\Xi_i^T(\tilde{X}_i(t),\bar{e}_i(t),t)\begin{bmatrix}\tilde{\bar{G}}_i(\tilde{X}_i(t),\bar{e}_i(t),t)\\ 0\end{bmatrix}R_i^{-1} \\
&\quad \times\begin{bmatrix}\tilde{\bar{G}}_i(\tilde{X}_i(t),\bar{e}_i(t),t)\\ 0\end{bmatrix}^T\left(\frac{\partial V(\tilde{X}_i(t),\bar{e}_i(t),t)}{\partial[\tilde{X}_i^T(t)\,\bar{e}_i^T(t)\,t]^T}\right) \\
&\quad -\frac{1}{4}\left(\frac{\partial V(\tilde{X}_i(t),\bar{e}_i(t),t)}{\partial[\tilde{X}_i^T(t)\,\bar{e}_i^T(t)\,t]^T}\right)^T\begin{bmatrix}\tilde{\bar{G}}_i(\tilde{X}_i(t),\bar{e}_i(t),t)\\ 0\end{bmatrix}R_i^{-1} \\
&\quad \times\begin{bmatrix}\tilde{\bar{G}}_i(\tilde{X}_i(t),\bar{e}_i(t),t)\\ 0\end{bmatrix}^T\Xi_i(\tilde{X}_i(t),\bar{e}_i(t),t) \\
&\quad -\frac{1}{4}\Xi_i^T(\tilde{X}_i(t),\bar{e}_i(t),t)\begin{bmatrix}\tilde{\bar{G}}_i(\tilde{X}_i(t),\bar{e}_i(t),t)\\ 0\end{bmatrix}R_i^{-1} \\
&\quad \times\begin{bmatrix}\tilde{\bar{G}}_i(\tilde{X}_i(t),\bar{e}_i(t),t)\\ 0\end{bmatrix}^T\Xi_i(\tilde{X}_i(t),\bar{e}_i(t),t) \\
&\quad +\frac{1}{4\rho_i^2}\Xi_i^T(\tilde{X}_i(t),\bar{e}_i(t),t)\begin{bmatrix}\tilde{\bar{D}}_i(\tilde{X}_i(t),\bar{e}_i(t),t)\ 0\\ 0\qquad\quad 0\end{bmatrix} \\
&\quad \times\left(\frac{\partial V(\tilde{X}_i(t),\bar{e}_i(t),t)}{\partial[\tilde{X}_i^T(t)\,\bar{e}_i^T(t)\,t]^T}\right)+\frac{1}{4\rho_i^2}\left(\frac{\partial V(\tilde{X}_i(t),\bar{e}_i(t),t)}{\partial[\tilde{X}_i^T(t)\,\bar{e}_i^T(t)\,t]^T}\right)^T \\
&\quad \times\begin{bmatrix}\tilde{\bar{D}}_i(\tilde{X}_i(t),\bar{e}_i(t),t)\ 0\\ 0\qquad\quad 0\end{bmatrix}\Xi_i(\tilde{X}_i(t),\bar{e}_i(t),t) \\
&\quad +\frac{1}{4\rho_i^2}\Xi_i^T(\tilde{X}_i(t),\bar{e}_i(t),t)\begin{bmatrix}\tilde{\bar{D}}_i(\tilde{X}_i(t),\bar{e}_i(t),t)\ 0\\ 0\qquad\quad 0\end{bmatrix} \\
&\quad \times\Xi_i(\tilde{X}_i(t),\bar{e}_i(t),t)+\frac{1}{4\rho_i^2}\Xi_i^T(\tilde{X}_i(t),\bar{e}_i(t),t) \\
&\quad \times\begin{bmatrix}\tilde{\bar{F}}_{-i}(\tilde{X}_i(t),\bar{e}_i(t),t)\ 0\\ 0\qquad\quad 0\end{bmatrix}\left(\frac{\partial V(\tilde{X}_i(t),\bar{e}_i(t),t)}{\partial[\tilde{X}_i^T(t)\,\bar{e}_i^T(t)\,t]^T}\right) \\
&\quad +\frac{1}{4\rho_i^2}\left(\frac{\partial V(\tilde{X}_i(t),\bar{e}_i(t),t)}{\partial[\tilde{X}_i^T(t)\,\bar{e}_i^T(t)\,t]^T}\right)^T\begin{bmatrix}\tilde{\bar{F}}_{-i}(\tilde{X}_i(t),\bar{e}_i(t),t)\ 0\\ 0\qquad\quad 0\end{bmatrix} \\
&\quad \times\Xi_i(\tilde{X}_i(t),\bar{e}_i(t),t)+\frac{1}{4\rho_i^2}\Xi_i^T(\tilde{X}_i(t),\bar{e}_i(t),t) \\
&\quad \times\begin{bmatrix}\tilde{\bar{F}}_{-i}(\tilde{X}_i(t),\bar{e}_i(t),t)\ 0\\ 0\qquad\quad 0\end{bmatrix}\Xi_i(\tilde{X}_i(t),\bar{e}_i(t),t), \\
&\quad \textit{for } i=1,\ldots,N
\end{aligned}
\tag{48}
$$

By the symmetric property, we have following equations:

$$
\begin{aligned}
&\Xi_i^T(\tilde{X}_i(t),\bar{e}_i(t),t)\begin{bmatrix}\tilde{\bar{G}}_i(\tilde{X}_i(t),\bar{e}_i(t),t)\\ 0\end{bmatrix}R_i^{-1} \\
&\quad \times\begin{bmatrix}\tilde{\bar{G}}_i(\tilde{X}_i(t),\bar{e}_i(t),t)\\ 0\end{bmatrix}^T\left(\frac{\partial V(\tilde{X}_i(t),\bar{e}_i(t),t)}{\partial[\tilde{X}_i^T(t)\,\bar{e}_i^T(t)\,t]^T}\right) \\
&= \left(\frac{\partial V(\tilde{X}_i(t),\bar{e}_i(t),t)}{\partial[\tilde{X}_i^T(t)\,\bar{e}_i^T(t)\,t]^T}\right)^T\begin{bmatrix}\tilde{\bar{G}}_i(\tilde{X}_i(t),\bar{e}_i(t),t)\\ 0\end{bmatrix}R_i^{-1} \\
&\quad \times\begin{bmatrix}\tilde{\bar{G}}_i(\tilde{X}_i(t),\bar{e}_i(t),t)\\ 0\end{bmatrix}^T\Xi_i(\tilde{X}_i(t),\bar{e}_i(t),t), \\
&\quad i=1,\ldots,N
\end{aligned}
\tag{49}
$$

$$
\begin{aligned}
&\Xi_i^T(\tilde{X}_i(t),\bar{e}_i(t),t)\begin{bmatrix}\tilde{\bar{D}}_i(\tilde{X}_i(t),\bar{e}_i(t),t)\ 0\\ 0\qquad\quad 0\end{bmatrix} \\
&\quad \times\left(\frac{\partial V(\tilde{X}_i(t),\bar{e}_i(t),t)}{\partial[\tilde{X}_i^T(t)\,\bar{e}_i^T(t)t]^T}\right) \\
&= \left(\frac{\partial V(\tilde{X}_i(t),\bar{e}_i(t),t)}{\partial[\tilde{X}_i^T(t)\,\bar{e}_i^T(t)\,t]^T}\right)^T\begin{bmatrix}\tilde{\bar{D}}_i(\tilde{X}_i(t),\bar{e}_i(t),t)\ 0\\ 0\qquad\quad 0\end{bmatrix} \\
&\quad \times\Xi_i(\tilde{X}_i(t),\bar{e}_i(t),t), \quad i=1,\ldots,N
\end{aligned}
\tag{50}
$$

$$
\begin{aligned}
&\Xi_i^T(\tilde{X}_i(t),\bar{e}_i(t),t)\begin{bmatrix}\tilde{\bar{F}}_{-i}(\tilde{X}_i(t),\bar{e}_i(t),t)\ 0\\ 0\qquad\quad 0\end{bmatrix} \\
&\quad \times\left(\frac{\partial V(\tilde{X}_i(t),\bar{e}_i(t),t)}{\partial[\tilde{X}_i^T(t)\,\bar{e}_i^T(t)\,t]^T}\right) \\
&= \left(\frac{\partial V(\tilde{X}_i(t),\bar{e}_i(t),t)}{\partial[\tilde{X}_i^T(t)\,\bar{e}_i^T(t)\,t]^T}\right)^T\begin{bmatrix}\tilde{\bar{F}}_{-i}(\tilde{X}_i(t),\bar{e}_i(t),t)\ 0\\ 0\qquad\quad 0\end{bmatrix} \\
&\quad \times\Xi_i(\tilde{X}_i(t),\bar{e}_i(t),t), \quad i=1,\ldots,N
\end{aligned}
\tag{51}
$$

By (49), (50) and (51), then (48) becomes

$$
\begin{aligned}
&\varepsilon_i(\theta_s(t)) \\
&= \Xi_i^T(\tilde{X}_i(t),\bar{e}_i(t),t)\{\begin{bmatrix}\tilde{\bar{F}}_i(\tilde{X}_i(t),\bar{e}_i(t),t)\\ 1\end{bmatrix} \\
&\quad -\frac{1}{2}\begin{bmatrix}\tilde{\bar{G}}_i(\tilde{X}_i(t),\bar{e}_i(t),t)\\ 0\end{bmatrix}R_i^{-1}\begin{bmatrix}\tilde{\bar{G}}_i(\tilde{X}_i(t),\bar{e}_i(t),t)\\ 0\end{bmatrix}^T \\
&\quad \times\left(\frac{\partial V(\tilde{X}_i(t),\bar{e}_i(t),t)}{\partial[\tilde{X}_i^T(t)\,\bar{e}_i^T(t)\,t]^T}\right)-\frac{1}{4}\left(\frac{\partial V(\tilde{X}_i(t),\bar{e}_i(t),t)}{\partial[\tilde{X}_i^T(t)\,\bar{e}_i^T(t)\,t]^T}\right)^T \\
&\quad \times\begin{bmatrix}\tilde{\bar{G}}_i(\tilde{X}_i(t),\bar{e}_i(t),t)\\ 0\end{bmatrix}R_i^{-1}\begin{bmatrix}\tilde{\bar{G}}_i(\tilde{X}_i(t),\bar{e}_i(t),t)\\ 0\end{bmatrix}_i^T \\
&\quad \times\Xi_i(\tilde{X}_i(t),\bar{e}_i(t),t)+\frac{1}{2\rho_i^2}\begin{bmatrix}\tilde{\bar{D}}_i(\tilde{X}_i(t),\bar{e}_i(t),t)\ 0\\ 0\qquad\quad 0\end{bmatrix} \\
&\quad \times\left(\frac{\partial V(\tilde{X}_i(t),\bar{e}_i(t),t)}{\partial[\tilde{X}_i^T(t)\,\bar{e}_i^T(t)\,t]^T}\right)+\frac{1}{4\rho_i^2}\begin{bmatrix}\tilde{\bar{D}}_i(\tilde{X}_i(t),\bar{e}_i(t),t)\ 0\\ 0\qquad\quad 0\end{bmatrix} \\
&\quad \times\Xi_i(\tilde{X}_i(t),\bar{e}_i(t),t)+\frac{1}{2\rho_i^2}\begin{bmatrix}\tilde{\bar{F}}_{-i}(\tilde{X}_i(t),\bar{e}_i(t),t)\ 0\\ 0\qquad\quad 0\end{bmatrix} \\
&\quad \times\left(\frac{\partial V(\tilde{X}_i(t),\bar{e}_i(t),t)}{\partial[\tilde{X}_i^T(t)\,\bar{e}_i^T(t)\,t]^T}\right)+\frac{1}{4\rho_i^2}\begin{bmatrix}\tilde{\bar{F}}_{-i}(\tilde{X}_i(t),\bar{e}_i(t),t)\ 0\\ 0\qquad\quad 0\end{bmatrix} \\
&\quad \times\Xi_i(\tilde{X}_i(t),\bar{e}_i(t),t)\}, \quad \textit{for } i=1,\ldots,N
\end{aligned}
\tag{52}
$$

If $\varepsilon_i(\theta_s(t)) \to 0$ in (45), then (52) can be written as

$$\begin{aligned}
&\varepsilon_i(\theta_s(t)) \\
&= \Xi_i^T(\tilde{X}_i(t), \bar{e}_i(t), t)\{\begin{bmatrix} \tilde{\bar{F}}_i(\tilde{X}_i(t), \bar{e}_i(t), t) \\ 1 \end{bmatrix} \\
&\quad -\frac{1}{2}\begin{bmatrix} \tilde{\bar{G}}_i(\tilde{X}_i(t), \bar{e}_i(t), t) \\ 0 \end{bmatrix} R_i^{-1} \begin{bmatrix} \tilde{\bar{G}}_i(\tilde{X}_i(t), \bar{e}_i(t), t) \\ 0 \end{bmatrix}^T \\
&\quad \times \left(\frac{\partial V(\tilde{X}_i(t), \bar{e}_i(t), t)}{\partial [\tilde{X}_i^T(t)\ \bar{e}_i^T(t)\ t]^T}\right) - \frac{1}{4}\left(\frac{\partial V(\tilde{X}_i(t), \bar{e}_i(t), t)}{\partial [\tilde{X}_i^T(t)\ \bar{e}_i^T(t)\ t]^T}\right)^T \\
&\quad \times \begin{bmatrix} \tilde{\bar{G}}_i(\tilde{X}_i(t), \bar{e}_i(t), t) \\ 0 \end{bmatrix} R_i^{-1} \begin{bmatrix} \tilde{\bar{G}}_i(\tilde{X}_i(t), \bar{e}_i(t), t) \\ 0 \end{bmatrix}^T \\
&\quad \times \Xi_i(\tilde{X}_i(t), \bar{e}_i(t), t) + \frac{1}{2\rho_i^2}\begin{bmatrix} \tilde{\bar{D}}_i(\tilde{X}_i(t), \bar{e}_i(t), t) & 0 \\ 0 & 0 \end{bmatrix} \\
&\quad \times \left(\frac{\partial V(\tilde{X}_i(t), \bar{e}_i(t), t)}{\partial [\tilde{X}_i^T(t)\ \bar{e}_i^T(t)\ t]^T}\right) + \frac{1}{4\rho_i^2}\begin{bmatrix} \tilde{\bar{D}}_i(\tilde{X}_i(t), \bar{e}_i(t), t) & 0 \\ 0 & 0 \end{bmatrix} \\
&\quad \times \Xi_i(\tilde{X}_i(t), \bar{e}_i(t), t) + \frac{1}{2\rho_i^2}\begin{bmatrix} \tilde{\bar{F}}_{-i}(\tilde{X}_i(t), \bar{e}_i(t), t) & 0 \\ 0 & 0 \end{bmatrix} \\
&\quad \times \left(\frac{\partial V(\tilde{X}_i(t), \bar{e}_i(t), t)}{\partial [\tilde{X}_i^T(t)\ \bar{e}_i^T(t)\ t]^T}\right) + \frac{1}{4\rho_i^2}\begin{bmatrix} \tilde{\bar{F}}_{-i}(\tilde{X}_i(t), \bar{e}_i(t), t) & 0 \\ 0 & 0 \end{bmatrix} \\
&\quad \times \Xi_i(\tilde{X}_i(t), \bar{e}_i(t), t)\} \to 0, \quad for\ i = 1, \ldots, N
\end{aligned} \tag{53}$$

Clearly, the term

$$\begin{aligned}
&\begin{bmatrix} \tilde{\bar{F}}_i(\tilde{X}_i(t), \bar{e}_i(t), t) \\ 1 \end{bmatrix} - \frac{1}{2}\begin{bmatrix} \tilde{\bar{G}}_i(\tilde{X}_i(t), \bar{e}_i(t), t) \\ 0 \end{bmatrix} R_i^{-1} \\
&\quad \times \begin{bmatrix} \tilde{\bar{G}}_i(\tilde{X}_i(t), \bar{e}_i(t), t) \\ 0 \end{bmatrix}^T \left(\frac{\partial V(\tilde{X}_i(t), \bar{e}_i(t), t)}{\partial [\tilde{X}_i^T(t)\ \bar{e}_i^T(t)\ t]^T}\right) \\
&\quad -\frac{1}{4}\left(\frac{\partial V(\tilde{X}_i(t), \bar{e}_i(t), t)}{\partial [\tilde{X}_i^T(t)\ \bar{e}_i^T(t)\ t]^T}\right)^T \begin{bmatrix} \tilde{\bar{G}}_i(\tilde{X}_i(t), \bar{e}_i(t), t) \\ 0 \end{bmatrix} R_i^{-1} \\
&\quad \times \begin{bmatrix} \tilde{\bar{G}}_i(\tilde{X}_i(t), \bar{e}_i(t), t) \\ 0 \end{bmatrix}^T \Xi_i(\tilde{X}_i(t), \bar{e}_i(t), t) \\
&\quad + \frac{1}{2\rho_i^2}\begin{bmatrix} \tilde{\bar{D}}_i(\tilde{X}_i(t), \bar{e}_i(t), t) & 0 \\ 0 & 0 \end{bmatrix} \left(\frac{\partial V(\tilde{X}_i(t), \bar{e}_i(t), t)}{\partial [\tilde{X}_i^T(t)\ \bar{e}_i^T(t)\ t]^T}\right) \\
&\quad + \frac{1}{4\rho_i^2}\begin{bmatrix} \tilde{\bar{D}}_i(\tilde{X}_i(t), \bar{e}_i(t), t) & 0 \\ 0 & 0 \end{bmatrix} \Xi_i(\tilde{X}_i(t), \bar{e}_i(t), t) \\
&\quad + \frac{1}{2\rho_i^2}\begin{bmatrix} \tilde{\bar{F}}_{-i}(\tilde{X}_i(t), \bar{e}_i(t), t) & 0 \\ 0 & 0 \end{bmatrix} \left(\frac{\partial V(\tilde{X}_i(t), \bar{e}_i(t), t)}{\partial [\tilde{X}_i^T(t)\ \bar{e}_i^T(t)\ t]^T}\right) \\
&\quad + \frac{1}{4\rho_i^2}\begin{bmatrix} \tilde{\bar{F}}_{-i}(\tilde{X}_i(t), \bar{e}_i(t), t) & 0 \\ 0 & 0 \end{bmatrix} \Xi_i(\tilde{X}_i(t), \bar{e}_i(t), t)
\end{aligned}$$

in $\{\cdot\}$ of (53) is not equal to zero for all $\tilde{X}_i(t)$ and $\bar{e}_i(t)$. If (53) holds, $\Xi_i(\tilde{X}_i(t), \bar{e}_i(t), t)$ must approach to zero. In this situation, from (46) we know that $\left(\frac{\partial V(\tilde{X}_i(t), \bar{e}_i(t), t)}{\partial [\tilde{X}_i^T(t)\ \bar{e}_i^T(t)\ t]^T}\right)_\varepsilon \to \left(\frac{\partial V(\tilde{X}_i(t), \bar{e}_i(t), t)}{\partial [\tilde{X}_i^T(t)\ \bar{e}_i^T(t)\ t]^T}\right)$. By Theorem 1, the proposed HJIE-reinforcement learning-based DNN can output $\left(\frac{\partial V(\tilde{X}_i(t), \bar{e}_i(t), t)}{\partial [\tilde{X}_i^T(t)\ \bar{e}_i^T(t)\ t]^T}\right)$ to generate control gain $K_i^*(\hat{\tilde{X}}_i(t),\ \bar{e}_i(t))$ in (21), observer gain $L_i^*(\hat{\tilde{X}}_i(t))$ in (22), and the proposed HJIE-reinforced DNN-based observer-based control method will approach to the theoretical decentralized H_∞ attack-tolerant observer-based formation tracking control design. The proof is finished. ■

Remark 7: According to Theorem 2, we can obtain the output $\left(\frac{\partial V(\tilde{X}_i(t), \bar{e}_i(t), t)}{\partial [\tilde{X}_i^T(t) \bar{e}_i^T(t)\ t]^T}\right)$ via training DNN by HJIE-reinforcement learning-based Adam algorithm to make $\varepsilon_i(\theta_s(t))$ approach zero and then use the output to calculate the control input $u^*(t)$ and observer gain $L_i^*(\hat{\tilde{X}}_i(t))$ in the off-line training phase as shown in Fig. 4. However, we will end the phase of off-line training when $|\varepsilon_i(\theta_s(t))| \le \psi$ for a certain low value ψ or the step size of training achieves a certain number S in (42) practical applications.

Remark 8: $Y_i(t)$ can be obtained through actual satellite dynamic (3) with real external disturbance $v_i(t)$, measurement noise $n_i(t)$ and interconnected coupling effect $X_j(t - \tau_{ij}(t))$ by H_∞ observer-based attack-tolerant decentralized formation reference tracking control $u_i^*(t)$ in the on-line operation phase. The reference tracking error $\bar{e}_i(t)$ and estimation error $\tilde{\bar{X}}(t)$ are fed into the well-trained DNN to output $\left(\frac{\partial V(\tilde{X}_i(t), \bar{e}_i(t), t)}{\partial [\tilde{X}_i^T(t)\ \bar{e}_i^T(t)\ t]^T}\right)$ and generate $u_i^*(t)$ and $L_i^*(\hat{\tilde{X}}_i(t))$ for the robust decentralized H_∞ observer-based attack-tolerant formation tracking control of NCS of large-scale satellites in (3). However, the weighting parameters $\theta_s(t)$ of DNN need to be updated by HJIE-reinforcement-based Adam learning algorithm in (42)-(44) if $|\varepsilon_i(\theta_s(t))| > \psi$ during on-line operation phase, and this will not have any influence on the reinforcement learning DNN-based observer-based tracking control scheme of team formation NCS of large-scale satellites.

In the practical application of wireless transmission network, the state informations are transmitted in the form of network packets. Therefore, the following nonlinear sample-data stochastic system with a sampling time h can be used to model the satellite formation NCS in (3).

$$\begin{aligned}
S_i: \frac{X_i(t+h)}{h} &= F_i(X_i(t)) + G_i(X_i(t))u_i(t) \\
&\quad + \sum_{j \in N_i} F_{ij}(X_i(t))X_j(t - \tau_{ij}(t)) \\
&\quad + D_i(X_i(t))v_i(t) + D_a^i \gamma_a^i(t) \\
Y_i(t) &= C_i(X_i(t)) + n_i(t) + D_s^i \gamma_s^i(t)
\end{aligned} \tag{54}$$

or

$$\begin{aligned}
S_i: X_i(t+h) &= (X_i(t) + hF_i(X_i(t))) + hG_i(X_i(t))u_i(t) \\
&\quad + h\sum_{j \in N_i} F_{ij}(X_i(t))X_j(t - \tau_{ij}(t)) \\
&\quad + hD_i(X_i(t))v_i(t) + D_a^i \gamma_a^i(t), \\
Y_i(t) &= C_i(X_i(t)) + n_i(t) + D_s^i \gamma_s^i(t)
\end{aligned} \tag{55}$$

From smoothed models of actuator malicious attacks in (6) and the sensor malicious attacks in (8), the augmented system (9) can be reformulated as follows:

$$\begin{aligned}\bar{X}_i(t+h) &= (\bar{X}_i(t) + h\bar{F}_i(\bar{X}_i(t)) + h\bar{G}_i(\bar{X}_i(t))u_i(t) \\ &\quad + h\sum_{j\in N_i}\bar{F}_{ij}(\bar{X}_i(t))\bar{X}_j(t-\tau_{ij}(t)) \\ &\quad + h\bar{D}_i(\bar{X}_i(t))\bar{v}_i(t) \\ Y_i(t) &= \bar{C}_i(X) + n_i(t)\end{aligned} \tag{56}$$

Similarly, we can rewritten the observer dynamic system (10) as follows:

$$\begin{aligned}\hat{\bar{X}}_i(t+h) &= (\hat{\bar{X}}_i(t) + hF_i(\hat{\bar{X}}_i(t))) + hG_i(\hat{\bar{X}}_i(t))u_i(t) \\ &\quad + hL_i(\hat{\bar{X}}_i(t))(Y_i(t) - \hat{Y}_i(t))dt \\ \hat{Y}_i(t) &= \bar{C}_i(\hat{\bar{X}}_i(t)),\ \hat{X}_i(0) = \hat{X}_{i,0}\end{aligned} \tag{57}$$

Accordingly, the tracking error dynamic equation in (13) and state estimation error dynamic equation in (15) are modified as:

$$\begin{aligned}\bar{e}_i(t+h) &= (\bar{e}_i(t) + hF_{e,i}(\bar{e}_i(t),t)) + hG_{e,i}(\bar{e}_i(t),t)u_i(t) \\ &\quad + h\sum_{j\in N_i}F_{e,ij}(\bar{e}_i(t),t)\bar{X}_j(t-\tau_{ij}(t)) \\ &\quad + hD_{e,i}(\bar{e}_i(t),t)\bar{v}_i(t)\end{aligned} \tag{58}$$

and

$$\begin{aligned}\tilde{X}_i(t+h) &= (\tilde{X}_i(t) + h\tilde{F}_i(\tilde{X}_i(t))) + h\tilde{G}_i(\tilde{X}_i(t))u_i(t) \\ &\quad + h\sum_{j\in N_i}\tilde{F}_{ij}(\hat{\bar{X}}_i(t) + \tilde{X}_i(t))\bar{X}_j(t-\tau_{ij}(t)) \\ &\quad + h\bar{D}_i(\hat{\bar{X}}_i(t) + \tilde{X}_i(t))\bar{v}_i(t)\end{aligned} \tag{59}$$

respectively. In Fig.3, the system states are measured through the sensor. These states must be sampled in the form of network packets before transmission through the wireless network. Therefore, the system architecture can be described as a nonlinear sample-data system in (54)-(59).

IV. SIMULATION EXAMPLE

In the future 6G wireless communication era, low-orbit satellites will be developed towards a large-scale satellite constellation. In the limited space, the crossing of satellite orbits is inevitable. In the simulation example, we not only consider the position and attitude of satellites in a single orbit, but also need to consider the team formation with crossing situation of two different satellite orbits at the same height. Under proper orbit planning and stable position control, these satellites can avoid the problem of collision. In order to validate the effectiveness of the proposed robust H_∞ observer-based reinforcement learning DNN-based attack-tolerant decentralized formation reference tracking control for large-scale satellite team, a simulation of the satellite team in different orbits under external disturbance and delayed CCI coupling effect is provided in this section. Moreover, in order to demonstrate the advantages of proposed method, the H_∞ T-S fuzzy control method [29] is also employed to compare with our proposed method.

A. DESIGN SPECIFICATION

There are 10 satellites in a team with two different orbits with an inclination of 53 degrees and an altitude of 550 km as shown in Fig. 6. $\omega_{ECI,z_i} = \sqrt{\frac{u_e}{R_o}}$ is the orbital velocity, where u_e and R_o are the earth gravitational parameter and distance from the virtual leader to the earth [46], respectively. The earth gravitational parameters u_e in (1) are 398600 km^3/s^2 and $R_o = 7921\ km$. The satellite mass $m_i = 260\ kg$ and the inertia matrix $J_k^i = diag\{35, 20, 16\}kg/m^2$, $k = 1, 2, 3$, $i = 1, \ldots 10$ [47]. Besides, the step size of sample-data in (54) is chosen to be $h = 0.01\ s$ in this simulation.

Due to the thrust of malicious attack signals on the wireless network channel, a fourth order ($k = 3$) smoothed model in (6) and a fourth order smoothed model in (8) are employed to describe actuator attack signal and sensor attack signal. Extrapolation parameters are specified as $a_0 = 0.8$, $a_1 = 0.1$, $a_2 = 0.075$, $a_3 = 0.025$, $b_0 = 0.9$, $b_1 = 0.05$, $b_2 = 0.035$, and $b_3 = 0.015$.

Moreover, we also take into account environmental disturbances in satellite orbits like solar radiation pressure, earth flattening, and aerodynamic drag in (46), (47) as follows [21], [47]:

$$\begin{aligned}D_{dx}^i &= 10^{-7}(38.9\sin^2\omega_{ECI,z_i}t \\ &\quad + 7.88\cos\omega_{ECI,z_i}t\sin\omega_{ECI,z_i}t - 88.8)\ Nm \\ D_{dy}^i &= 10^{-8}(-131\sin^2\omega_{ECI,z_i}t + 833\cos^2\omega_{ECI,z_i}t \\ &\quad - 4.96\cos\omega_{ECI,z_i}t - 13.5)\ Nm \\ D_{dz}^i &= -6.28\times10^{-6}\sin\omega_{ECI,z_i}t\ Nm \\ D_{\theta_1}^i &= 0.005\sin(0.1t)\ Nm \\ D_{\theta_2}^i &= 0.005\cos(0.1t)\ Nm \\ D_{\theta_3}^i &= 0.005\sin(0.15t)\ Nm\end{aligned} \tag{60}$$

The co-channel interference (CCI) may occur among satellites. According to the property of co-channel interference, the CCI strength is related to the distance between the two transmitters. That is to say, the closer two satellites are together, the greater the impact of CCI. Therefore, CCI mainly occurs between two adjacent satellites in the formation team. In this simulation, the coupling terms are used to represent the effect of CCI on the ith satellite system as follows:

$$\begin{aligned}&F_{ij}(X_i(t))X_j(t-\tau_{ij}(t)) \\ &= [0,0,0,0.01\dot{x}_i(t)\dot{x}_j(t-0.1), 0.01\dot{y}_i(t)\dot{y}_j(t-0.1), \\ &\quad 0.01\dot{z}_i(t)\dot{z}_j(t-0.1), 0,0,0, 0.01\dot{\theta}_1^i(t)\dot{\theta}_1^j(t-0.1), \\ &\quad 0.01\dot{\theta}_2^i(t)\dot{\theta}_2^j(t-0.1), 0.01\dot{\theta}_3^i(t)\dot{\theta}_3^j(t-0.1)]^T \\ &\quad \text{for } j\neq i, j = 1,\ldots,10.\end{aligned} \tag{61}$$

where $\dot{x}_j, \dot{y}_j, \dot{z}_j, \dot{\theta}_1^j, \dot{\theta}_2^j, \dot{\theta}_3^j$ denote the CCI effect caused by the jth neighboring satellite on the ith satellite.

For the robust H_∞ observer-based attack-tolerant decentralized team formation tracking control strategy in (18), the weighting matrices $Q_{1,i}, Q_{2,i}, R_i$ and the prescribed

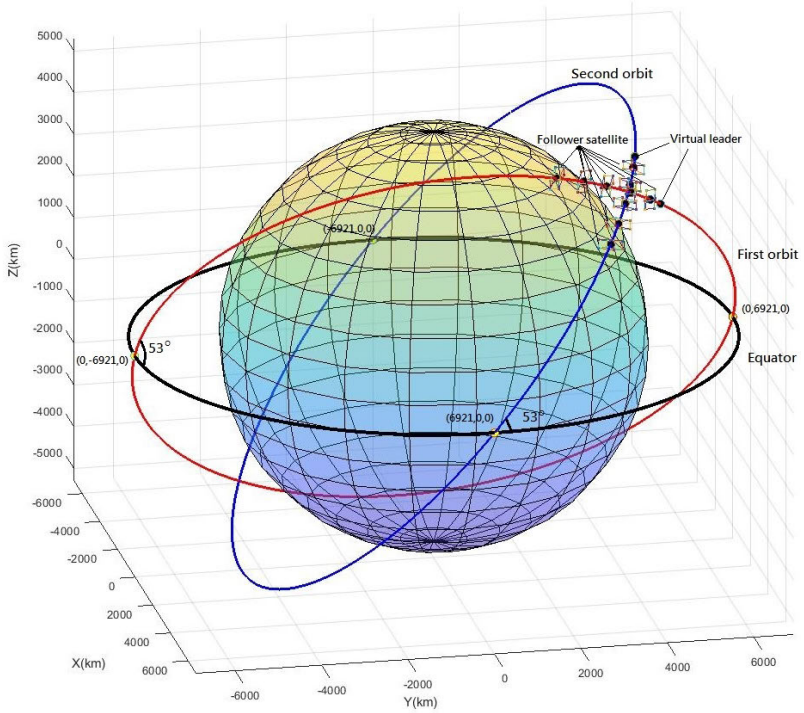

FIGURE 6. A team with 10 LEO satellites with crossing situation of two different orbits for some mission in ECI frame.

attenuated level ρ_i are specified for some mission as follows:

$$\begin{aligned} Q_{1,i} &= diag\{1,1,1,10^{-3},10^{-3},10^{-3},1,1,1,\\ &\qquad 10^{-3},10^{-3},10^{-3}\}\\ Q_{2,i} &= diag\{1,1,1,1,1,1,1,1,1,1,1,10^{-3},10^{-3},\\ &\qquad 10^{-3},1,1,1,10^{-3},10^{-3},10^{-3}\}\\ R_i &= diag\{1,1,1,1,1,1\}\\ \rho_i &= 2 \end{aligned} \tag{62}$$

In this simulation, the virtual leader of one orbit is along the inclination angle of 53 degrees and intersects the equator at two points (0,-6921,0) and (0,6921,0) of ECI frame, and the other virtual leader is along the inclination angle of 53 degrees and the intersection with the equator at the two points (-6921,0,0) and (6921,0,0) of ECI frame as shown in the Fig. 6. In the satellite attitude for some task, the desired attitude reference trajectory is specified as follows [47]:

$$\theta^i_{r_1}(t) = \begin{cases} \frac{4}{3}\pi\frac{t}{t_f}, & \text{for } t < \frac{t_f}{4}\\ \frac{\pi}{3}, & \text{for } \frac{t_f}{4} \le t < \frac{3t_f}{4}\\ -\frac{4}{3}\pi\frac{t}{t_f}+\frac{4}{3}\pi, & \text{for } \frac{3t_f}{4} \le t < t_f \end{cases}$$

$$\theta^i_{r_2}(t) = \begin{cases} \pi\frac{t}{t_f}, & \text{for } t < \frac{t_f}{4}\\ -\pi\frac{t}{t_f}+\frac{\pi}{2}, & \text{for } \frac{t_f}{4} \le t < \frac{3t_f}{4}\\ \pi\frac{t}{t_f}-\pi, & \text{for } \frac{3t_f}{4} \le t < t_f \end{cases}$$

TABLE 1. The reference states of 10 LEO satellites of a team formation for some mission in two orbits in simulation.

Satellite	The reference $r_i(t)$
$Satellite1$	$r_1(t) = [50,0,0,0,0,0,0,\theta^1_{r_1},\theta^1_{r_2},\theta^1_{r_3}]^T$
$Satellite2$	$r_2(t) = [675,0,0,0,0,0,0,\theta^2_{r_1},\theta^2_{r_2},\theta^2_{r_3}]^T$
$Satellite3$	$r_3(t) = [1300,0,0,0,0,0,0,\theta^3_{r_1},\theta^3_{r_2},\theta^3_{r_3}]^T$
$Satellite4$	$r_4(t) = [1925,0,0,0,0,0,0,\theta^4_{r_1},\theta^4_{r_2},\theta^4_{r_3}]^T$
$Satellite5$	$r_5(t) = [2550,0,0,0,0,0,0,\theta^5_{r_1},\theta^5_{r_2},\theta^5_{r_3}]^T$
$Satellite6$	$r_6(t) = [50,0,0,0,0,0,0,\theta^6_{r_1},\theta^6_{r_2},\theta^6_{r_3}]^T$
$Satellite7$	$r_7(t) = [675,0,0,0,0,0,0,\theta^7_{r_1},\theta^7_{r_2},\theta^7_{r_3}]^T$
$Satellite8$	$r_8(t) = [1300,0,0,0,0,0,0,\theta^8_{r_1},\theta^8_{r_2},\theta^8_{r_3}]^T$
$Satellite9$	$r_9(t) = [1925,0,0,0,0,0,0,\theta^9_{r_1},\theta^9_{r_2},\theta^9_{r_3}]^T$
$Satellite10$	$r_{10}(t) = [2550,0,0,0,0,0,0,\theta^{10}_{r_1},\theta^{10}_{r_2},\theta^{10}_{r_3}]^T$

$$\theta^i_{r_3}(t) = \begin{cases} \frac{4}{3}\pi\frac{t}{t_f}, & \text{for } t < \frac{t_f}{4}\\ \frac{\pi}{3}, & \text{for } \frac{t_f}{4} \le t < \frac{3t_f}{4}\\ -\frac{4}{3}\pi\frac{t}{t_f}+\frac{4}{3}\pi, & \text{for } \frac{3t_f}{4} \le t < t_f \end{cases} \tag{63}$$

for $i = 1,\ldots,10$, $k = 1,2,3$, and t_f is the terminal time.

In a large-scale LEO satellite team formation, each orbiting satellite will maintain a certain distance and attitude from the virtual leader to form a line-shaped satellite formation. For the convenience of observation and the consideration of the limitation of communication distance, we choose five follower satellites in each orbit. The reference state $r_i(t)$ of each satellite in the team are given as Table 1, and the initial states are given in Table 2.

TABLE 2. The initial states of 10 LEO satellites in the team formation in the simulation.

Satellite	The initial conditions
$Satellite1$	$X_1(0) = [54.9527, 0.5002, 0.3984, 0, 0, 0, 0.3017, 0.3314, -0.4986, 0, 0, 0]^T$
$Satellite2$	$X_2(0) = [671.5324, 3.2331, -1.7468, 0, 0, 0, 0.4724, -0.2885, -0.2675, 0, 0, 0]^T$
$Satellite3$	$X_3(0) = [1304.2578, 2.4571, 4.2579, 0, 0, 0, -0.5012, 0.8369, 0.3695, 0, 0, 0]^T$
$Satellite4$	$X_4(0) = [1931.7621, -6.7234, -2.1409, 0, 0, 0, -0.6251, -0.7723, 0.5506, 0, 0, 0]^T$
$Satellite5$	$X_5(0) = [2544.8354, -4.4710, 5.5519, 0, 0, 0, 0.9635, -0.1463, 0.6997, 0, 0, 0]^T$
$Satellite6$	$X_6(0) = [52.9475, -2.2114, 5.0472, 0, 0, 0, 0.3779, 0.7030, 0.3399, 0, 0, 0]^T$
$Satellite7$	$X_7(0) = [668.7789, 4.2581, -4.6837, 0, 0, 0, -0.4410, 0.3678, 0.5238, 0, 0, 0]^T$
$Satellite8$	$X_8(0) = [1294.2156, 4.2581, -4.6837, 0, 0, 0, 0.5102, -0.3260, 0.6367, 0, 0, 0]^T$
$Satellite9$	$X_9(0) = [1920.5293, 3.6211, 0.3785, 0, 0, 0, 0.8671, -0.1682, -0.3263, 0, 0, 0]^T$
$Satellite10$	$X_{10}(0) = [2555.5965, -5.6028, 2.0263, 0, 0, 0, 0.3258, -0.5563, -0.2769, 0, 0, 0]^T$

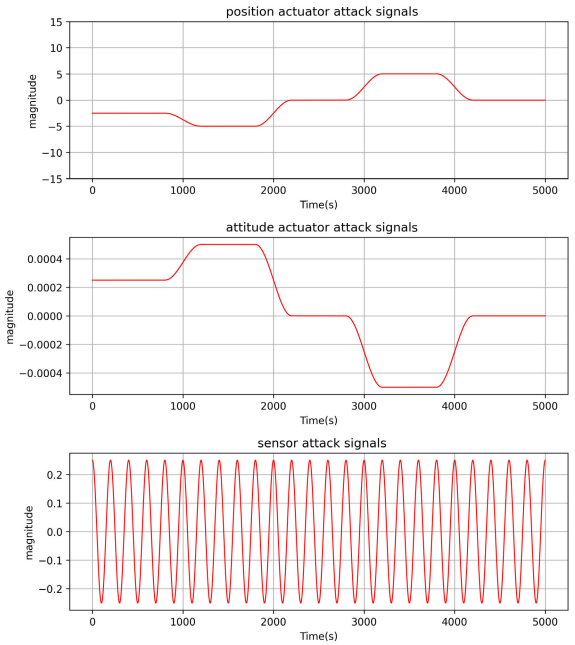

FIGURE 7. The actuator attack signal $\gamma_a^i(t)$ and sensor attack signal $\gamma_s^i(t)$ in each satellite NCS in the team.

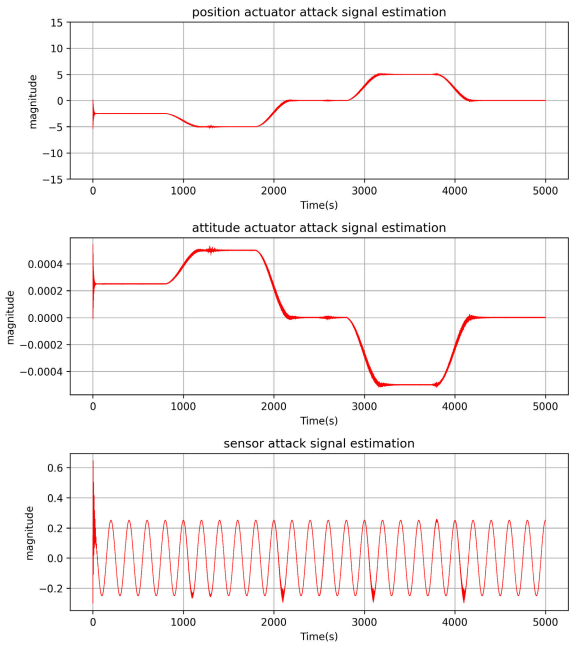

FIGURE 8. The estimations of actuator attack signals and sensor attack signals by the proposed decentralized H_∞ attack-tolerant Luenberger-type observers in (10) of 10 satellites in the team.

According to Theorem 1, in order to achieve the robust H_∞ decentralized observer-based attack-tolerant formation tracking control strategy in (18), we need to solve the $HJIE_i$ for H_∞ control gain $K_i(\hat{\hat{X}}_i(t), \bar{e}_i(t))$ in (21) and H_∞ observer gain $L_i^*(\hat{\hat{X}}_i(t))$ in (22) for the observer-based reference tracking control of the ith satellite in (17). With the help of reinforcement learning-based DNN, the solutions $\left(\frac{\partial V(\tilde{X}_i(t),\bar{e}_i(t),t)}{\partial[\tilde{X}_i^T(t)\ \bar{e}_i^T(t)\ t]^T}\right)$ of $HJIE_i$ can be outputted from the trained DNN via the HJIE-reinforcement Adam learning algorithm in the off-line training phase, then $\left(\frac{\partial V(\tilde{X}_i(t),\bar{e}_i(t),t)}{\partial[\tilde{X}_i^T(t)\bar{e}_i^T(t)\ t]^T}\right)$ can be used to calculate the control input, the observer gain in the on-line operation phase. Therefore, the decentralized H_∞ attack-tolerant observer-based reference tracking control strategy of team formation tracking of 10 satellites can be achieved.

The architecture of DNN consists of one input layer with inputs $\tilde{X}_i(t)$ and $\bar{e}_i(t)$, four feedforward hidden layers, four batch normalization layers and one output layer to be trained by HJIE-reinforcement Adam learning algorithm to output the desired output $\left(\frac{\partial V(\tilde{X}_i(t),\bar{e}_i(t),t)}{\partial[\tilde{X}_i^T(t)\bar{e}_i^T(t)\ t]^T}\right)$. Each hidden layer has 128, 256, 64, and 32 neurons, sequentially. The parameters of the Adam learning algorithm in (42), (43) and (44) are set as $\alpha_1 = 0.9$, $\alpha_2 = 0.999$, $\psi = 10^{-3}$, $\lambda = 10^{-7}$. Training steps S is set as 30, and batch size P is 800. In the off-line training phase, 20000 initial tracking errors $\bar{e}_i(0)$ and estimation errors $\tilde{X}_i(0)$ are randomly selected around the origin $X_i(0)$.

B. SIMULATION RESULT

In the results of this simulation, the 10 LEO satellites in orbit should be able to be decentralized controlled to efficiently attenuate the effect of external disturbance, measurement noise, CCI coupling and attack signals to maintain a specific distance from the leader satellite and make attitude changes

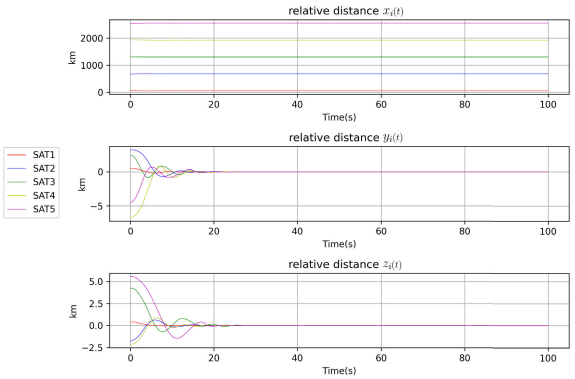

FIGURE 9. The relative distance tracking trajectories of the first five satellites in the first orbit team formation system in 100 seconds. The effect of external disturbance, measurement noise, malicious attack signal and delayed coupling caused by adjacent satellites can be efficiently attenuated by the proposed robust decentralized H_∞ observer-based attack-tolerant team formation tracking control strategy via HJIE-reinforcement learning-based DNN scheme by Adam learning algorithm.

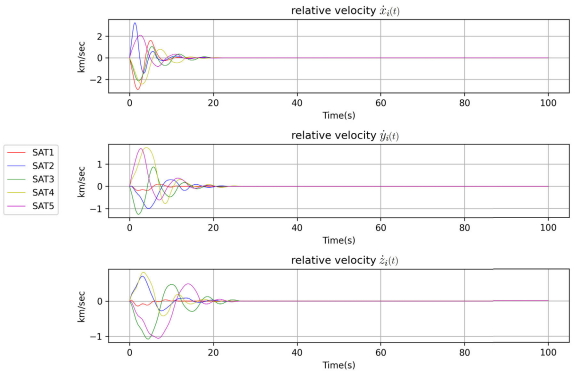

FIGURE 10. The relative velocity tracking trajectories of the first five satellites in the first orbit of team formation system in 100 seconds. The effect of external disturbance, measurement noise, malicious attack signal and delayed coupling caused by adjacent satellites on each satellite can be efficiently attenuated by the proposed robust decentralized H_∞ observer-based attack-tolerant team formation tracking control strategy via reinforcement learning-based DNN scheme by Adam learning algorithm.

according to their desired mission in Table 1. The satellite network control system will suffer from malicious attack signals in the wireless transmission channel when receiving and sending state and control information. The equivalent actuator attack signal $\gamma_a^i(t)$ and sensor attack signal $\gamma_s^i(t)$ of each satellite in the team are shown in Fig. 7, and the estimated actuator attack signal and sensor attack signal are shown in Fig. 8. Due to the large initial state, the initial estimation error is also large for each satellite, too. After the transient state, the attack signals can be estimated precisely by the proposed robust H_∞ attack-tolerant decentralized observer for the compensation of their effect. For the structure of Luenberger-type observer in (10), the estimation $\hat{X}_i(t)$ of state variables $X_i(t)$ of the ith satellite is influenced by the sensor attack signal corrupted on $Y_i(t)$. Therefore, the estimation of the actuator attack signal is slightly fluctuated by the effect of sensor attack signal. Although there is a

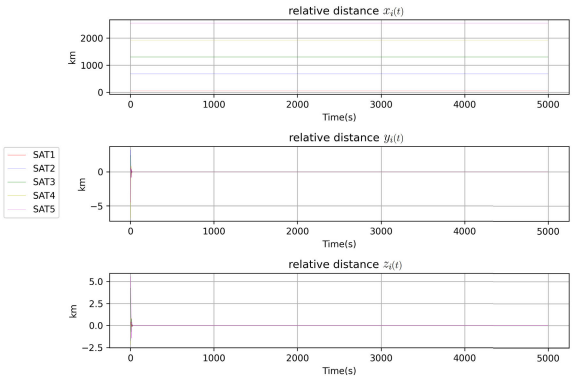

FIGURE 11. The relative distance tracking trajectories of the first five satellites of the formation team in the first orbit in 5000 seconds. The effect of external disturbance, measurement noise, malicious attack signal and delayed coupling caused by adjacent satellites on each satellite can be efficiently attenuated by the proposed robust decentralized H_∞ observer-based attack-tolerant team formation tracking control strategy via HJIE-reinforcement learning-based DNN scheme by Adam algorithm.

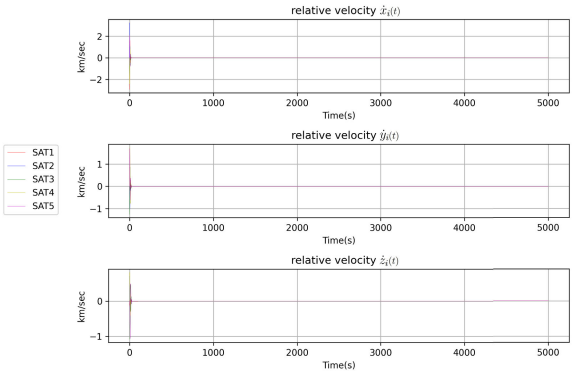

FIGURE 12. The relative velocity tracking trajectories of the first five satellites of the formation team in the first orbit in 5000 seconds. The effect of external disturbance, measurement noise, malicious attack signal and delayed coupling caused by adjacent satellites of five satellites can be efficiently attenuated by the proposed robust decentralized H_∞ observer-based attack-tolerant team formation tracking control strategy via reinforcement learning-based DNN scheme through Adam learning algorithm.

small estimation error, the estimated attack signal can be effectively fedback to eliminate the effect of actuator attack signal on control signal and sensor attack signal on state estimation.

The tracking trajectories of relative position and relative velocity of the follower satellites are given in Fig. 9 and Fig. 10 within 100 seconds, respectively. Under the influence of transient response of initial conditions, the relative position of each satellite can reach a desired steady state within 30 seconds under malicious attack signal, internal connection coupling, external interference and measurement noise. Fig. 11 and Fig. 12 show the relative position state and relative velocity state of each follower satellite for up to 5000 seconds, respectively. It can be seen that the relative position of the satellite team formation can be kept the desired

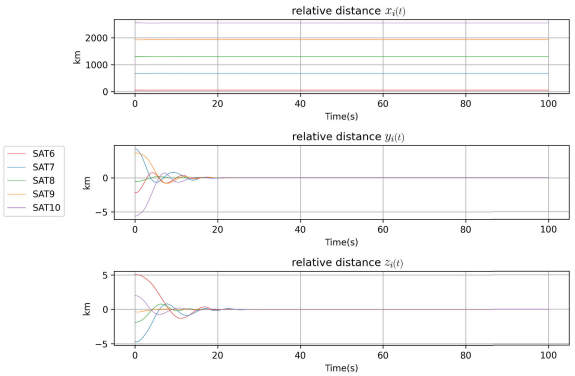

FIGURE 13. The relative distance tracking trajectories of the last five satellites in the second orbit formation system in 100 seconds. The effect of external disturbance, measurement noise, malicious attack signal and delayed coupling caused by adjacent satellites on each satellite can be efficiently attenuated by the proposed robust decentralized H_∞ observer-based attack-tolerant team formation tracking control strategy via reinforcement learning-based DNN scheme by Adam learning algorithm.

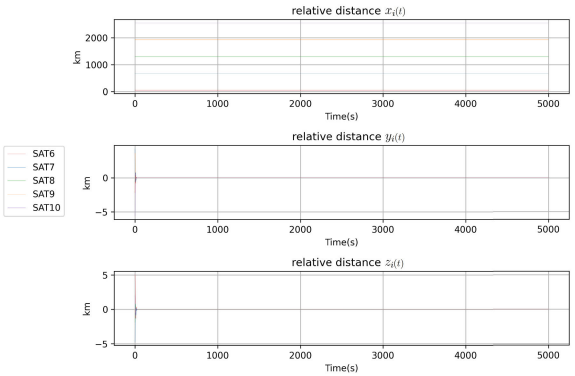

FIGURE 15. The relative distance tracking trajectories of the last five satellites in the second orbit of team formation in 5000 seconds. The effect of external disturbance, measurement noise, malicious attack signal and delayed coupling caused by adjacent satellites on each satellite can be efficiently attenuated by the proposed robust decentralized H_∞ observer-based attack-tolerant team formation tracking control strategy via reinforcement learning-based DNN scheme through Adam learning algorithm.

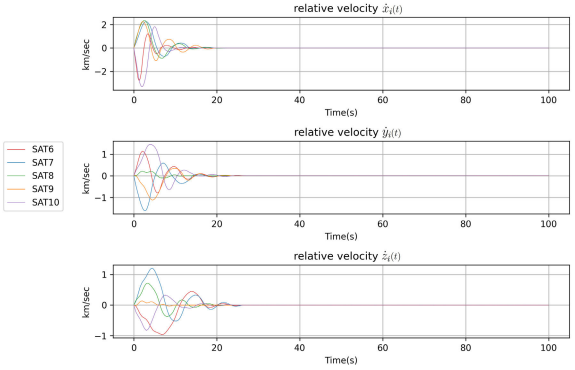

FIGURE 14. The relative velocity tracking trajectories of the last five satellites in the second orbit formation system in 100 seconds. The effect of external disturbance, measurement noise, malicious attack signal and delayed coupling caused by adjacent satellites of five satellites can be efficiently attenuated by the proposed robust decentralized H_∞ observer-based attack-tolerant team formation tracking control strategy via reinforcement learning-based DNN scheme by Adam learning algorithm.

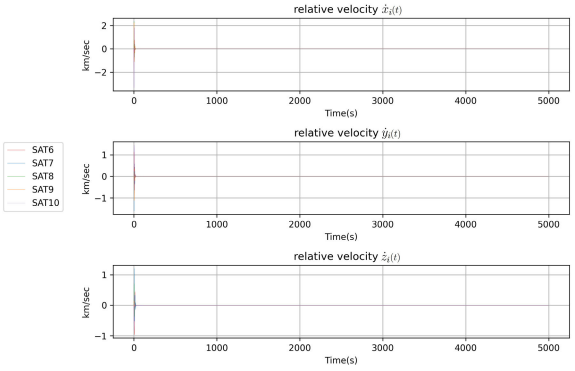

FIGURE 16. The relative velocity tracking trajectories of the last five satellites in the second orbit of team formation in 5000 seconds. The effect of external disturbance, measurement noise, malicious attack signal and delayed coupling caused by adjacent satellites on each satellite can be efficiently attenuated by the proposed robust decentralized H_∞ observer-based attack-tolerant team formation tracking control strategy via reinforcement learning-based DNN scheme through Adam learning algorithm.

team formation during the period of the satellite orbiting around the earth. The positions and velocity states of the last five satellites in another orbit are shown in Fig. 13-Fig. 16, respectively.

During the satellite orbiting process, the desired attitude angular of each satellite is time-varying for some specified missions. The attitude tracking trajectories of the satellite angle and the attitude tracking trajectory of the angular velocity of first five satellites in the first orbit are given in Fig. 17 and Fig. 18, respectively. From the simulation results under the influence of malicious attack signal, internal connection coupling, external interference and measurement noise, the attitude of each satellite can reach the relative angular we specified within 50 seconds. In addition, when the reference attitude angular changes, the relative angular error of the follower satellites can also converge rapidly. The attitude states of the last five satellites in another orbit are shown in Fig. 19-Fig. 20.

For the convenience of illustration, Fig. 21 shows the snapshots of the 10-satellite team in two-orbit under the Earth-Centered-Inertial frame. In the beginning, all satellites are scattered around two-orbits and have different initial attitude angles. After 100 seconds, follower satellites can maintain the desired relative distances and specific relative attitude angular in the team formation. Namely, the satellite team can operate on the two orbits. When t=1820, the satellite team flies to the crossing area of the two different orbits. Under the decentralized H_∞ attack-tolerant position control, the follower satellites in two different orbits can pass through without collision. At t=5000, the satellite team formation can still maintain a desired relative position and relative attitude angular.

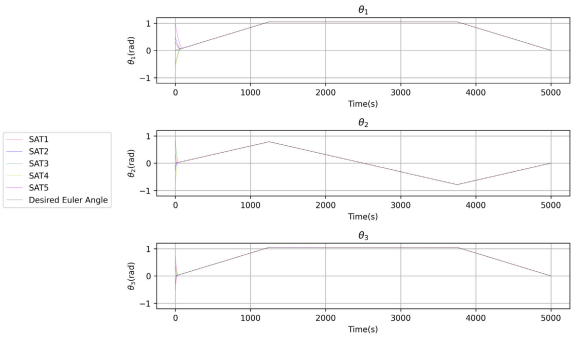

FIGURE 17. The relative angular tracking trajectories of the first five satellites in the first orbit formation in 5000 seconds. The effect of external disturbance, measurement noise, malicious attack signal and delayed coupling caused by adjacent satellites on each satellite can be efficiently attenuated by the proposed robust decentralized H_∞ observer-based attack-tolerant team formation tracking control strategy via reinforcement learning-based DNN scheme by Adam learning algorithm.

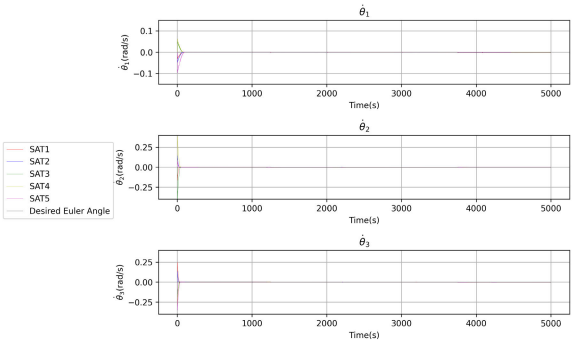

FIGURE 18. The relative angle velocity tracking trajectories of the first five satellites in the first orbit of team formation in 5000 seconds. The effect of external disturbance, measurement noise, malicious attack signal and delayed coupling from adjacent satellites of five satellites can be efficiently attenuated by the proposed robust decentralized H_∞ observer-based attack-tolerant team formation tracking control strategy via reinforcement learning-based DNN scheme by Adam learning algorithm.

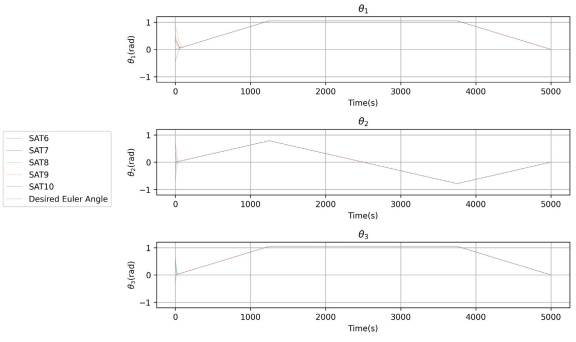

FIGURE 19. The relative angular tracking trajectories of the last five satellites in the second orbit formation system in 5000 seconds. The effect of external disturbance, measurement noise, malicious attack signal and delayed coupling caused by adjacent satellites on each satellite can be efficiently attenuated by the proposed robust decentralized H_∞ observer-based attack-tolerant team formation tracking control strategy via reinforcement learning-based DNN approach via Adam learning algorithm.

Fig. 22 shows the control inputs for the 1st and 5th satellites in the team. The position estimation error and

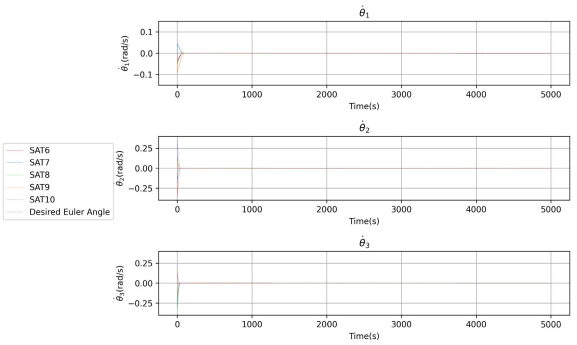

FIGURE 20. The relative angle velocity tracking trajectories of the last five satellites in the second orbit of team formation in 5000 seconds. The effect of external disturbance, measurement noise, malicious attack signal and delayed coupling caused by adjacent satellites on each satellite can be efficiently attenuated by the proposed robust decentralized H_∞ observer-based attack-tolerant team formation tracking control strategy via reinforcement learning-based DNN scheme through Adam learning algorithm.

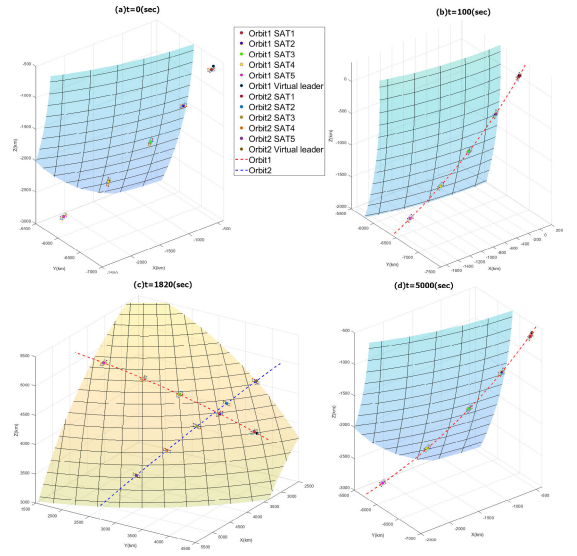

FIGURE 21. The snapshots of the proposed robust H_∞ observer-based attack-tolerant reinforcement learning DNN-based decentralized team formation tracking control scheme of 10 satellite. The two-orbit formation shape of 10 satellite formation team in the orbital flighting process is shown at (a) t = 0(sec), (b) t = 100(sec), (c) t = 1820(sec) and (d) t = 5000(sec), respectively.

attitude estimation error of the first satellite are shown in Fig. 23 and Fig. 24, respectively. In Fig. 22, due to the change of the reference attitude and the influence of coupling and external environment interference, the control input on the attitude has slightly jittery. Moreover, it can be found that when a malicious attack occurs, the control input will change the amplitude to compensate for the impact of the malicious attack. According to the simulation results, it can be validated that under the proposed robust H_∞ observer-based attack-tolerant reinforcement learning DNN-based control strategy, the satellite team formation can achieve the desired formation shape and attitude under malicious attack signal, external disturbance, measurement noise and delayed coupling effect.

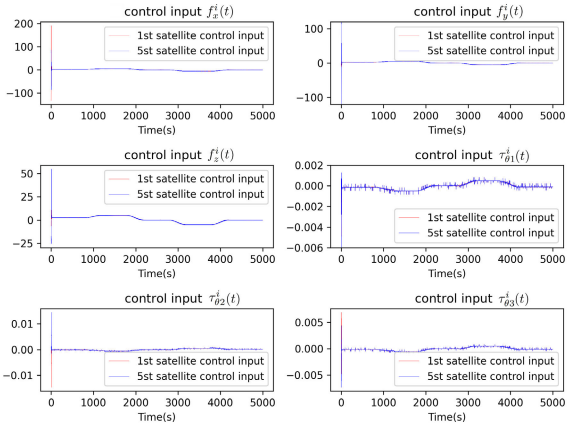

FIGURE 22. The control inputs $u_i(t) = [f_x^i(t), f_y^i(t), f_z^i(t), \tau_{\theta 1}^i, \tau_{\theta 2}^i, \tau_{\theta 3}^i]^T$ in (3) for the 1th and 5th satellite (i.e.,i = 1,5) of 10-satellite formation team by the proposed robust H_∞ observer-based attack-tolerant HJIE-reinforcement learning DNN-based decentralized team formation tracking control scheme.

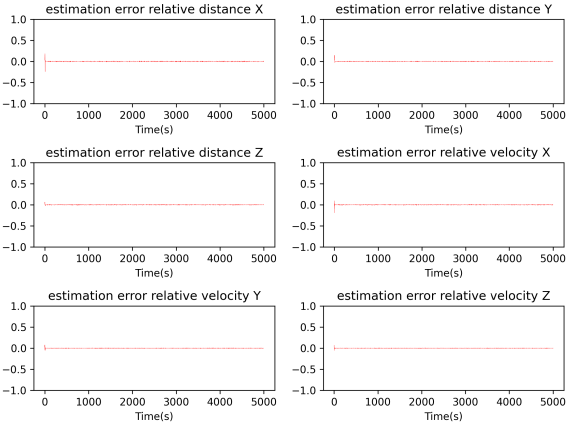

FIGURE 23. The position estimation error of the first satellite by the proposed robust H_∞ observer-based attack-tolerant reinforcement learning DNN-based decentralized team formation tracking control scheme.

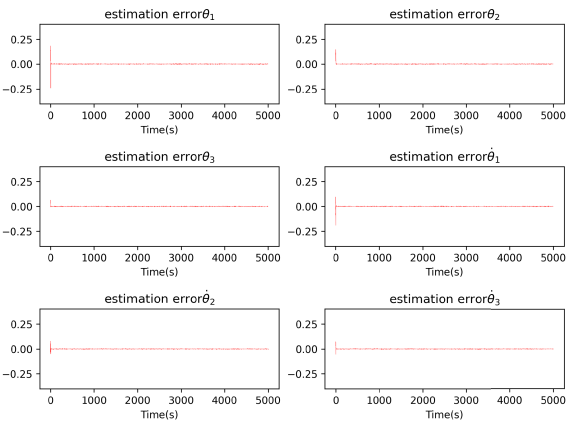

FIGURE 24. The attitude estimation error of the first satellite by the proposed robust H_∞ observer-based attack-tolerant reinforcement learning DNN-based decentralized team formation tracking control scheme.

The real average H_∞ observer-based attack-tolerant team formation tracking performance of 10 satellites in the team

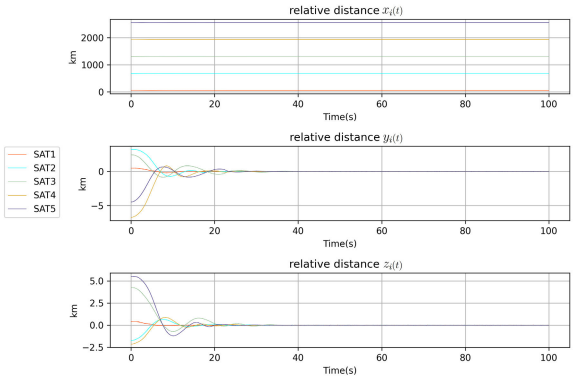

FIGURE 25. The relative distance tracking trajectories of the first five satellites in the first orbit team formation by H_∞ T-S fuzzy control strategy in 100 seconds [29].

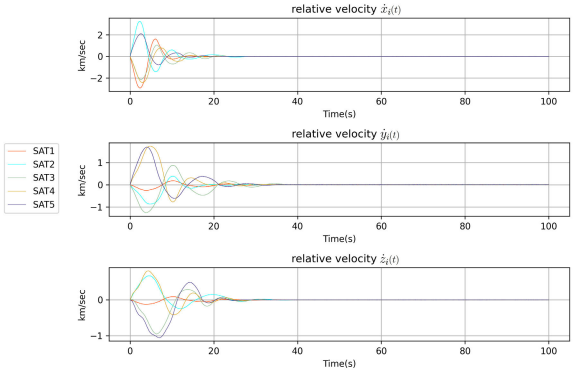

FIGURE 26. The relative velocity tracking trajectories of the first five satellites in the first orbit of team formation by H_∞ T-S fuzzy control strategy in 100 seconds [29].

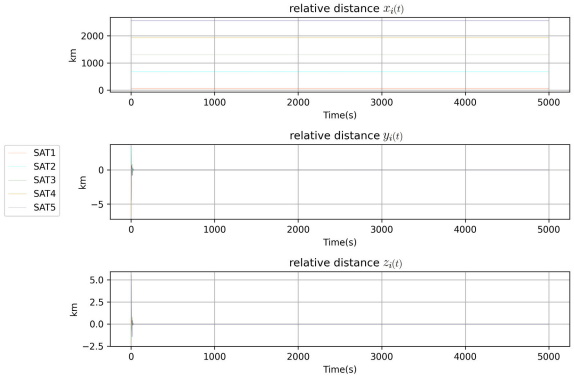

FIGURE 27. The relative distance tracking trajectories of the first five satellites of the formation team in the first orbit by H_∞ T-S fuzzy control strategy in 5000 seconds.

formation satellite system is calculated as:

$$(1/10)\sum_{i=1}^{10} \times \frac{\{\int_0^{5000} \tilde{\tilde{X}}^T(t)\tilde{Q}_i\tilde{\tilde{X}}(t) + u_i(t)^T R_i u_i(t)dt - V(\tilde{\tilde{X}}_i(0),0)\}}{\{\int_0^{5000}(\tilde{\tilde{v}}_i^T(t)\tilde{\tilde{v}}_i(t) + \tilde{\tilde{X}}_{-i}^T(t-\tau_{-i}(t))\tilde{\tilde{X}}_{-i}(t-\tau_{-i}(t)))dt\}} = (1.76)^2 \le 2^2 \quad (64)$$

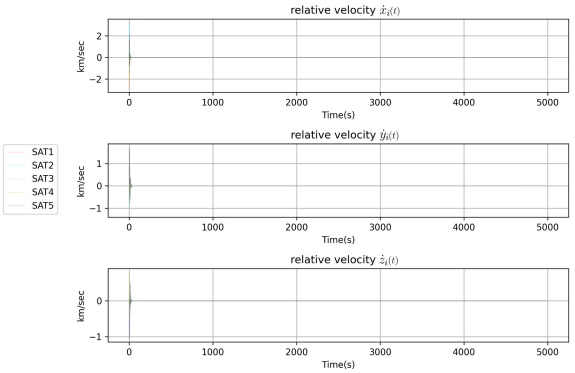

FIGURE 28. The relative velocity tracking trajectories of the first five satellites of the formation team in the first orbit by H_∞ T-S fuzzy control strategy in 5000 seconds.

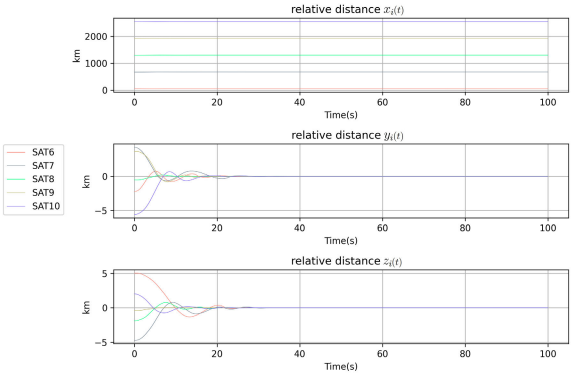

FIGURE 29. The relative distance tracking trajectories of the last five satellites in the second orbit formation by H_∞ T-S fuzzy control strategy in 100 seconds.

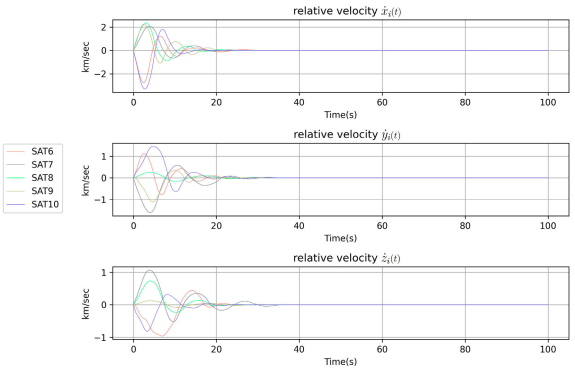

FIGURE 30. The relative velocity tracking trajectories of the last five satellites in the second orbit formation by H_∞ T-S fuzzy control strategy in 100 seconds.

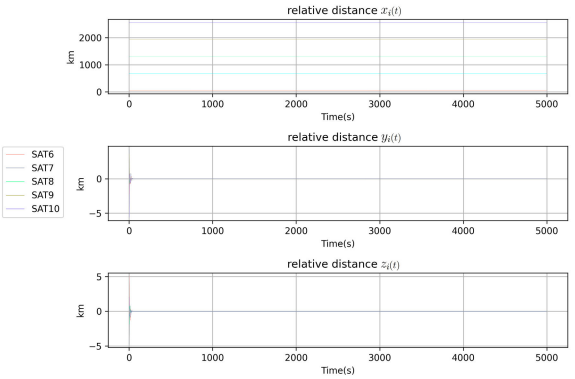

FIGURE 31. The relative distance tracking trajectories of the last five satellites in the second orbit of team formation by H_∞ T-S fuzzy control strategy in 5000 seconds.

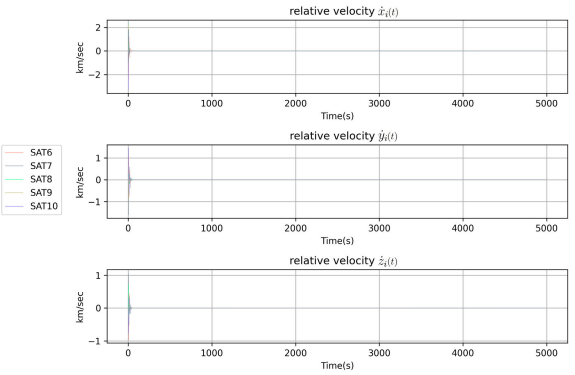

FIGURE 32. The relative velocity tracking trajectories of the last five satellites in the second orbit of team formation by H_∞ T-S fuzzy control strategy in 5000 seconds.

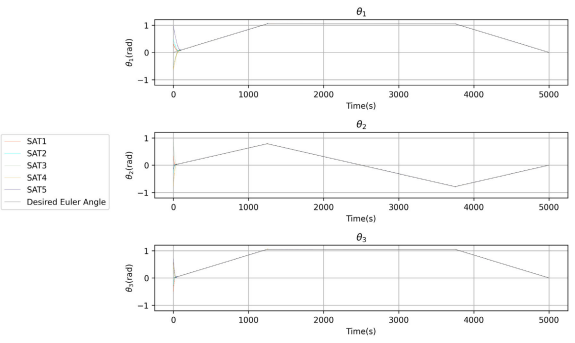

FIGURE 33. The relative angular tracking trajectories of the first five satellites in the first orbit formation by H_∞ T-S fuzzy control strategy in 5000 seconds.

C. COMPARISON RESULT AND DISCUSSION

In this subsection, the H_∞ T-S fuzzy control strategy [29] is employed to simulate the satellite formation control under the same desired formation shape.

By the H_∞ T-S fuzzy control strategy, the tracking trajectory of relative position and relative velocity of the follower satellites are given in Fig. 25-Fig. 32, and the attitude tracking trajectory of the follower satellite angle and the attitude tracking trajectory of the angular velocity are given in Fig. 33-Fig. 36. Fig. 37 shows the control inputs for the 1st and 5th satellites in the team. From the above simulation results, we can know that the H_∞ T-S fuzzy control takes a longer time to enter the steady state, and is also more affected by external disturbance when compared with our proposed method. This is because fuzzy control solves linear matrix inequalities instead of directly solving HJIEs, which leads to a very conservative result. The converting of LMIs by a series of inequality operations and the quadratic

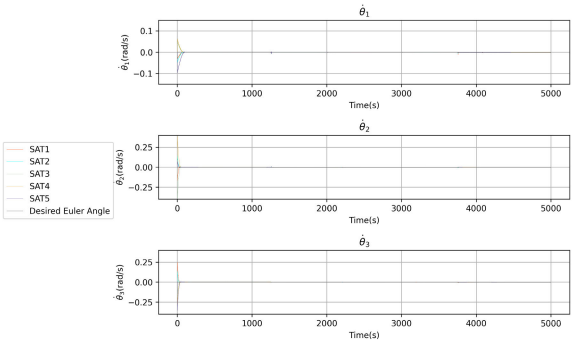

FIGURE 34. The relative velocity tracking trajectories of the first five satellites in the first orbit of team formation by H_∞ T-S fuzzy control strategy in 5000 seconds.

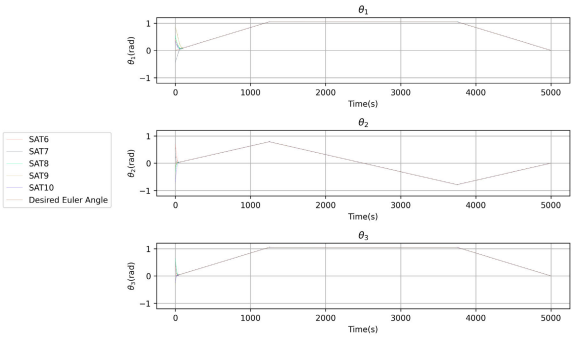

FIGURE 35. The relative angular tracking trajectories of the last five satellites in the second orbit formation by H_∞ T-S fuzzy control strategy in 5000 seconds.

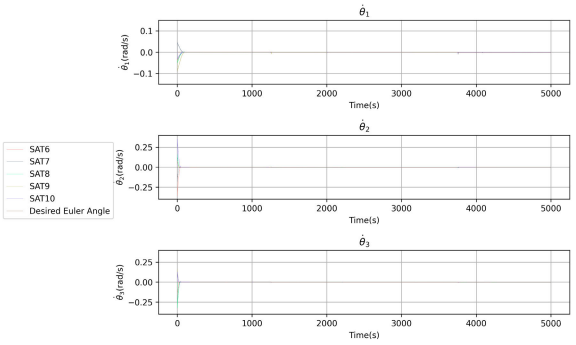

FIGURE 36. The relative velocity tracking trajectories of the last five satellites in the second orbit of team formation by H_∞ T-S fuzzy control strategy in 5000 seconds.

Lyapunov $V(\tilde{X}_i(t), \bar{e}_i(t), t) = \tilde{X}_i^T(t)P_1\tilde{X}_i(t) + \bar{e}_i^T(t)P_2\bar{e}_i(t)$ will make the results more conservative. In addition, the approximating nonlinear system with interpolation from local linear systems will generate interpolation errors and degrade control performance. The real tracking control performance of the H_∞ T-S fuzzy formation tracking control design is also calculated as $\rho_i^* = 5.21$ which is poor than the proposed method. Further, it needs to calculate a very complicated T-S fuzzy observer-based tracking control law at every time instant, in which 4096 local linearized observer-based control laws are interpolated by fuzzy base to approach the nonlinear

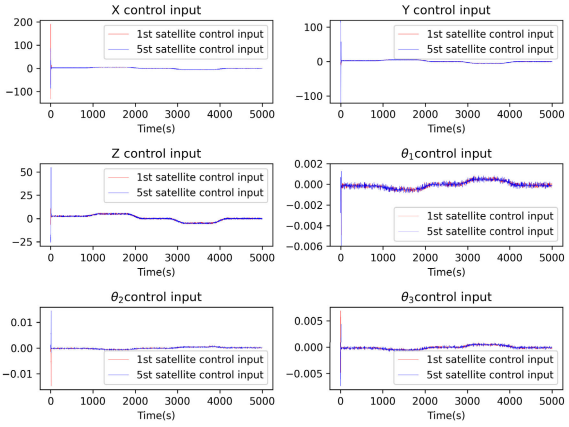

FIGURE 37. The control inputs for the 1th and 5th satellite of 10-satellite formation team by the H_∞ T-S fuzzy control strategy.

observer-based control law in (10), and makes it not easy for practical applications at present.

V. CONCLUSION

In this paper, a robust H_∞ attack-tolerant decentralized observer-based formation tracking control strategy is proposed for a large-scale team formation satellite NCS with the consideration of external disturbance, measurement noise, coupling effect and attack signals from the wireless communication channel. By using smoothed models to describe the behaviors of attack signals, the conventional Luenberger observer is used to estimate system state of each satellite and the attack signals on sensors and actuators for compensation to avoid their corruption, and through the robust decentralized H_∞ observer-based reference tracking control method, the influence of external disturbance, measurement noise and coupling from other satellites on the estimation error and tracking error of each satellite in the team formation system is reduced to a desired attenuation level. From the energy perspective, the robust H_∞ attack-tolerant decentralized observer-based reference tracking control of large-scale team formation satellite NCS can efficiently attenuate effects of the external disturbance, measurement noise and interconnected coupling effect under a prescribed disturbance attenuation level. Consequently, the robust H_∞ decentralized observer-based attack-tolerant control design of team formation of large-scale satellites can be transformed into a problem of solving a decoupled set of highly nonlinear partial differential HJIEs for each satellite in the team. We incorporate reinforcement learning-based DNN with the robust H_∞ attack-tolerant decentralized observer-based tracking control strategy into co-design to solve a control-observer-coupled HJIE for each satellite of the formation team. By training HJIE-reinforcement-learning-based-DNN by Adam learning algorithm, control-observer-coupled HJIE of the robust H_∞ decentralized observer-based attack-tolerant control strategy can be solved for each satellite to achieve the desired team formation tracking control. Moreover, it has been

demonstrated that the proposed DNN-based observer-based reference tracking control scheme can achieve the theoretical robust decentralized H_∞ observer-based reference tracking control strategy of large-scale satellite team formation system in the low earth orbit with external disturbance, malicious attack signal, coupling effect and measurement noise if the error of HJIE approximated by the proposed reinforcement learning-based DNN can approach to zero. The main advantages of HJIE-reinforcement deep learning approach are two-fold: (1) HJIE-reinforcement deep learning approach can directly solve the general solution from HJIE in (25) for H_∞ control law in (21) and observer law in (22) unlike the conventional T-S fuzzy method and global linearization method can only solve a conservative quadratic Lyapunov solution from HJIE in (25). (2) We don't need to compute very complicated L^2 interpolatory control law and observer law at every time instant when nonlinear stochastic system in (3) is interpolated by L local linear systems via T-S fuzzy method [29] and global linearization method [30]. So the proposed HJIE-reinforcement method can save much computation time. A simulation example of 10-LEO satellite formation in two-crossing orbits is given to validate the effectiveness of proposed method with comparison. 10 LEO satellites in two different orbits of the team formation can maintain the desired relative distance and attitude during flight under the influence of external disturbances, measurement noise, CCI coupling from other satellites and attack signals through wireless communication channel.

REFERENCES

[1] G. Liu and S. Zhang, "A survey on formation control of small satellites," *Proc. IEEE*, vol. 106, no. 3, pp. 440–457, Mar. 2018.

[2] S. Ren, X. Yang, R. Wang, S. Liu, and X. Sun, "The interaction between the LEO satellite constellation and the space debris environment," *Appl. Sci.*, vol. 11, no. 20, p. 9490, Oct. 2021.

[3] A. U. Chaudhry and H. Yanikomeroglu, "Laser intersatellite links in a starlink constellation: A classification and analysis," *IEEE Veh. Technol. Mag.*, vol. 16, no. 2, pp. 48–56, Jun. 2021.

[4] D. P. Scharf, F. Y. Hadaegh, and S. R. Ploen, "A survey of spacecraft formation flying guidance and control (part 1): Guidance," in *Proc. Amer. Control Conf.*, 2003, pp. 1733–1739.

[5] P. K. C. Wang and F. Y. Hadaegh, "Minimum-fuel formation reconfiguration of multiple free-flying spacecraft," *J. Astron. Sci.*, vol. 47, nos. 1–2, pp. 77–102, Mar. 1999.

[6] A. Essghaier, L. Beji, M. A. E. Kamel, A. Abichou, and J. Lerbet, "Co-leaders and a flexible virtual structure based formation motion control," *Int. J. Vehicle Auto. Syst.*, vol. 9, nos. 1–2, p. 108, 2011.

[7] R. W. Beard, J. Lawton, and F. Y. Hadaegh, "A coordination architecture for spacecraft formation control," *IEEE Trans. Control Syst. Technol.*, vol. 9, no. 6, pp. 777–790, Nov. 2001.

[8] Y. Huang and Y. Jia, "Adaptive finite-time 6-DOF tracking control for spacecraft fly around with input saturation and state constraints," *IEEE Trans. Aerosp. Electron. Syst.*, vol. 55, no. 6, pp. 3259–3272, Dec. 2019.

[9] C. B. Low, "Adaptable virtual structure formation tracking control design for nonholonomic tracked mobile robots, with experiments," in *Proc. IEEE 18th Int. Conf. Intell. Transp. Syst.*, Sep. 2015, pp. 1868–1875.

[10] G. Pola, P. Pepe, and M. D. D. Benedetto, "Decentralized supervisory control of networks of nonlinear control systems," *IEEE Trans. Autom. Control*, vol. 63, no. 9, pp. 2803–2817, Sep. 2018.

[11] A. Yang, W. Naeem, G. W. Irwin, and K. Li, "Stability analysis and implementation of a decentralized formation control strategy for unmanned vehicles," *IEEE Trans. Control Syst. Technol.*, vol. 22, no. 2, pp. 706–720, Mar. 2014.

[12] Y.-H. Chang, C.-W. Chang, C.-L. Chen, and C.-W. Tao, "Fuzzy sliding-mode formation control for multirobot systems: Design and implementation," *IEEE Trans. Syst., Man, Cybern. B, Cybern.*, vol. 42, no. 2, pp. 444–457, Apr. 2012.

[13] M.-Y. Lee, B.-S. Chen, Y. Chang, and C.-L. Hwang, "Stochastic robust team formation tracking design of multi-VTOL-UAV networked control system in smart city under time-varying delay and random fluctuation," *IEEE Access*, vol. 8, pp. 131310–131326, 2020.

[14] X. Liu, S. S. Ge, C.-H. Goh, and Y. Li, "Event-triggered coordination for formation tracking control in constrained space with limited communication," *IEEE Trans. Cybern.*, vol. 49, no. 3, pp. 1000–1011, Mar. 2019.

[15] X. Liu and K. D. Kumar, "Network-based tracking control of spacecraft formation flying with communication delays," *IEEE Trans. Aerosp. Electron. Syst.*, vol. 48, no. 3, pp. 2302–2314, Jul. 2012.

[16] A. Shui, W. Chen, P. Zhang, S. Hu, and X. Huang, "Review of fault diagnosis in control systems," in *Proc. Chin. Control Decis. Conf.*, Guilin, China, 2009, pp. 5324–5329.

[17] S. Harshavarthini, R. Sakthivel, and C. K. Ahn, "Finite-time reliable attitude tracking control design for nonlinear quadrotor model with actuator faults," *Nonlinear Dyn.*, vol. 96, no. 4, pp. 2681–2692, Jun. 2019.

[18] R. Sakthivel, T. Satheesh, S. Harshavarthini, and D. J. Almakhles, "Design of resilient reliable control for uncertain periodic piecewise systems with time-varying delay and disturbances," *J. Franklin Inst.*, vol. 357, no. 17, pp. 12326–12345, Nov. 2020.

[19] M.-Y. Lee, B.-S. Chen, C.-Y. Tsai, and C.-L. Hwang, "Stochastic H_∞ robust decentralized tracking control of large-scale team formation UAV network system with time-varying delay and packet dropout under interconnected couplings and Wiener fluctuations," *IEEE Access*, vol. 9, pp. 41976–41997, 2021.

[20] R. K. Saha, "Spectrum sharing in satellite-mobile multisystem using 3D in-building small cells for high spectral and energy efficiencies in 5G and beyond era," *IEEE Access*, vol. 7, pp. 43846–43868, 2019.

[21] Z. Zhang, Y. Shi, Z. Zhang, H. Zhang, and S. Bi, "Modified order-reduction method for distributed control of multi-spacecraft networks with time-varying delays," *IEEE Trans. Control Netw. Syst.*, vol. 5, no. 1, pp. 79–92, Mar. 2018.

[22] P. Razzaghi and N. Assadian, "Study of the triple-mass tethered satellite system under aerodynamic drag and J_2 perturbations," *IEEE Access*, vol. 7, pp. 43846–43868, 2019.

[23] R. Vijayan, M. Bilal, and K. Schilling, "Nonlinear dynamic modeling of satellite relative motion with differential J_2 and drag," in *Proc. IEEE Aerosp. Conf.*, Mar. 2020, pp. 1–8.

[24] C. S. Wu and B. S. Chen, "Adaptive attitude control of spacecraft: A mixed H_2 and H_∞ approach," *AIAA. J. Guid., Control Dyn.*, vol. 24, no. 4, pp. 755–766, 2001.

[25] C. Liu, Z. Sun, D. Ye, and K. Shi, "Robust adaptive variable structure tracking control for spacecraft chaotic attitude motion," *IEEE Access*, vol. 6, pp. 3851–3857, 2018.

[26] C.-S. Tseng, B.-S. Chen, and H.-J. Uang, "Fuzzy tracking control design for nonlinear dynamic systems via T-S fuzzy model," *IEEE Trans. Fuzzy Syst.*, vol. 9, no. 3, pp. 381–392, Jun. 2001.

[27] C.-S. Tseng and B.-S. Chen, "H_∞ decentralized fuzzy model reference tracking control design for nonlinear interconnected systems," *IEEE Trans. Fuzzy Syst.*, vol. 9, no. 6, pp. 795–809, Dec. 2001.

[28] G. Feng, "A survey on analysis and design of model-based fuzzy control systems," *IEEE Trans. Fuzzy Syst.*, vol. 14, no. 5, pp. 676–697, Oct. 2006.

[29] B. S. Chen, Y. S. Ma, and M. Y. Li, "Stochastic robust H_∞ decentralized network formation tracking control of large-scale team satellites via event-triggered mechanism," *IEEE Access*, vol. 10, pp. 62011–62036, 2022.

[30] B. S. Chen, W. H. Chen, and H. L. Wu, "Robust H_2/H_∞ global linearization filter design for nonlinear stochastic systems," *IEEE Trans. Circuits Syst. I, Reg. Papers, Reg. Papers*, vol. 56, no. 7, pp. 1441–1454, Jul. 2009.

[31] K. A. Hoo and J. C. Kantor, "Global linearization and control of a mixed-culture bioreactor with competition and external inhibition," *Math. Bioscience*, vol. 82, no. 1, pp. 43–62, Nov. 1986.

[32] S. Boyd, L. E. Ghaoui, E. Feron, and V. Balakrishan, *Linear Matrix Inequalities in System and Control Theory*. Philadelphia, PA, USA: SIAM, 1994.

[33] R. A. Nichols, R. T. Reichert, and W. J. Rugh, "Gain scheduling for H_∞ controllers: A flight control example," *IEEE Trans. Control Syst. Technol.*, vol. 1, no. 2, pp. 69–79, Jun. 1993.
[34] B.-S. Chen and C.-F. Wu, "Robust scheduling filter design for a class of nonlinear stochastic Poisson signal systems," *IEEE Trans. Signal Process.*, vol. 63, no. 23, pp. 6245–6257, Dec. 2015.
[35] D. P. Kingma and J. Ba, "Adam: A method for stochastic optimization," 2014, *arXiv:1412.6980*.
[36] A. L. Maas, P. Qi, Z. Xie and A. Y. Hannun, "Building DNN acoustic models for large vocabulary speech recognition," *Comput. Speech Lang.*, vol. 41, pp. 195–213, Jan. 2017.
[37] D. Ciresan, U. Meier, and J. Schmidhuber, "Multi-column deep neural networks for image classification," in *Proc. IEEE Conf. Comput. Vis. Pattern Recognit.*, Jun. 2012, pp. 3642–3649.
[38] Y. N. Dong and G. S. Lian, "Research and discussion on image recognition and classification algorithm based on deep learning," in *Proc. Int. Conf. Mach. Learn., Big Data Bus. Intell. (MLBDBI)*, Jan. 2020, pp. 274–278.
[39] H.-C. Shin et al., "Deep convolutional neural networks for computer-aided detection: CNN architectures, dataset characteristics and transfer learning," *IEEE Trans. Med. Imag.*, vol. 35, no. 5, pp. 1285–1298, Feb. 2016.
[40] B. S. Chen, M. Y. Lee, and T. H. Lin, "DNN-based H_∞ control scheme of nonlinear time-varying dynamic systems with external disturbance and its application to UAV tracking design," *IEEE Access*, vol. 9, pp. 69635–69653, 2021.
[41] B. S. Chen, M. Y. Li, and X. H. Chen, "Security-enhanced filter design for stochastic systems under malicious attack via smoothed signal model and multiobjective estimation method," *IEEE Trans. Signal Process.*, vol. 68, pp. 4971–4986, 2020.
[42] S. X. Du, A. Dekka, and B. Wu, *Modular Multilevel Converters: Analysis, Control, and Applications*. Hoboken, NJ, USA: Wiley-IEEE Press, Jan. 2018.
[43] T. Basar and P. Bernhard, *H_∞ Optimal Control and Related Minmax Design Problems: A Dynamic Game Approach*. Boston, MA, USA: Birkhäuser, 1995.
[44] W. Zhang, L. Xie, and B. S. Chen, *Stochasitc H_2/H_∞ Control: A Nash Game Approach*. Boca Raton, FL, USA: CRC Press, 2017.
[45] Y. N. Dauphin, H. D. Vries, J. Chung, and Y. Bengio, "RMSProp and equilibrated adaptive learning rates for non-convex optimization," *Mach. Learn.*, vol. 1, pp. 1504–1512, Feb. 2015.
[46] D. Wang, B. Wu, and E. K. Poh, *Satellite Formation Flying. Relative Dynamics* (Fuel Optimal Maneuvers and Formation Maintenance).
[47] S. Bahrami and M. Namvar, "Rigid body attitude control with delayed attitude measurement," *IEEE Trans. Control Syst. Technol.*, vol. 23, no. 5, pp. 1961–1969, Sep. 2015.
[48] X. Li, C. Ahn, D. Lu, and S. Guo, "Robust simultaneous fault estimation and nonfragile output feedback fault-tolerant control for Markovian jump systems," *IEEE Trans. Syst., Man, Cybern. Syst.*, vol. 49, no. 9, pp. 1769–1776, Sep. 2019.
[49] B. S. Chen, C. S. Wu, and Y. W. Jan, "Adaptive fuzzy mixed H_2/H_∞ attitude control of spacecraft," *IEEE Trans. Aerosp. Electron. Syst.*, vol. 36, no. 4, pp. 1343–1359, Nov. 2000.
[50] L. Chen, Y. Zhu, F. Wu, and Y. Zhao, "Fault estimation observer design for stochastic switched systems with sensor and non-differentiable actuator failures," *IEEE Trans. Cybern.*, to be published.
[51] Y. Zhu and W. X. Zheng, "Observer-based control for cyber-physical systems with periodic DoS attacks via a cyclic switching strategy," *IEEE Trans. Autom. Control*, vol. 65, no. 8, pp. 3714–3721, Aug. 2020.

BOR-SEN CHEN (Life Fellow, IEEE) received the B.S. degree in electrical engineering from the Tatung Institute of Technology, Taipei, Taiwan, in 1970, the M.S. degree in geophysics from National Central University, Chungli, Taiwan, in 1973, and the Ph.D. degree in electrical engineering from the University of Southern California, Los Angeles, CA, USA, in 1982. He has been a Lecturer, an Associate Professor, and a Professor with the Tatung Institute of Technology, from 1973 to 1987. Currently, he is a Tsing Hua Distinguished Chair Professor in electrical engineering and computer science with National Tsing Hua University, Hsinchu, Taiwan. His current research interests include control engineering, signal processing, and systems biology. He has received the Distinguished Research Award from the National Science Council of Taiwan four times. He is also a National Chair Professor of the Ministry of Education of Taiwan.

HUNG-YU LIN received the B.S. degree from the Department of Communication, Navigation and Control Engineering, National Taiwan Ocean University, Keelung, Taiwan, in 2020, and the M.S. degree from the Department of Electrical Engineering, National Tsing Hua University, Hsinchu, Taiwan, in 2022. His current research interests include robust control, fuzzy control, and nonlinear stochastic systems.